SPECTROSCOPIC PROBES OF HYDROGEN BONDING NETWORKS AND PROTON TRANSFER IN PHOTOSYNTHETIC WATER OXIDATION

A Dissertation
Presented to
The Academic Faculty

by

Udita Brahmachari

In Partial Fulfillment
of the Requirements for the Degree
Doctor of Philosophy in the
School of Chemistry and Biochemistry

Georgia Institute of Technology
December 2018

SPECTROSCOPIC PROBES OF HYDROGEN BONDING NETWORKS AND PROTON TRANSFER IN PHOTOSYNTHETIC WATER OXIDATION

Approved by:

Dr. Bridgette A. Barry, Advisor
School of Chemistry and Biochemistry
Georgia Institute of Technology

Dr. Pamela P. Peralta-Yahya
School of Chemistry and Biochemistry
Georgia Institute of Technology

Dr. Mostafa El-Sayed
School of Chemistry and Biochemistry
Georgia Institute of Technology

Dr. Jennifer E. Curtis
School of Physics
Georgia Institute of Technology

Dr. Adegboyega K. Oyelere
School of Chemistry and Biochemistry
Georgia Institute of Technology

Date Approved: October 30, 2018

ACKNOWLEDGEMENTS

I want to thank everyone who helped me complete my thesis work. I am grateful to my committee members Dr. Mostafa El-Sayed, Dr. Adegboyega Oyelere, Dr. Pamela Peralta-Yahya and Dr. Jennifer Curtis for their encouragement and valuable input throughout my time at Georgia Tech. My Ph.D. adviser Dr. Bridgette Barry is not only an excellent scientist but also an outstanding mentor. She trained me to be analytical and incisive in my thinking as well as planning comprehensive experiments to answer challenging scientific questions. Her enthusiasm for science is truly infectious. It has been an honor to work so closely with her and I will always cherish this experience.

I am grateful to the Barry lab members for being outstanding colleagues, mentors and friends. Parts of my project truly required a team effort and the Barry lab members were incredibly supportive. Dr. Adam Offenbacher and Dr. Brandon Polander were my first mentors. Both were excellent teachers with wildly different approaches and successfully converted me from a physical chemist to a biochemist over a period of six months. Dr. Zhanjun Guo was my companion on the PSII project and we spent many years working together in the dark to shed light on the oxygen evolution reaction. He was also an excellent friend who is compassionate and understanding (and introduced us to a whole array of new food). I thank Tyler Mccaslin for all the wonderful scientific and non-scientific discussions over the years. He was the undisputed expert on tools in the lab (a skillset from which I benefited immensely). Jiayuan “Nancy” He has been a delightful mentee-turned-collaborator with amazing persistence and attentiveness. I am grateful that I got the opportunity to work with her in the Barry lab. I am thankful to Dr. Yusuf Uddin for

camaraderie and companionship on our Ph.D. journey. He was not a Barry lab member in letter, but he definitely in spirit. I thank Dr. Atlee Watson for making the lab a fun place, Dr. Cynthia Pagba for being the ultimate lab spectroscopy expert (after Dr. Barry), Dr. Jiafeng Geng for career counselling and advice (besides Raman training), Sara Konecny and Emmanuela "Chichi" Obi for being patient mentees with an impatient mentor like me.

I thank Dr. Amy Ehrenworth, Dr. Pranav Karelkar, Dr. Swe-Htet Naing, David Hanna and Verjine Khodaverdian for their support and friendship. I want to especially thank Amy, my first friend in the US, for making me feel welcome and sharing numerous new experiences with me. My friends Dr. Reema Kundu, Dr. Tanushree Mitra and Dr. Shauvik Roy Choudhury provided support and understanding through the challenges of graduate school. I thank my sister, Dr. Sayanti Brahmachari for guidance throughout my life. I obtained an extremely patient mentor in her at birth and through the life challenges we faced together, we became the best of friends, counselors and comrades. I am grateful to my parents, Dr. Sunil Kumar Brahmachari and Dr. Ruby Bandyopadhyay for fostering curiosity, and valuing learning above all else. My parents, especially my mother, ensured we got every possible opportunity to excel and succeed in life and protected us in an environment where women were not highly valued or welcome. Lastly, I want to express my gratitude to my husband, Dr. Dwaipayan Mukhpadhyay, my partner and true confidant. He broadened my mind with new ideas and helped me craft a philosophy for my life. Being with him, I have learnt to live with myself and all my doubts. I thank him for believing in me and constantly challenging me to seek an improved version of myself.

TABLE OF CONTENTS

LIST OF TABLES

LIST OF FIGURES

LIST OF SYMBOLS AND ABBREVIATIONS

Å	angstrom
Abs	absorbance
ATP	adenosine triphosphate
AU	absorbance units
Ca PSII	calcium reconstituted photosystem II
CD PSII	calcium depleted photosystem II
Chl *a*	chlorophyll *a*
DD	double difference
DCBQ	2,6-dichloro-1,4-benzoquinone
DFT	density functional theory
EPR	electron paramagnetic resonance
ENDOR	electron nuclear double resonance
HEPES	4-(2-hydroxyethyl)-1-piperazineethanesulfonic acid
FTIR	Fourier transform infrared
MES	2-(*N*-morpholino) ethanesulfonic acid
OEC	oxygen-evolving complex
OTG	*n*-octyl-beta-D-thioglucoside
Pheo *a*	pheophytin *a*
PSII	photosystem II
Q_A	plastoquinone acceptor (bound)
Q_B	plastoquinone acceptor (mobile)
QM/MM	quantum mechanical/molecular mechanical

SDS-PAGE	sodium dodecyl sulfate polyacrylamide gel electrophoresis
Sr PSII	strontium reconstituted photosystem II
T. elongatus	*Thermosynechococcus elongatus*
UV	ultraviolet
V	volt
Y_D	tyrosine 160 of the D2 polypeptide
Y_Z	tyrosine 161 of the D1 polypeptide

Additional abbreviations are explained in the text.

SUMMARY

After decades of study, the mechanistic details of photosynthetic oxygen evolution still remain unclear. It is an important outstanding problem in biological chemistry. Photosynthetic oxygen production in the reaction center, photosystem II, is responsible for the maintenance of aerobic heterotrophic life and is thus of intrinsic importance in biological chemistry. In photosystem II, sequential light-induced oxidations of the oxygen evolving Mn_4CaO_5 cluster drive water oxidation and produce molecular oxygen and protons. The sequentially oxidized forms of this metal cluster are called the S_n states, where n refers to the number of oxidizing equivalents stored on the cluster. Efficient proton translocation and deprotonation of substrate water are critical for activity. Chloride, an essential cofactor, has been proposed to regulate proton transfer in the proton coupled electron transfer reactions (PCET) of the PSII OEC that accompany the S-state cycle. Chloride is an uncommon cofactor and is found in only a few enzymes besides PSII. Simulations have suggested that chloride exerts its effect by conformationally gating proton transfer and affecting the pK_a of amino acid residues directly involved in this pathway. Reaction-induced FTIR difference spectroscopy allows for monitoring long lived structural changes that accompany each S state transition. The spectral signature of an intermediary protonated water cluster, peptide carbonyl groups, hydrogen bonding perturbations and anion exchange will be used to investigate proton transfer in PSII. Theoretical calculations will be used alongside experiments to investigate the mechanism of chloride dependence of PSII. Elucidating proton transfer events and the role of chloride will aid in the design of new biomimetic catalysts for harvesting solar energy.

CHAPTER 1. INTRODUCTION

1.1 Proton transfer reactions

1.1.1 Grotthuss mechanism of proton-hopping

Protons exhibit anomalously high mobility in water.[1] It is approximately seven times that of a sodium ion, or about five times that of a potassium cation at room temperature. The first mechanism attempting to rationalize this discrepancy came from von Grotthuss.[2] He proposed that water molecules play the role of intermediates in a stepwise proton-hopping mechanism. The excess proton moves from one water molecule to the next using the existing hydrogen bonded network in aqueous solutions (Figure 1.1).

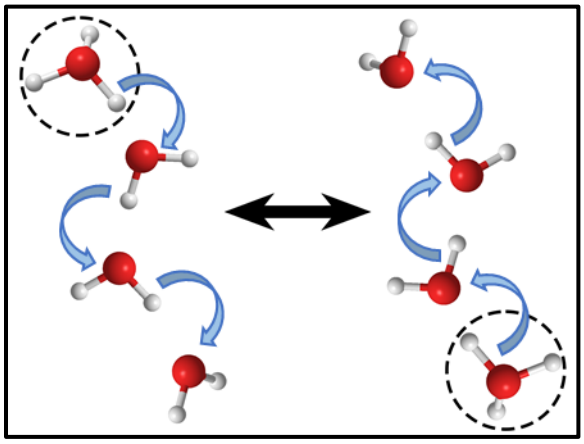

Figure 1.1 Schematic representation of the Grotthuss mechanism of proton transfer in aqueous solutions.

1.1.2 Eigen or Zundel?

The structure of the intermediary protonated water has been the subject of extensive debate.[3-4] The two primary candidates have been proposed; the hydronium ion, H_3O^+, also

referred to as the Eigen cation[5], and the Zundel ion[6], $H_5O_2^+$ (Figure 1.2). Both these ions are solvated by neighbouring waters connected by hydrogen bonds. In the gas phase, spectral signatures of both forms the Eigen and Zundel ions have been obtained.[7] The size of the cluster, determined by the number of water molecules solvating the protonated core, dictates the structure adopted by the core. In aqueous solutions, the spectral signature of the Eigen cation was observed in an acid-base neutralization reactions[8] and the Zundel cation in aqueous hydrochloric acid solutions.[9] Computational studies have proposed an "Eigen−Zundel−Eigen" (EZE) mechanism for proton transport.[3]

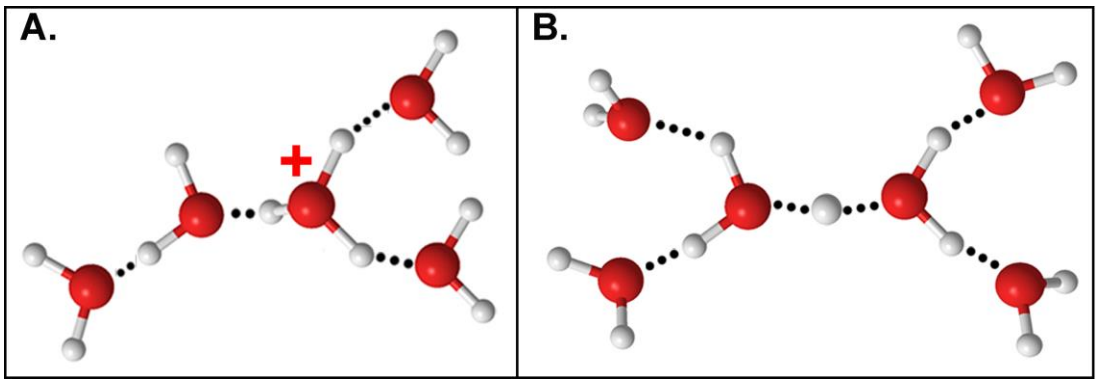

Figure 1.2 Structure of an (A) Eigen cation (H_3O^+) with four solvating water molecules, and (B) Zundel cation with four waters solvating the $H_5O_2^+$ core. Colors of atoms: Oxygen (red), hydrogen (white).

1.1.3 Enzymatic proton transfer in biology

Proton transfer in proteins can occur by several mechanisms. In a Grotthuss mechanism, proton transfer occurs between hydrogen bonded donor and acceptor pairs, through a free energy ladder, which favors directional transfer. The donor and acceptor pairs may be amino acid side chains or internal water molecules.[3] Alternatively, the proton transfer pathway may be regulated by a protein or chromophore-derived conformational

change, as in bacteriorhodopsin,[10] yellow photoactive protein,[11] and cytochrome c oxidase.[12] It may also be regulated by water dynamics, as in bacteriorhodopsin,[13] or by enhanced mobility of a proton-shuttling amino acid side chain, as in carbonic anhydrase.[14] In these cases, the rate of transfer through the pathway may be more adaptable and less sensitive to changes in thermodynamic driving force. Figure 1.3 shows the structures of some of these enzymes.

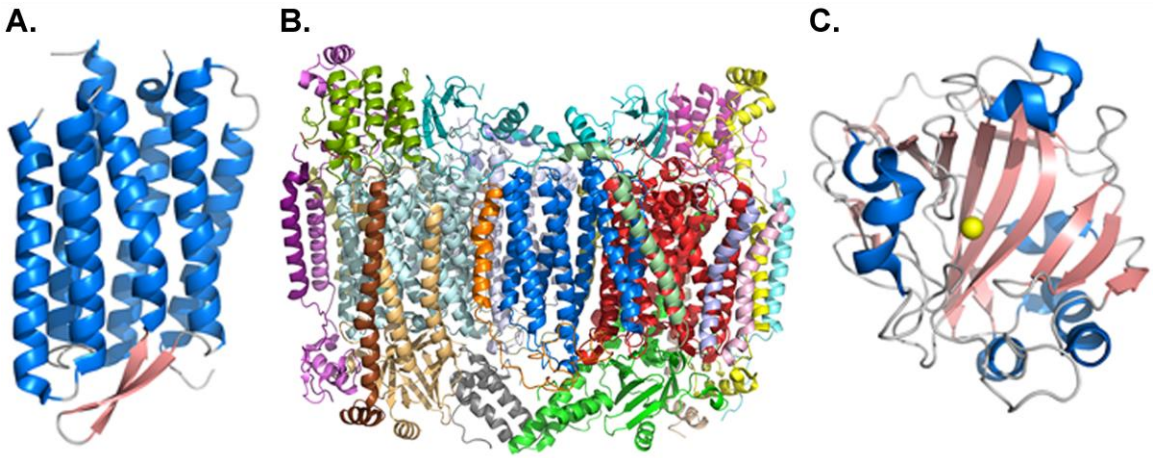

Figure 1.3 Some examples of proton shuttling enzymes. (A) Bacteriorhodopsin (PDB ID: 2NTU[15]), (B) Cytochrome c oxidase (PDB ID: 3WG7[16]), and (C) Carbonic anhydrase (PDB ID: 1TBT[17]). All three enzymes require proton transfer for activity.

In photosynthetic oxygen evolution, proton transfer from the catalytic site to the lumen is necessary to maintain optimal activity. Photosystem II (PSII) contains two potential proton transfer pathways containing hydrogen-bonded peptide carbonyl groups, amino acid side chains and internal water molecules (Figure 1.4). The mechanism of photosynthetic proton transfer will be investigated in this study.

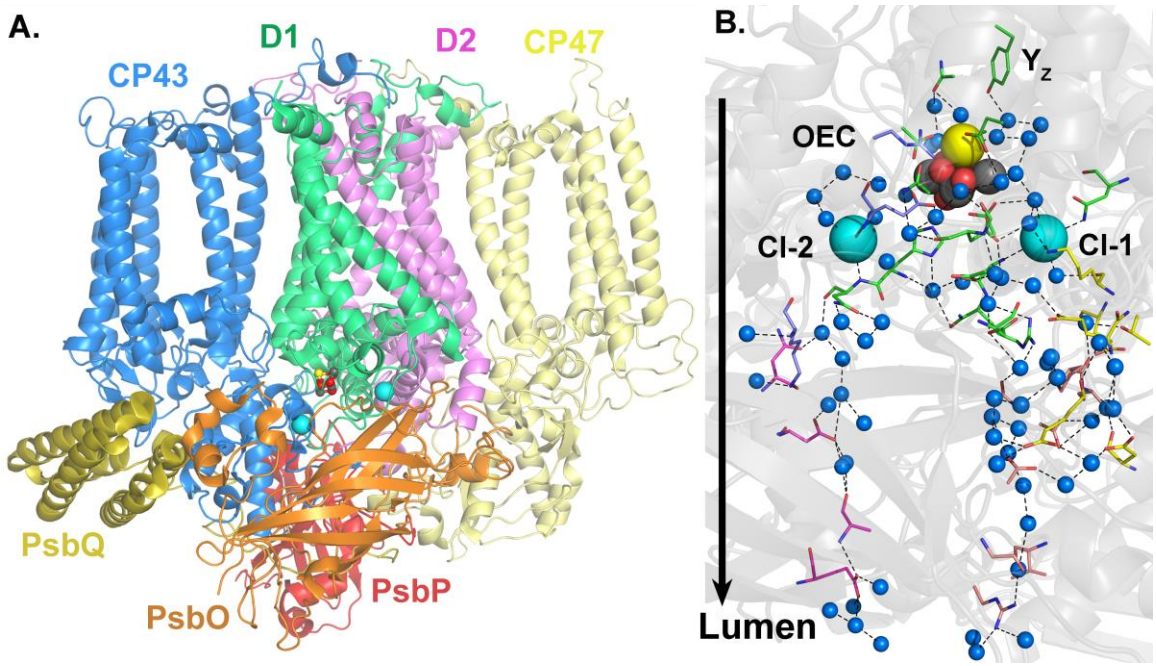

Figure 1.4 (A) Monomeric unit of PSII from Spinach at 3.2 Å resolution (PDB ID: 3JCU[18]) showing the cofactor-binding subunits and extrinsic subunits (D1, green; D2, magenta; CP47, yellow; CP43 blue; PsbO, orange; PsbP, red; PsbQ, olive). (B) Putative proton transfer pathways extending from the OEC to the lumen (PDB ID: 4UB6[19])

1.2 Photosynthetic oxygen evolution

1.2.1 Photosystem II

Photosystem II (PSII), the site of photosynthetic oxygen evolution, is a complex membrane protein comprised of both intrinsic transmembrane subunits along with extrinsic ones. Recently, a cryo EM structure of spinach PSII has been obtained.[18] A PSII monomer is comprised of several integral membrane spanning subunits and three extrinsic subunits (Figure 1.4).[18-20] The reaction center is made up of the primary subunits D1, D2, CP47 and CP43 which bind the redox active cofactors (Figure 1.5).

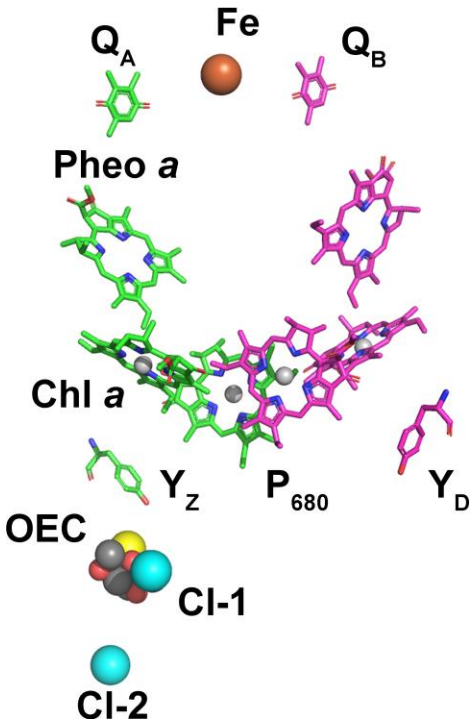

Figure 1.5 Cofactor arrangement in the cyanobacterial reaction center. Amino acid residues, chlorophyll *a* (Chl *a*), pheophytin *a* (Pheo *a*), and quinones (Q_A and Q_B) responsible for photoinduced charge separation across the membrane bilayer (PDB ID: 4UB6[19]).

Reaction is initiated by light-induced charge separation across the membrane bilayer. An accessory chlorophyll molecule, $Chl_{acc(D1)}$, absorbs light energy and transfers it to the reaction center (Figure 1.5).[21] An electron is lost from the excited state of $Chl_{acc(D1)}$ to the intermediate acceptor pheophytin (Pheo). The hole on $Chl_{acc(D1)}^{+}$ moves to the dimeric cholorophyll, P_{680}. The radical pair, P_{680}^{+}/$Pheo^{-}$ is thereby generated. It is stabilized through oxidation of $Pheo^{-}$ by a bound plastoquinone acceptor, Q_A and reduction of P_{680}^{+} by the redox-active tyrosine, Y_Z (Y161 of D1 polypeptide).[22] The neutral tyrosyl radical, $Y_Z^{\bullet}$, is a powerful oxidant and oxidizes the oxygen evolving complex (OEC).[23] The terminal electron acceptor in PSII is a second plastoquinone molecule, Q_B which reduces Q_A. A doubly reduced Q_B (Q_B^{-2}) is generated by two complete rounds of electron transfer

in the reaction center. Q_B^{-2} then exits the Q_B site and is subsequently replaced by a fully oxidized Q_B molecule.[24]

1.2.2 Oxygen evolving complex and S-state cycle of water oxidation

A Mn_4CaO_5 cluster constitutes the oxygen evolving complex (OEC) (Figure 1.6)[20]. Four sequential photooxidations of this cluster generates oxygen.[25] Oxygen evolution oscillates with period four. These oxidized states of the OEC are termed S_n states, where n=0-4 (Figure 1.6). A single flash of light oxidizes the OEC from the dark-adapted S_1 state to S_2.[26] The next flash promotes the OEC to the S_3 state. S_4 is a transient metastable state[27]. The OEC proceeds to the S_0 state directly from S_3 during the next photooxidation event. Substrate water oxidation accompanies this transition and the OEC gets restored to its most reduced (S_0) state. Proton release occurs concomitantly with the oxidations of the OEC. The liberated protons are transported to the interior lumen of the thylakoid membrane. The stoichiometry of proton release determined experimentally is 1:0:1:2 (Figure 1.6A)[28].

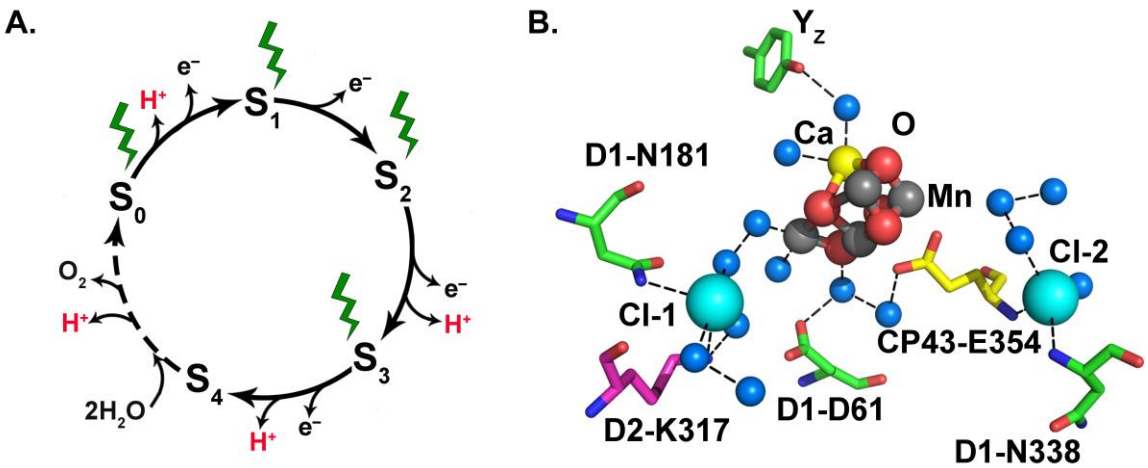

Figure 1.6 (A) S-state cycle[29] of water oxidation. (B) Chloride binding sites in PSII (PDB ID: 4UB6[19]). Metal ions: calcium, yellow; chloride, cyan; iron, brown; magnesium, white; manganese, gray; oxygen, red.

1.3 Reaction-induced FTIR difference spectroscopy

Reaction-induced infrared difference spectroscopy technique has the capability to reveal detailed structural information about proteins that precludes the need for invasive labeling.[30] It yields information about the conformational and chemical state of the molecules present in a system of interest by monitoring bond vibrations.[31-32] To detect conformational changes at the single amino acid level, reaction induced FT-IR (RIFT-IR) spectroscopy is employed.[33] The high signal to noise ratio and internal frequency calibration permits accurate background subtraction. This technique can be effective for monitoring photoinduced reactions in PSII.

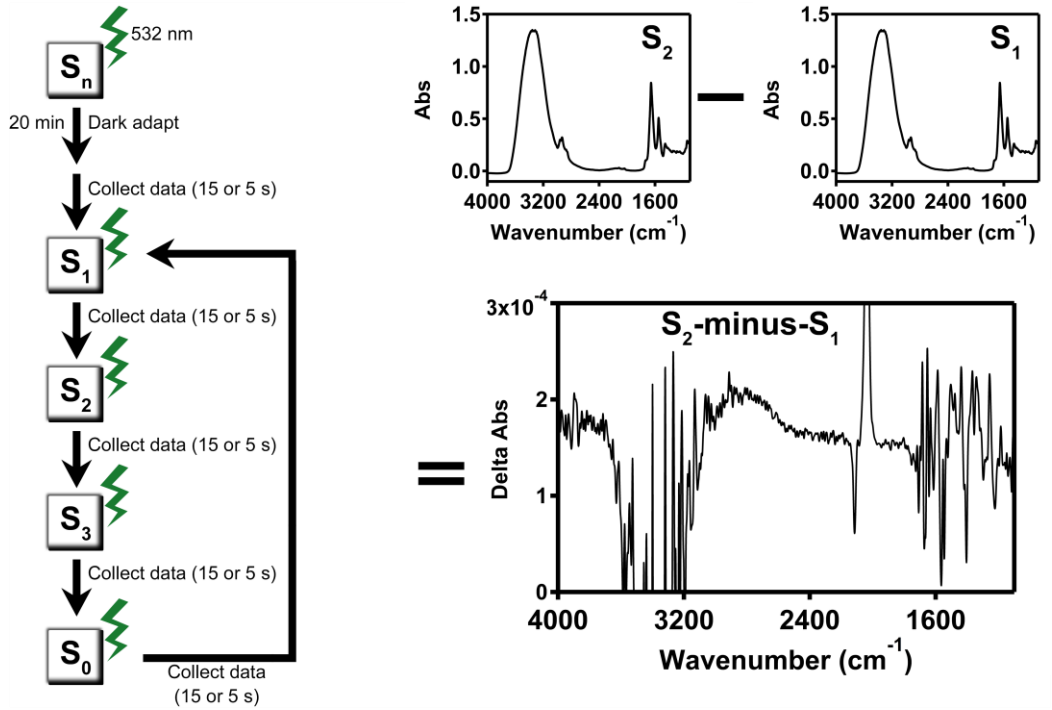

Figure 1.7 Spectroscopic methods employed to measure RIFT-IR spectra as a function of S state. Green arrows depict 532 nm flashes (7 ns).[34]

In PSII, short nanosecond laser pulses can be used to progress the system through different S-states.[35-36] The difference between the spectra associated with the two states is then analyzed (Figure 1.7). Electron transfer along the reaction center in PSII occurs on the microsecond to millisecond time scale.[37] In our experiments, difference FTIR spectra reflect structural changes at the oxygen-evolving complex that persist on the seconds time scale. These long-lived structural changes are likely attributable to be changes in hydrogen-bonding, electrostatics, polarity, and backbone conformation of PSII.[38] Each difference spectrum generated therefore reflect structural changes occurring on transition from S_n to S_{n+1}. These transitions are triggered by 532 nm laser flashes. Thus flash-induced FTIR spectroscopy is extremely well-suited to study structural changes that occur in PSII.

1.4 Probes for photosynthetic proton transfer

1.4.1 The essential cofactor chloride

Chloride ions have been found to be necessary for optimal oxygen evolution activity of PSII particles.[39-40] In the cyanobacterial crystal structure, two chloride ions, Cl-1 and Cl-2, are located 6.7 and 7.4 Å away from the OEC, respectively (Figure 1.6B). The exact role of the chloride ion is poorly understood.[41-42] A number of monovalent ions have been tested for their ability to support oxygen evolution activity ($Cl^- > Br^- >> NO_3^- > NO_2^- > I^-$).[43] Chloride binding is affected by the presence or absence of the smaller extrinsic subunits PsbP and PsbQ which is reflected in variation of K_D values.[44-45] In a flash based UV-visible spectrophotometric experiment conducted on isolated spinach PSII particles, it was shown that Cl^- is required only for the latter two S-state transitions (S_2 to S_3 and S_3 to S_0).[46] chloride has been proposed to mediate proton transfer reactions in PSII.[42]

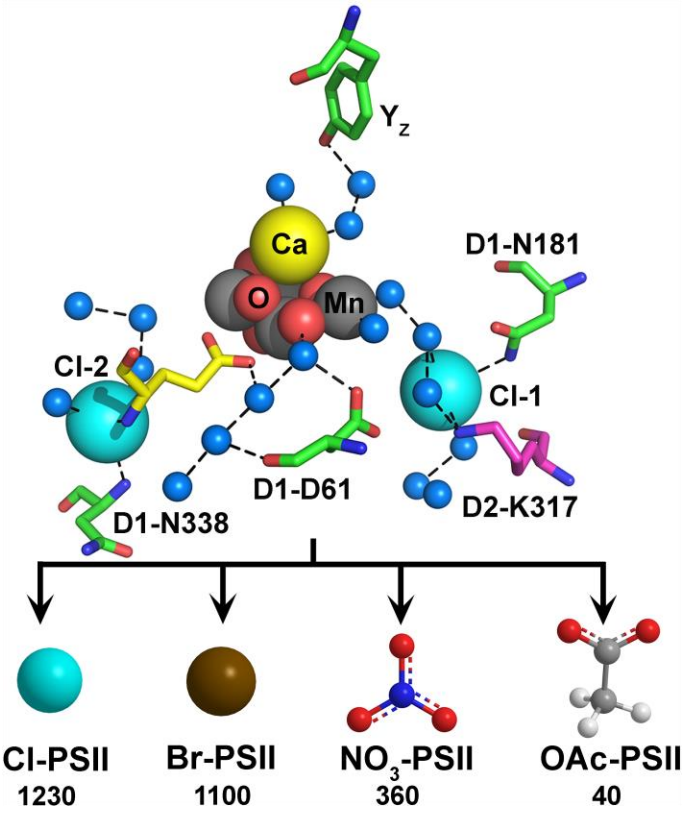

Figure 1.8 Chloride ions and their ligand environment. Bromide, nitrate and acetate were substituted at the chloride site. Below each ion, oxygen evolution rates, in µmol O_2/(mg Chl.hr)$^{-1}$, are shown. (PDB ID: 4UB6[19])

Substitutions at the chloride site will be carried out using the activating bromide and nitrate and the inhibitory acetate anions (Figure 1.8). Bromide supports 89% and nitrate supports 29% of the control chloride activity. Acetate substitution results in dramatically lowered oxygen evolution rates. The infrared spectrum with these anion-exchanged samples will be recorded and analyzed to investigate the role of chloride.

1.4.2 Internal protonated water cluster

Previously, a unique infrared signal has been detected from an internal water cluster in PSII. The broad band centered around 2,880 cm^{-1} wavenumbers was attributed to a cationic water cluster based on experiments using ammonia and $D_2{}^{16}O$.[29] By comparison

of the experimental data with studies on protonated water clusters of varying lengths in the gas phase, this water cluster was proposed to comprise of five water molecules.[47] Ca^{2+}-dependence and flash dependence were observed for this band. The water band originates during the S_1 to S_2 transition and is therefore a result of coupled proton transfer to an internal water cluster which forms a part of the hydrogen bonded network around the OEC. This proton gets released to bulk solvent during subsequent S-state transitions.[29] Therefore, the spectral signal arises from an intermediate in the proton transfer pathway. This IR signal will be used as a spectroscopic probe to monitor Cl-dependence of proton transfer during S-state transitions.

1.4.3 HB network

There exists an extensive hydrogen-bonded network in PSII, spanning over 35 Å and comprising of peptide carbonyl groups, amino acid side chains and internal water molecules. The vibrations of backbone amide C=O are excellent spectroscopic markers for monitoring hydrogen bonding changes. Previously, the substrate analogue ammonia was used to disrupt the hydrogen bonded network in PSII in sucrose containing buffers.[33] The cryoprotectant trehalose (Figure 1.9), known for its ability to stabilize proteins against denaturation under adverse conditions, was able to mitigate ammonia induced changes in the infrared spectrum.[48] The vibrational frequencies of the amide carbonyl groups will be exploited to investigate changes in the hydrogen bonding network in response to proton transfer events. The effects of cryoprotectants on this network will also be studied to assign a role for chloride in photosynthetic proton transfer.

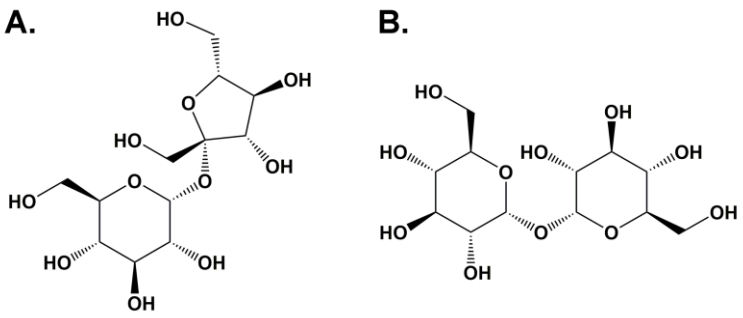

Figure 1.9 Structures of (A) sucrose and (B) trehalose used as cryoprotectants to probe hydrogen bonding networks in PSII.

1.5 Overview of the thesis

In Chapter 2, we attempted to use solvent isotope exchange to probe the role of internal water molecules in photosynthetic proton transfer. Both $D_2{}^{16}O$ and $H_2{}^{18}O$ exchange were performed on PSII core complexes. A novel 3074 cm^{-1} infrared band was identified during the S_3 to S_0 transition. We assigned this S_0 3074 cm^{-1} band to a protonated, internal water cluster, based on its sensitivity to calcium removal, frequency, $D_2{}^{16}O$ isotope shift, and significant (58 cm^{-1}) $H_2{}^{18}O$-induced frequency shift. When compared to the protonated water cluster that gives rise to the 2830 cm^{-1} band in the S_2 state, the S_0 hydronium ion is likely to be coordinated by additional water molecules. The S_2 band also exhibited $D_2{}^{16}O$ and $H_2{}^{18}O$ sensitivity. These data are consistent with transient proton transfer to water during the S_1 to S_2 and the S_3 to S_0 transitions; these protons may be derived from terminal water or hydroxide ligands to the Mn_4CaO_5 cluster. $H_2{}^{18}O$ had no effect on the mid-infrared (1800-1100 cm^{-1}) region of any S-state transition; $D_2{}^{16}O$ caused significant changes only in the S_1 to S_2 spectrum. The effect of $D_2{}^{16}O$ supports the conclusion that the S_1 to S_2 transition alters hydrogen bonding in the OEC water network.

This evidence shows that water plays two roles in photosynthetic oxygen evolution, the first as the substrate and the second as a transient proton donor and acceptor.

Chapter 3 investigated the role of chloride using RIFT-IR spectroscopy and quantum mechanical calculations. Anion exchange was performed using the activating anions bromide and nitrate. At 283 K, the spectral signature of the protonated water cluster was observed in the S_2 state which exhibited $H_2{}^{18}O$-induced shift. This result matched those in Chapter 2 at 263 K. QM computations on small models of the OEC predicted that a hydronium ion is stabilized by chloride. The model predicted the upshift and downshift of a H_3O^+ stretching mode by bromide and nitrate substitution, respectively. To test for this effect in anion-exchanged PSII, a single laser flash was applied to a dark adapted S_1 sample to generate the S_2 state, and difference RIFT-IR spectra were obtained. Anion exchange shows that an infrared band at 2830 cm^{-1}, assigned to W_n^+, a protonated water cluster, shifts up with bromide substitution and shifts down with nitrate substitution. Both anions support oxygen evolution activity. When compared to the QM derived results, the W_n^+ band frequencies support the conclusion that chloride plays a direct role in internal proton transfer during oxygen evolution.

Chapter 4 probed the hydrogen bonded proton transfer network of PSII using anion exchange in conjunction with infrared signals from W_n^+ and peptide carbonyl groups during the S_1 to S_2 transition. The increased ionic radius of bromide elicits a spectral Stark shift. The inhibitory anion, nitrate, caused a reorganization of the hydrogen-bonding network, which manifested as changes in the amide I and II regions of the vibrational spectrum. Trehalose, which is known to increase the strength of hydrogen-bonding interactions in proteins, reverses these nitrate-induced effects on backbone hydrogen

bonding. This is detected as a recovery of a differential band at 1530/1522 cm^{-1}, as well as a positive signal at 1630 cm^{-1}, when nitrate-PSII is suspended in trehalose buffer. Previously, these bands have been shown to be sensitive to site-directed mutations at amino acid residues, predicted to participate in the proton transfer pathway. Notably, trehalose also causes a frequency shift of the internal hydronium ion signal, W_n^+. These experiments provide evidence that nitrate inhibition involves alterations in hydrogen-bonding interactions in the oxygen evolving complex. Because nitrate targets the chloride site, these data also imply that chloride maintains a network, which plays a functional role in photosynthetic oxygen evolution.

Chapter 5 presents the effects of substituting acetate, an oxygen evolution inhibitor, for chloride. QM calculations on the small model of the OEC used in Chapter 3 indicates that acetate effectively intercalates into the proton transfer network and acts as a proton acceptor. Two different binding modes of acetate were tested in the model. In both modes, the carboxylate group accepts a proton, which chloride had stabilized on a nearby water molecule. In the infrared spectrum, the W_n^+ band at 2830 cm^{-1} is no longer evident. Isotope editing with ^{13}C-acetete provides evidence of the protonation event. These results show that the robust proton transfer network of PSII uses proton hopping via intermediary water molecules. Substituting an alternate proton acceptor to water such as acetate is detrimental for activity.

1.6 References

1. Agmon, N. The Grotthuss Mechanism. *Chem. Phys. Lett.* **1995,** *244,* 456-462.

2. de Grotthuss, C. J. T. *Ann. Chim.* **1806,** *58,* 54-74.

3. Knight, C.; Voth, G. A. The Curious Case of the Hydrated Proton. *Acc. Chem. Res.* **2012,** *45,* 101-9.

4. Agmon, N. The Acid Test for Water Structure. *Nature Chemistry* **2016,** *8,* 206.

5. Eigen, M. Proton Transfer, Acid-Base Catalysis, and Enzymatic Hydrolysis. Part I: Elementary Processes. *Angewandte Chemie International Edition in English* **1964,** *3,* 1-19.

6. Zundel, G. Hydration Structure and Intermolecular Interaction in Polyelectrolytes. *Angewandte Chemie International Edition in English* **1969,** *8,* 499-509.

7. Headrick, J. M.; Diken, E. G.; Walters, R. S.; Hammer, N. I.; Christie, R. A.; Cui, J.; Myshakin, E. M.; Duncan, M. A.; Johnson, M. A.; Jordan, K. D. Spectral Signatures of Hydrated Proton Vibrations in Water Clusters. *Science* **2005,** *308,* 1765-1769.

8. Mohammed, O. F.; Pines, D.; Dreyer, J.; Pines, E.; Nibbering, E. T. Sequential Proton Transfer through Water Bridges in Acid-Base Reactions. *Science* **2005,** *310,* 83-86.

9. Thämer, M.; De Marco, L.; Ramasesha, K.; Mandal, A.; Tokmakoff, A. Ultrafast 2d Ir Spectroscopy of the Excess Proton in Liquid Water. *Science* **2015,** *350,* 78-82.

10. Garczarek, F.; Gerwert, K. Functional Waters in Intraprotein Proton Transfer Monitored by Ftir Difference Spectroscopy. *Nature* **2006,** *439,* 109-112.

11. Borgstahl, G. E.; Williams, D. R.; Getzoff, E. D. 1.4. Ang. Structure of Photoactive Yellow Protein, a Cytosolic Photoreceptor: Unusual Fold, Active Site, and Chromophore. *Biochemistry* **1995,** *34,* 6278-6287.

12. Seibold, S. A.; Mills, D. A.; Ferguson-Miller, S.; Cukier, R. I. Water Chain Formation and Possible Proton Pumping Routes in *Rhodobacter Sphaeroides* Cytochrome

C Oxidase: A Molecular Dynamics Comparison of the Wild Type and R481k Mutant. *Biochemistry* **2005,** *44*, 10475-10485.

13. Garczarek, F.; Wang, J.; El-Sayed, M. A.; Gerwert, K. The Assignment of the Different Infrared Continuum Absorbance Changes Observed in the 3000–1800-Cm^{-1} Region During the Bacteriorhodopsin Photocycle. *Biophys. J.* **2004,** *87*, 2676-2682.

14. Silverman, D. N.; McKenna, R. Solvent-Mediated Proton Transfer in Catalysis by Carbonic Anhydrase. *Acc. Chem. Res.* **2007,** *40*, 669-675.

15. Luecke, H.; Richter, H.-T.; Lanyi, J. K. Proton Transfer Pathways in Bacteriorhodopsin at 2.3 Angstrom Resolution. *Science* **1998,** *280*, 1934-1937.

16. Hirata, K.; Shinzawa-Itoh, K.; Yano, N.; Takemura, S.; Kato, K.; Hatanaka, M.; Muramoto, K.; Kawahara, T.; Tsukihara, T.; Yamashita, E., et al. Determination of Damage-Free Crystal Structure of an X-Ray-Sensitive Protein Using an Xfel. *Nature methods* **2014,** *11*, 734-6.

17. Fisher, Z.; Hernandez Prada, J. A.; Tu, C.; Duda, D.; Yoshioka, C.; An, H.; Govindasamy, L.; Silverman, D. N.; McKenna, R. Structural and Kinetic Characterization of Active-Site Histidine as a Proton Shuttle in Catalysis by Human Carbonic Anhydrase Ii. *Biochemistry* **2005,** *44*, 1097-105.

18. Wei, X.; Su, X.; Cao, P.; Liu, X.; Chang, W.; Li, M.; Zhang, X.; Liu, Z. Structure of Spinach Photosystem Ii–Lhcii Supercomplex at 3.2 Å Resolution. *Nature* **2016,** *534*, 69-74.

19. Suga, M.; Akita, F.; Hirata, K.; Ueno, G.; Murakami, H.; Nakajima, Y.; Shimizu, T.; Yamashita, K.; Yamamoto, M.; Ago, H., et al. Native Structure of Photosystem Ii at 1.95 Å Resolution Viewed by Femtosecond X-Ray Pulses. *Nature* **2015,** *517*, 99-103.

20. Umena, Y.; Kawakami, K.; Shen, J.-R.; Kamiya, N. Crystal Structure of Oxygen-Evolving Photosystem Ii at a Resolution of 1.9 Å. *Nature* **2011,** *473*, 55-60.

21. Holzwarth, A.; Müller, M.; Reus, M.; Nowaczyk, M.; Sander, J.; Rögner, M. Kinetics and Mechanism of Electron Transfer in Intact Photosystem Ii and in the Isolated Reaction Center: Pheophytin Is the Primary Electron Acceptor. *Proc. Natl. Acad. Sci. U.S.A.* **2006,** *103*, 6895-6900.

22. Barry, B. A. The Role of Redox-Active Amino Acids in the Photosynthetic Water-Oxidizing Complex. *Photochem. Photobiol.* **1993,** *57*, 179-188.

23. Boerner, R.; Barry, B. Isotopic Labeling and Epr Spectroscopy Show That a Tyrosine Residue Is the Terminal Electron Donor, Z, in Manganese-Depleted Photosystem Ii Preparations. *J. Biol. Chem.* **1993,** *268*, 17151-17154.

24. Diner, B. A.; Babcock, G. T., *Oxygenic Photosynthesis: The Light Reactions*, Springer: 1996, pp 213-247.

25. Kok, B.; Forbush, B.; McGloin, M. Cooperation of Charges in Photosynthetic O_2 Evolution-I. A Linear Four Step Mechanism. *Photochem. Photobiol.* **1970,** *11*, 457-75.

26. Haumann, M.; Grabolle, M.; Neisius, T.; Dau, H. The First Room-Temperature X-Ray Absorption Spectra of Higher Oxidation States of the Tetra-Manganese Complex of Photosystem Ii. *FEBS Lett.* **2002,** *512*, 116-120.

27. Barry, B. A.; Cooper, I. B.; De Riso, A.; Brewer, S. H.; Vu, D. M.; Dyer, R. B. Time-Resolved Vibrational Spectroscopy Detects Protein-Based Intermediates in the Photosynthetic Oxygen-Evolving Cycle. *Proc. Natl. Acad. Sci. U.S.A.* **2006,** *103*, 7288-7291.

28. Bao, H.; Dilbeck, P. L.; Burnap, R. L. Proton Transport Facilitating Water-Oxidation: The Role of Second Sphere Ligands Surrounding the Catalytic Metal Cluster. *Photosynth. Res.* **2013,** *116*, 215-229.

29. Polander, B. C.; Barry, B. A. Detection of an Intermediary, Protonated Water Cluster in Photosynthetic Oxygen Evolution. *Proc. Natl. Acad. Sci. U.S.A.* **2013,** *110*, 10634-9.

30. Zscherp, C.; Barth, A. Reaction-Induced Infrared Difference Spectroscopy for the Study of Protein Reaction Mechanisms. *Biochemistry* **2001,** *40*, 1875-1883.

31. Barth, A. Fine-Structure Enhancement—Assessment of a Simple Method to Resolve Overlapping Bands in Spectra. *Spectrochimica Acta Part A: Molecular and Biomolecular Spectroscopy* **2000,** *56*, 1223-1232.

32. Mantsch, H. H.; Moffatt, D. J.; Casal, H. L. Fourier Transform Methods for Spectral Resolution Enhancement. *J. Mol. Struct.* **1988,** *173*, 285-298.

33. Polander, B. C.; Barry, B. A. A Hydrogen-Bonding Network Plays a Catalytic Role in Photosynthetic Oxygen Evolution. *Proc. Natl. Acad. Sci. U.S.A.* **2012,** *109*, 6112-6117.

34. Barry, B. A.; Brahmachari, U.; Guo, Z. Tracking Reactive Water and Hydrogen-Bonding Networks in Photosynthetic Oxygen Evolution. *Acc. Chem. Res.* **2017,** *50*, 1937-1945.

35. Noguchi, T.; Sugiura, M. Flash-Induced Fourier Transform Infrared Detection of the Structural Changes During the S-State Cycle of the Oxygen-Evolving Complex in Photosystem Ii. *Biochemistry* **2001,** *40*, 1497-1502.

36. Hillier, W.; Babcock, G. T. S-State Dependent Fourier Transform Infrared Difference Spectra for the Photosystem Ii Oxygen Evolving Complex. *Biochemistry* **2001,** *40*, 1503-1509.

37. Cooper, I. B.; Barry, B. A. Azide as a Probe of Proton Transfer Reactions in Photosynthetic Oxygen Evolution. *Biophys. J.* **2008,** *95*, 5843-5850.

38. Cooper, I. B.; Barry, B. A. Perturbations at the Chloride Site During the Photosynthetic Oxygen-Evolving Cycle. *Photosynth. Res.* **2007,** *92*, 345-356.

39. Pokhrel, R.; McConnell, I. L.; Brudvig, G. W. Chloride Regulation of Enzyme Turnover: Application to the Role of Chloride in Photosystem Ii. *Biochemistry* **2011,** *50*, 2725-2734.

40. Yocum, C. F. The Calcium and Chloride Requirements of the O_2 Evolving Complex. *Coord. Chem. Rev.* **2008,** *252*, 296-305.

41. Popelková, H.; Yocum, C. F. Current Status of the Role of Cl− Ion in the Oxygen-Evolving Complex. *Photosynth. Res.* **2007,** *93*, 111-121.

42. Rivalta, I.; Amin, M.; Luber, S.; Vassiliev, S.; Pokhrel, R.; Umena, Y.; Kawakami, K.; Shen, J.-R.; Kamiya, N.; Bruce, D. Structural–Functional Role of Chloride in Photosystem Ii. *Biochemistry* **2011,** *50*, 6312-6315.

43. Wincencjusz, H.; Yocum, C. F.; Van Gorkom, H. J. Activating Anions That Replace Cl-in the O2-Evolving Complex of Photosystem Ii Slow the Kinetics of the Terminal Step in Water Oxidation and Destabilize the S2 and S3 States. *Biochemistry* **1999,** *38*, 3719-3725.

44. Lindberg, K.; Andréasson, L.-E. A One-Site, Two-State Model for the Binding of Anions in Photosystem Ii. *Biochemistry* **1996,** *35*, 14259-14267.

45. Homann, P. H. Chloride Relations of Photosystem Ii Membrane Preparations Depleted of, and Resupplied with, Their 17 and 23 Kda Extrinsic Polypeptides. *Photosynth. Res.* **1988,** *15*, 205-220.

46. Wincencjusz, H.; van Gorkom, H. J.; Yocum, C. F. The Photosynthetic Oxygen Evolving Complex Requires Chloride for Its Redox State S2→ S3 and S3→ S0 Transitions but Not for S0→ S1 or S1→ S2 Transitions. *Biochemistry* **1997,** *36*, 3663-3670.

47. Douberly, G.; Walters, R.; Cui, J.; Jordan, K. D.; Duncan, M. Infrared Spectroscopy of Small Protonated Water Clusters, $H^+(H_2o)_N$ (N= 2− 5): Isomers, Argon Tagging, and Deuteration. *J Phys Chem A* **2010,** *114*, 4570-4579.

48. Jain, N. K.; Roy, I. Effect of Trehalose on Protein Structure. *Protein Sci.* **2009,** *18*, 24-36.

CHAPTER 2. DYNAMICS OF PROTON TRANSFER TO INTERNAL WATER DURING THE PHOTOSYNTHETIC OXYGEN-EVOLVING CYCLE

Reprinted with permission from *The Journal of Physical Chemistry B*

Brahmachari, U. and Barry, B. A. Dynamics of Proton Transfer to Internal Water During the Photosynthetic Oxygen-Evolving Cycle. *J. Phys. Chem. B* **2016** *120,* 11464–11473

2.1 Abstract

In photosynthesis, the light-driven oxidation of water is a sustainable process, which converts solar to chemical energy and produces protons and oxygen. To enable biomimetic strategies, the mechanism of photosynthetic oxygen evolution must be elucidated. Here, we provide information concerning a critical step in the oxygen-evolving, or S-state, cycle. During this S_3 to S_0 transition, oxygen is produced, and substrate water binds to the manganese-calcium catalytic site. Our spectroscopic and $H_2{}^{18}O$ labeling experiments show that this S_3 to S_0 step is associated with the protonation of an internal water cluster in a hydrogen-bonding network, which contains calcium. When compared to the protonated water cluster, formed during a preceding step, the S_1 to S_2 transition, the S_3 to S_0 hydronium ion is likely to be coordinated by additional water molecules. This evidence shows that internal water and the hydrogen bonding network act as a transient proton acceptor at multiple points in the oxygen-evolving cycle.

2.2 Introduction

Proton transfer in enzymes occurs via hydrogen-bonded chains of amino acid side chains. In some cases, hydrogen bonded, internal water also plays a role in proton movement. Three representative examples in which the role of internal water has been successfully elucidated are bacteriorhodopsin,[1-3] carbonic anhydrase,[4] and cytochrome c oxidase.[5]

Water is the substrate of the photosynthetic oxygen-evolving complex (OEC) in photosystem II (PSII). During oxygenic photosynthesis, molecular oxygen is generated through photo-induced oxidation of these substrate water molecules.[6-7] This multi-electron reaction yields molecular oxygen and protons. The protons are transferred over 35 Å to

the thylakoid lumen and generate a proton gradient. A cyanobacterial PSII monomer is comprised of 17 integral membrane-spanning subunits and 3 extrinsic subunits.[8-10] Photoexcitation leads to a charge separation involving the primary chlorophyll donor, P_{680}, and a quinone acceptor, Q_A. The radical pair is stabilized when reduction of P_{680}^+ by the redox-active tyrosine, Y_Z (Y161 of D1 polypeptide) occurs.[7, 11] The tyrosyl radical, $Y_Z^\bullet$, in turn oxidizes a Mn_4CaO_5 cluster, which is the site of water oxidation (Figure 2.1).[12-13] This metal cluster (Figure 2.1A), or OEC, undergoes four Y_Z-mediated oxidation reactions (Figure 2.1B).[12, 14] The oxidized states are termed S_n states, where n=0-4 and refers to the number of oxidizing equivalents stored (Figure 2.1B). A short, saturating flash oxidizes the OEC from the dark-adapted S_1 state to S_2, corresponding to the oxidation of Mn(III) to Mn(IV) (see ref 6 but see also ref 15). The second flash generates the S_3 state, and a third flash generates the S_4 metastable state.[12-13] S_4 converts to S_0 in the dark, and oxygen release accompanies this transition. Calcium and chloride ions are required for optimal oxygen evolution.[16] The extrinsic subunits of PSII, called PsbP and PsbQ, modulate its calcium and chloride requirement.[17-18]

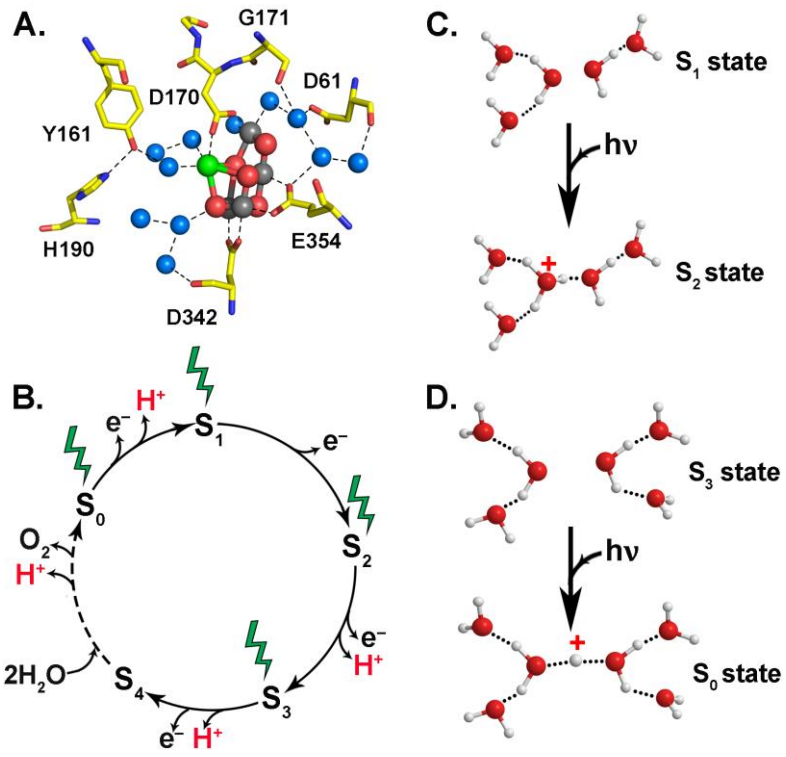

Figure 2.1 Photosynthetic water oxidation. (A) The OEC of cyanobacterial PSII and its predicted hydrogen-bonding network (PDB ID: 4UB6).[9] Amino acids are shown as sticks, water oxygens are shown as blue spheres, and hydrogen-bonding interactions are shown as dashed lines. Residues from the PSII subunits, D1 and CP43, are shown in green and yellow, respectively. Mn_4CaO_5 cluster: calcium, yellow; manganese, gray; oxygen, red. (B) Flash-induced S-state cycle of photosynthetic water oxidation.[12] (C) Schematic depiction of a cationic cluster of five water molecules, proposed to be produced during the flash-induced S_1 to S_2 transition. (D) Schematic depiction of a cationic cluster of six water molecules, proposed to be produced during the flash-induced S_3 to S_0 transition. Atoms: red, oxygen; white, hydrogen.

To make the reactions thermodynamically accessible, proton release is expected to occur concomitantly with the oxidation of water.[19] A 1:0:1:2 stoichiometry of proton release, corresponding to the S_0 to S_1, S_1 to S_2, S_2 to S_3, and S_3 to S_0 transitions, respectively, has been measured in sucrose buffers (Figure 2.1B).[20] Under this condition, the S_1 to S_2 transition is unique in that no proton release is detected. X-ray structures and site-directed mutagenesis have been used to propose proton-transfer pathways from the buried OEC to the lumen.[21-23] Previously, our group has detected an infrared signal

attributed to protonation of this internal water network during the S_1 to S_2 transition.[24-25] In this paper, we provide the first evidence for the protonation of this internal water network during the S_3 to S_0 transition, which is the catalytic step in the water-oxidizing chemistry.

2.3 Materials and Methods

Photosystem II (PSII) samples were obtained from market spinach. PSII-enriched membrane particles were prepared by treatment with Triton X-100.[26] These particles were then solubilized using another detergent, 0.4% octylthioglucoside (0.4%). Subsequent treatment with 10 mM $MgCl_2$ depletes the light-harvesting complexes, LHCII, CP24, CP26 and CP29.[27] PSII samples thus obtained were suspended into buffer containing 0.4 M sucrose, 50 mM 2-(N-morpholino)ethanesulfonic acid (MES)-NaOH, pH 6, and 15 mM NaCl and frozen at -70^{o}C.

Calcium depletion was performed using 10 mM ethylene glycol-bis(2,2-aminoethylether)-N,N,N',N'-tetraacetic acid (EGTA).[28] Samples were washed twice with 10 mM EGTA in 0.4 M sucrose, 50 mM 2-[4-(2-hydroxyethyl)piperazin-1-yl]ethanesulfonic acid (HEPES)-NaOH, pH 7.5, and 15 mM NaCl buffer. After the second wash, samples (calcium-depleted PSII or CD-PSII) were divided into small aliquots and frozen at -70^{o}C.

To perform calcium reconstitution for oxygen evolution assays,[28] a CD-PSII sample was thawed and pelleted by centrifugation (50,000 x *g*, 10 minutes, 4^{o}C). The pellet was resuspended in 0.4 M sucrose, 50 mM HEPES-NaOH, pH 7.5 and 15 mM NaCl (one EGTA-free wash). To reconstitute calcium, 20 mM calcium was added to this sample from

a 3 M buffered stock to give a calcium-reconstituted PSII (Ca-PSII) sample. The chloride concentration was maintained at 155 mM by addition from a 3 M buffered NaCl stock.

Oxygen assays were performed using a Clark-type oxygen electrode.[29] Freshly prepared solutions of recrystallized 0.5 mM 2,6-dichlorobenzoquinone and 1 mM potassium ferricyanide ($K_3[Fe(CN)_6]$) were used as the external acceptors. In some experiments, the inhibitor, 3-(3,4-dichlorophenyl)-1,1-dimethylurea (DCMU, Serva, Islandia, NY) was used at a concentration of 10 μM. Stocks (10 mM in ethanol) were made up immediately before the measurement. The assay was performed in buffer containing 0.4 M sucrose, 50 mM HEPES-NaOH, pH 7.5 and 15 mM NaCl or 0.4 M sucrose, 50 mM MES-NaOH, pH 6.0 and 15 mM NaCl. When required, chloride and calcium concentrations were adjusted by addition from 3 M buffered stocks.

As isolated and assayed at pH 6.0, PSII had oxygen evolution rates of 1,000 ± 170 μmol O_2 (mg Chl-h)$^{-1}$. After resuspension into pH 7.5 buffer with no EGTA treatment, the rate decreased to 520 ± 50 μmol O_2 (mg Chl-h)$^{-1}$. Oxygen evolution rates in the pH 7.5 sample were restored by addition of calcium and chloride to the assay media. For example, when 155 mM chloride was added, the rate of oxygen evolution was 750 ± 50 μmol O_2 (mg Chl-h)$^{-1}$ at pH 7.5. When assayed in the presence of 20 mM calcium and 155 mM chloride, the rate increased to 1,100 ± 120 μmol O_2 (mg Chl-h)$^{-1}$ at pH 7.5. Given the standard deviation, this calcium chloride induced rate is similar to the oxygen evolution rate reported for the pH 6 control, as described above (1,000 ± 170 μmol O_2 (mg Chl-h)$^{-1}$). This reversible decrease in oxygen evolution rate is expected at pH 7.5 and is due to loss of extrinsic subunits, PsbP and PsbQ.[2-5] These subunits are not absolutely required for activity, but modulate the requirement for calcium and chloride.[2-5] Addition of the PSII

inhibitor, 10 μM DCMU, which disrupts light-induced electron transfer, was used to give an estimate of the background. The DCMU background was 140 ± 10 μmol O_2 (mg Chl-h)$^{-1}$.

In CD-PSII samples, which were treated with EGTA at pH 7.5, the oxygen evolution rate decreased to 360 ± 60 μmol O_2 (mg Chl-h)$^{-1}$ (assayed with 155 mM chloride). Thus, CD-PSII samples exhibit little residual oxygen evolution; this decrease in activity is expected when calcium is depleted.[2-5] Previously, it was reported that CD-PSII exhibits no significant oxygen evolution when assayed in the presence of EGTA, which binds adventitious calcium.[28, 30] In the CD-PSII samples employed here, the rate of oxygen evolution in the presence of 10 mM EGTA was 270 ± 10 μmol O_2 (mg Chl-h)$^{-1}$ (assayed with 155 mM chloride). Given the standard deviation, there was little significant difference between the oxygen evolution activity of CD-PSII when assayed either in the presence (360 ± 60 μmol O_2 (mg Chl-h)$^{-1}$ or absence (270 ± 10 μmol O_2 (mg Chl-h)$^{-1}$) of EGTA. This observation agrees with our previous reports[28, 30] and indicates that pH 7.5 EGTA treatment is effective in removing calcium in the preparations employed here. These results are also consistent with previous results obtained using another calcium depletion method, which employed a high salt concentration to remove calcium.[31]

Reconstitution of calcium, generating Ca-PSII, restored oxygen evolution and gave a rate of 890 ± 70 μmol O_2 (mg Chl-h)$^{-1}$ at pH 7.5, when assayed with 20 mM calcium and 155 mM chloride. As expected, this is 79% of the control PSII rate measured at pH 7.5 under the same conditions.[31] We conclude that EGTA treatment at pH 7.5 depletes calcium from the majority of PSII centers and that the reconstitution method repletes calcium in the majority of PSII centers.

To prepare Ca-PSII and CD-PSII samples for the reaction-induced FT-IR (RIFT-IR) experiments, a CD sample was pelleted by centrifugation (50,000 x *g*, 10 minutes, 4°C) after thawing. Resuspension of the pellet was performed in a buffer containing 0.4 M sucrose, 50 mM HEPES-NaOH, pH 7.5 and 15 mM NaCl prepared in $H_2{}^{16}O$ (first EGTA-free wash). The sample was centrifuged again (50,000 x *g*, 15 minutes, 4°C), and the pellet was resuspended in 0.4 M sucrose, 50 mM HEPES-NaOH, pH 7.5 and 15 mM NaCl, prepared either in $H_2{}^{16}O$, $D_2{}^{16}O$, or $H_2{}^{18}O$. In the case of $H_2{}^{16}O$, calcium and chloride were added from buffered stock solutions to give Ca-PSII. For CD-PSII in $H_2{}^{16}O$, chloride alone was added from a 3 M buffered NaCl stock. In the case of $D_2{}^{16}O$ and $H_2{}^{18}O$, the $D_2{}^{16}O$ or $H_2{}^{18}O$ resuspension buffer already contained the appropriate amount of calcium and chloride to produce Ca-PSII or CD-PSII (second EGTA-free wash). For Ca-PSII, the calcium concentration was 20 mM, and the chloride concentration was 155 mM. For CD-PSII, no calcium was added, and the chloride concentration was 155 mM. Before the final centrifugation (50,000 x *g*, 15 minutes, 4°C), 7 mM $K_3[Fe(CN)_6]$ was added to the sample from a freshly prepared 800 mM stock either in $H_2{}^{16}O$ or $D_2{}^{16}O$. After the addition of 7 mM ferricyanide, samples were centrifuged (50,000 x g, 10 min, 4°C) to form a pellet.

Samples for 283 K experiments were prepared by washing OTG-PSII samples twice with buffer containing 0.4 M sucrose, 50 mM 2-[4-(2-hydroxyethyl)piperazin-1-yl]ethanesulfonic acid (HEPES)-NaOH, pH 7.5, and 15 mM NaCl. The oxygen evolution rate was >1200 μmol O_2 (mg Chl-h)$^{-1}$ at pH 7.5. FTIR data were collected in the presence of 20 mM calcium and 155 mM chloride. 7 mM freshly prepared potassium ferricyanide was added to each FTIR sample. Five loops of data collection was carried out for each

sample at 283 K with a wait time of 15 minutes in between loops. All other experimental paramenters were the same as the methods employed for the Ca-PSII and CD-PSII samples.

Literature protocols were used to perform RIFT-IR spectroscopy[24, 28, 32] at pL 7.5 and 263 K. In some cases, RIFT-IR experiments were also performed at 283 K. Briefly, the pelleted sample was spread on a CaF_2 window (25 x 2 mm) and concentrated under nitrogen gas. The sample was never completely dehydrated. The concentration time was adjusted to maintain an absorbance ratio of the O-H stretch (3,370 cm^{-1}) to amide II (1,550 cm^{-1}) of 2.8-3.8. The sample was covered with a second CaF_2 window. The edge of the windows was sealed with high vacuum grease to prevent sample dehydration. A parafilm wedge was used as a spacer between the windows to maintain a constant path length and to prevent interference fringes.

RIFT-IR spectroscopy was performed on a Bruker IFS 66v/S instrument with the following acquisition parameters:[3,4] 8 cm^{-1} spectral resolution; Happ-Genzel apodization function; 60 kHz mirror speed; four levels of zero filling; and Mertz phase correction. Samples were dark adapted for 20 minutes following a single saturated preflash from a 532 nm laser (at 40 mJ/cm^2 power density). A germanium window was used to block illumination of the sample by the spectrometer's internal HeNe laser. Following dark adaptation, samples were subjected to a series of five actinic flashes. Each was preceded and followed by 15 seconds of rapid scan data collection (first loop of data collection). When data was acquired at 263 K, the sample was annealed between flash cycles. After the first loop at 263 K, the temperature was raised to 283 K, and the sample annealed for 10 minutes. Subsequent to this, the entire experiment (including the dark adaptation) was repeated again at 263 K (second loop of data collection). From each RIFT-IR sample,

three-five loops of data were collected at 263 K, with 10 minutes of annealing at 283 K in between the loops. The single channel data collected before and after each laser flash were ratioed to obtain the difference spectra. The difference spectra was normalized to an Amide II intensity of 0.5 to account for differences in sample thickness and path length. The absorbance spectra for each sample was collected at the beginning of data collection loop (before the preflash) against an open beam background. The intensity of the amide II band was determined from these absorption spectra. Blank windows with a parafilm wedge were used to record background "difference" spectra, using the subtraction and laser flash protocol described above. This background spectrum was subtracted from the RIFT-IR data in order to provide a flat baseline (Figure 2.2). The difference spectra obtained after background correction were normalized to the intensity of the CN bands of ferricyanide/ferrocyanide in the $H_2{}^{16}O$ control spectrum, which was recorded with the same number of flashes. To correct a small offset in the mid-IR region of the $D_2{}^{16}O$ data (Figure 2.3), a straight-line baseline correction was applied to the $D_2{}^{16}O$ spectra in Figure 2.3, A-E. The data presented in some of the figures were smoothed using a 17 point Savitzky–Golay algorithm in Bruker OPUS software (see figure legends). The averaged, baseline-corrected, and normalized spectra were fit and plotted using IGOR (Wavemetrics, Lake Oswego, OR) software**.**

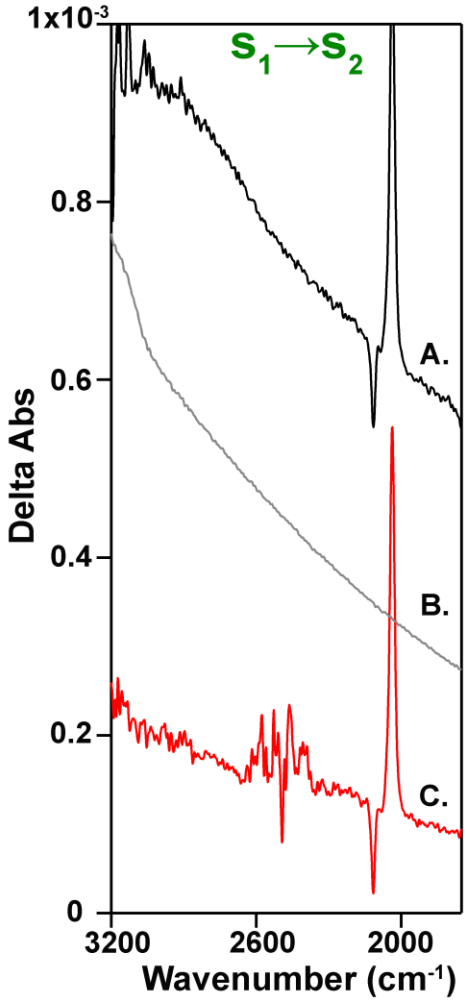

Figure 2.2 Examples of uncorrected RIFT-IR spectra at 263 K. (A) Ca-PSII in $H_2{}^{16}O$ buffer, pL 7.5 during the S_1 to S_2 transition. (B) Laser flash-induced background recorded using only CaF_2 windows. (C) Ca-PSII in $D_2{}^{16}O$ buffer, pL 7.5 during the S_1 to S_2 transition. Spectra are average 3-5 loops of (A) 12 and (C) 3 different samples. The background in (B) represents an average of 90 data sets and were collected using the same laser flash method as employed for the PSII spectra.

To summarize the information above, RIFT-IR spectra of the entire S-state cycle were obtained by ratioing a 15 sec single channel spectra recorded before and after a 532 nm laser flash. RIFT-IR spectra acquired in this fashion from PSII have been reported to exhibit period four oscillation associated with oxygen evolution.[32-33] Most of the experiments were carried out in pL 7.5 buffers at 263 K using 0.4 M sucrose as

cryoprotectant. These are optimal conditions for observing the 3,000-2,000 cm^{-1} spectral band of the S_1 to S_2 transition.[24] There is no expected Y_Z contribution to these spectra, due to the time scale of the measurements and the integrity of the preparations, which are highly active in oxygen evolution. Ref 24 reported that annealing was required to regenerate the broad spectral features at ~2,800 cm^{-1} in a second cycle of flashes at 263 K. Therefore, in this current study, each sample was subjected to three-five reaction cycles at 263 K with 10 minutes of 283 K annealing time between successive 263 K loops. There was no difference between the loops, which was significant relative to the signal-to-noise ratio. Due to the timescale used, these spectra reflect long-lived conformational changes in the OEC.[34-35]

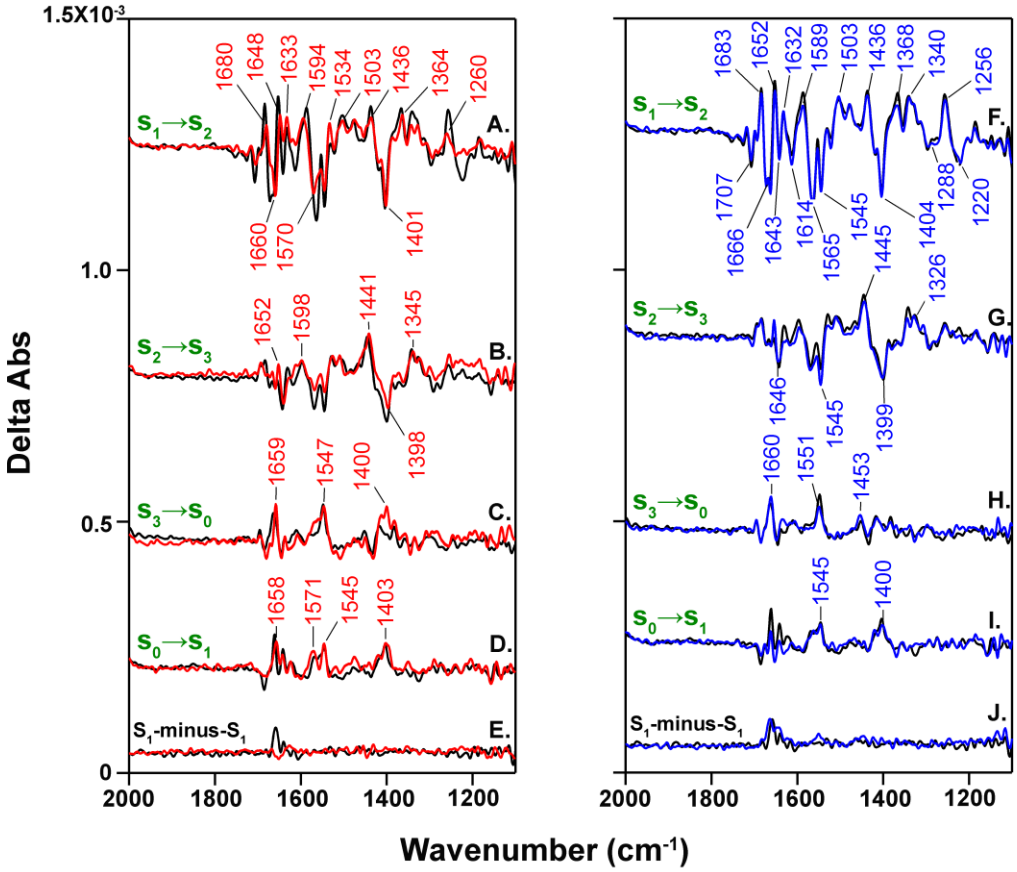

Figure 2.3 RIFT-IR spectra (2,000-1,100 cm^{-1} region) of Ca-PSII in $H_2{}^{16}O$ (black), $D_2{}^{16}O$ (red), and $H_2{}^{18}O$ (blue) buffer, associated with the entire S-state cycle at pL 7.5 and 263 K. In (A, F) S_2-minus-S_1 spectrum, (B, G) S_3-minus-S_2 spectrum, (C, H) S_0-minus-S_3 spectrum, and (D, I) S_1-minus-S_0 spectrum. In (E, J), Data obtained from S_1-minus-S_1 spectra of respective samples. Red labels, $D_2{}^{16}O$ (red); blue labels, $H_2{}^{18}O$ (blue). Each spectrum is an average of 3-5 loops obtained on 12 (A-J, black), 3 (A-E, red) and 11 (F-J, blue) different samples.

2.4 Results

Figure 2.4 presents the 3,200-1,750 cm^{-1} region of the RIFT-IR spectra, derived from oxygen-evolving PSII at 263 K. The sample was flashed to advance from the dark-adapted S_1 state, sequentially generating the S_2, S_3, S_0, and S_1 states (Figure 2.1b). Difference spectra were constructed for each S state transition, corresponding to the S_1 to S_2, S_2 to S_3, S_3 to S_0, and S_0 to S_1 transitions (Figure 2.4, A-D). To obtain this oxygen-

evolving PSII sample, EGTA was used to generate CD-PSII at pH 7.5, and calcium was then reconstituted to generate Ca-PSII. This Ca-PSII sample is active in steady state oxygen evolution and can complete the S state cycle. Calcium depletion decreases steady state oxygen evolution rate, as described in Methods. While the CD-PSII preparation is inhibited in steady-state oxygen evolution, this sample can form an S_2-like state[28, 36] on the first flash. We employ the CD-PSII sample as a control, in which the internal water network of PSII is disrupted.[8-10]

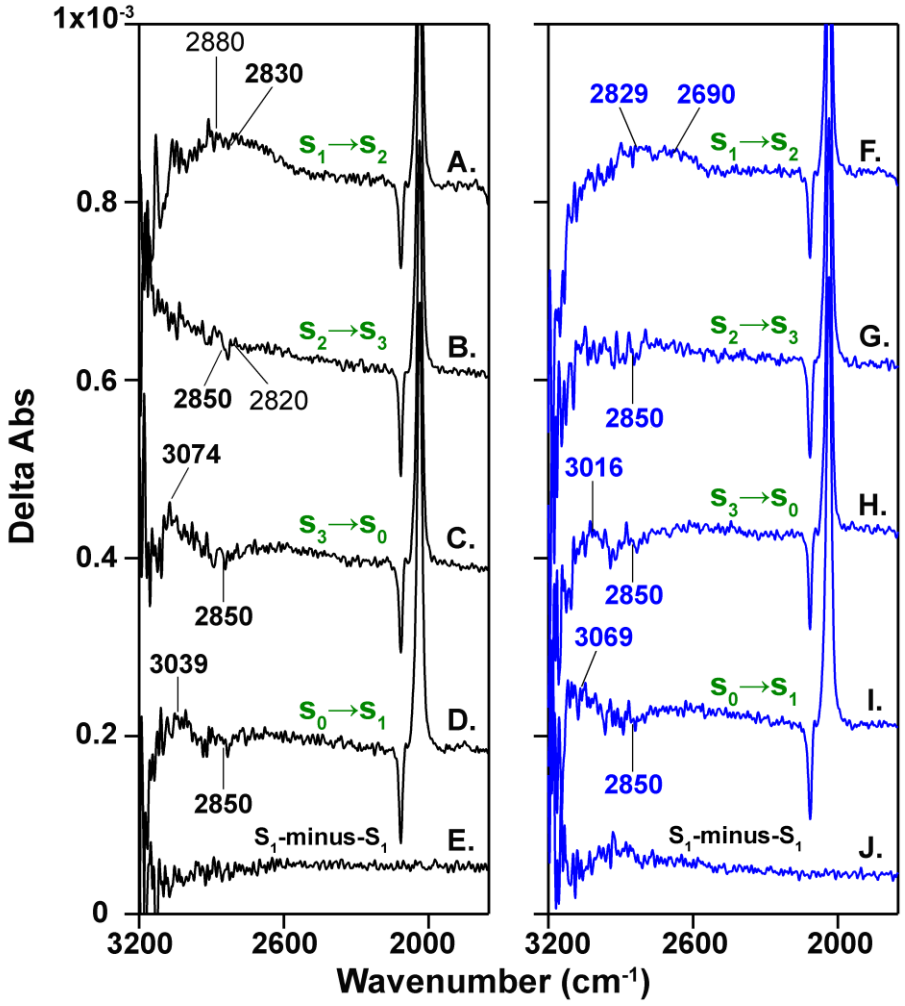

Figure 2.4 RIFT-IR spectra (3,200-1,750 cm^{-1} region) of Ca-PSII samples; spectra are associated with the entire S-state cycle at pL 7.5 and 263 K. Measurements were performed either in $H_2{}^{16}O$ buffer (A-E, black) or in $H_2{}^{18}O$ buffer (F-J, blue). (A, F)

S_2-minus-S_1 spectrum; (B, G) S_3-minus-S_2 spectrum; (C, H) S_0-minus-S_3 spectrum; and (D, I) S_1-minus-S_0 spectrum. (E, J) Data obtained from the S_1-minus-S_1 spectra of Ca-PSII samples. Each spectrum is an average of 3-5 data acquisition loops acquired from (A-E) 12 and (F-J) 11 different samples.

In Ca-PSII (Figure 2.4, A-D), 2,115/2,035 cm^{-1} CN stretching bands are observed on each flash and are therefore associated with each accessible S state transition. These bands originate from the reduction of potassium ferricyanide, which is used as the external electron acceptor. The intensity of the ferricyanide/ferrocyanide bands is consistent with S state advancement. Previous work using a variety of techniques has shown that this laser flash procedure is efficacious in S state advancement.[37-39] An overlay of Ca-PSII spectra with CD-PSII data is presented in Figure 2.5. In contrast to our earlier work,[24] these spectra were baseline-corrected (Figure 2.2), in order to enhance detection of isotope-induced shifts on a flat baseline. Figure 2.5, A-D shows that calcium depletion alters the intensity of bands in this 3,200-1,750 cm^{-1} spectral region on each transition.

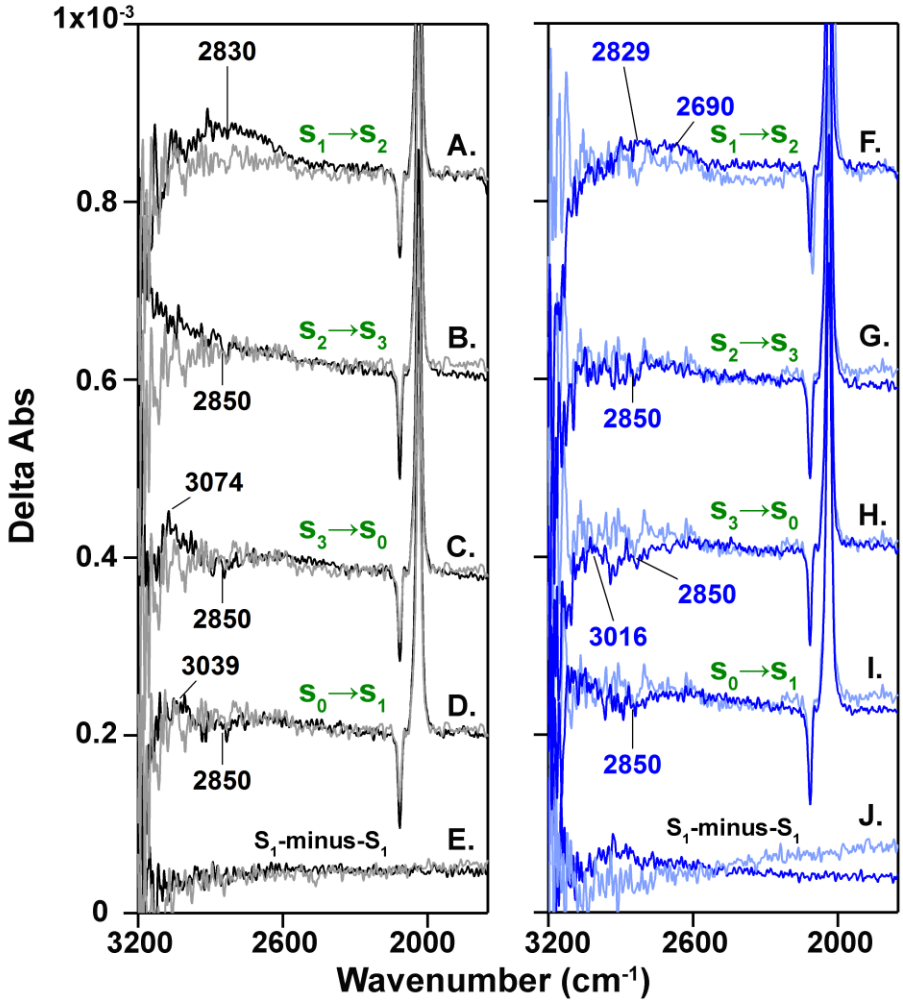

Figure 2.5 RIFT-IR spectra of Ca-PSII (black or dark blue) and CD-PSII (gray or light blue) at 263 K and pL 7.5. Measurements were performed either in (A-E) $H_2{}^{16}O$ buffer or (F-J) $H_2{}^{18}O$ buffer. CD-PSII generates an inhibited form of the S_2-minus-S_1 spectrum on the first flash. (A, F) Ca-PSII S_2-minus-S_1 (black, dark blue) and CD-PSII (gray, light blue). (B, G) Ca-PSII S_3-minus-S_2 (black, dark blue) and CD-PSII (gray, light blue). (C, H) Ca-PSII S_0-minus-S_3 (black, dark blue) and CD-PSII (gray, light blue). (D, I) Ca-PSII S_1-minus-S_0 (black, dark blue) and CD-PSII (gray, light blue). (E, J) Data obtained from the S_1-minus-S_1 spectra of respective samples. Each spectrum is an average of 3-5 loops obtained on (A-E, black) 12, (A-E, gray) 6, (F-J, dark blue) 11 and (F-J, light blue) 5 different samples. A 17 point smoothing Savitzky–Golay algorithm was employed.

To discuss selected spectral features in more detail, Figure 2.6 presents expanded 263 K spectra derived from the first and third flash. In Figure 2.6A, a positive infrared band is observed for the 263 K S_1 to S_2 transition, as reported previously under the same

conditions.[24] With our current method of baseline subtraction and subsequent curve fitting (Figure 2.6A), the center of the band is now estimated as 2830 cm^{-1}. As reported in ref 24, negative bands are also observed in spectra associated with each transition. In the current baseline-corrected spectra, the centers of the negative bands are estimated as 2,850 cm^{-1} (Figure 2.4, B-D). At 190 K, where only the S_1 to S_2 transition occurs, a similar infrared band was sensitive to the concentration of NaCl and was reported at 2740 cm^{-1} (pH 7.5).[25]

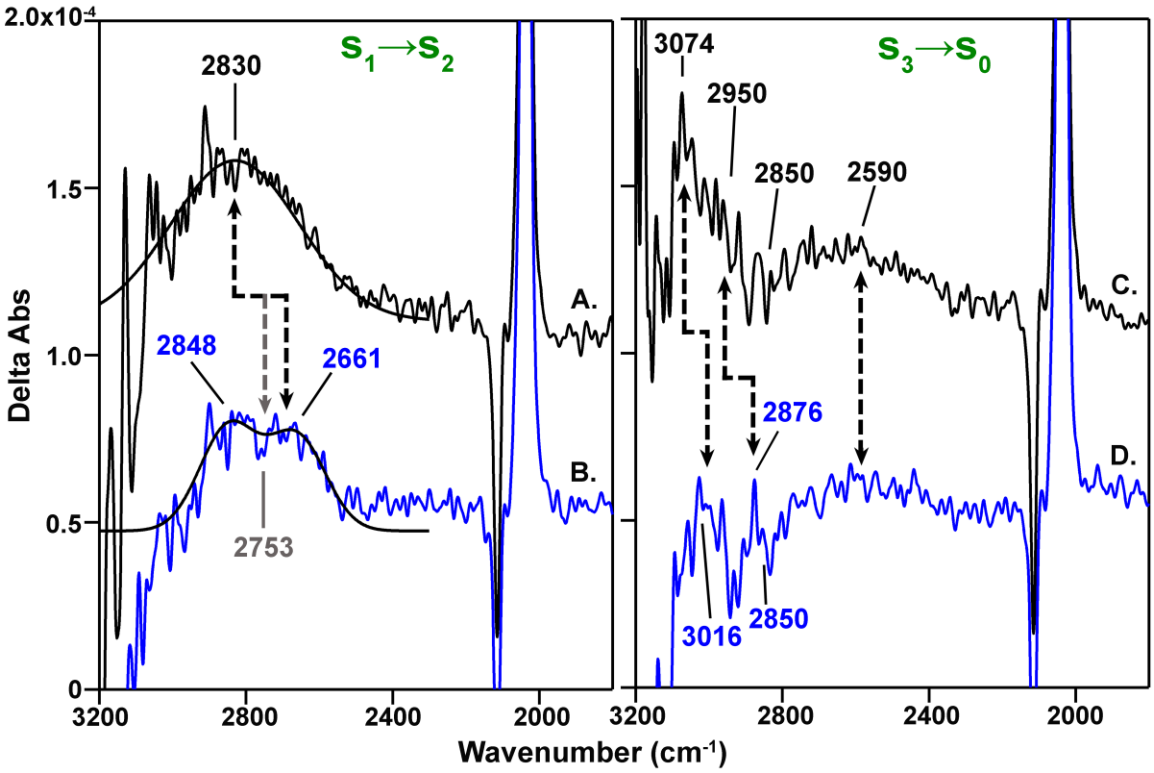

Figure 2.6 Expanded RIFT-IR spectra (3,200-1,800 cm^{-1} region), reproduced from Fig, 2A, C, F and H, associated with the S_1 to S_2 transition (A, B) and the S_3 to S_0 transition (C, D) either in $H_2{}^{16}O$ buffer (A, C, black) or $H_2{}^{18}O$ buffer (B, D, blue). Gaussian fits to the data are shown superimposed in (A and B). The black arrows in A and B illustrate the ^{18}O isotope shift, assuming that the exchanged peak has two components. The gray arrow in A and B illustrates the ^{18}O isotope shift, assuming that the exchanged peak has one component. The data were smoothed using a 17 point Savitzky–Golay algorithm.

Notably, Figure 2.4C exhibits a positive band at 3074 cm^{-1}, which is associated with the S_3 to S_0 transition. This positive S_0 band has not been reported previously. Expanded comparisons of the S_1 to S_2 (A,B) and S_3 to S_0 spectra (C,D) in Ca-PSII (A, C) and CD-PSII (B, D) samples are presented in Figure 2.7. Positive bands at 2830 and 3074 cm^{-1} are significantly more intense in Ca-PSII samples, compared to CD-PSII samples. This loss of intensity when calcium is depleted is attributed to the disruption of the OEC hydrogen bond network.

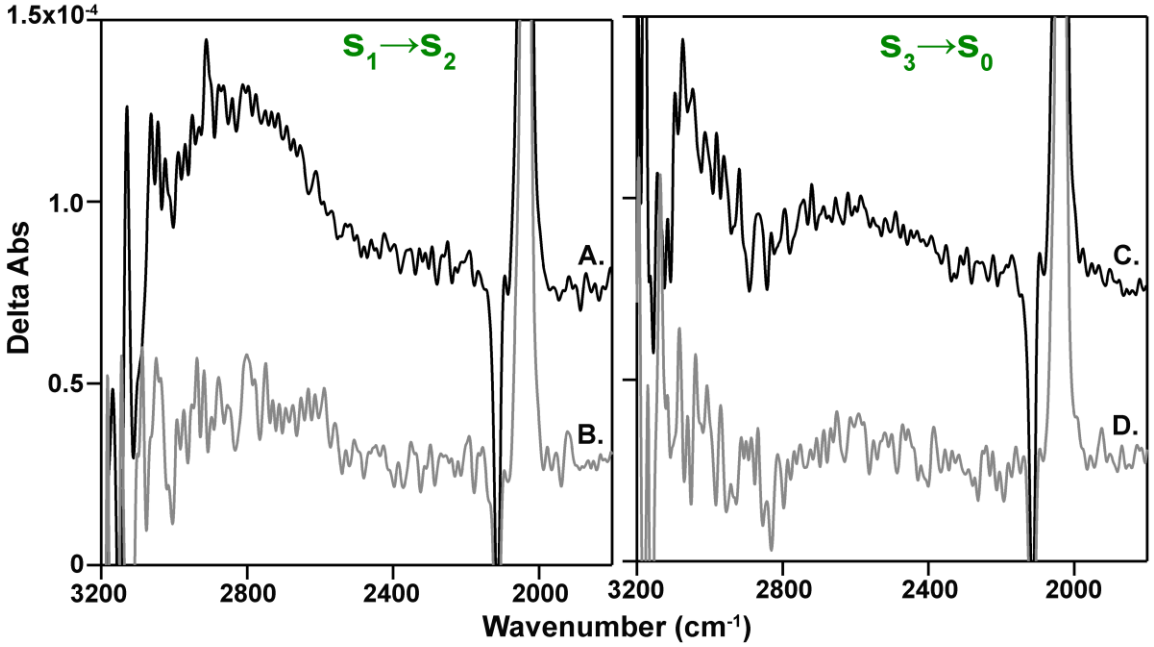

Figure 2.7 Expanded RIFT-IR spectra of Ca-PSII (black) and CD-PSII (gray) at 263 K and pL 7.5. Measurements were performed in $H_2{}^{16}O$ buffer. (A, B) Ca-PSII S_2-minus-S_1 (black) and CD-PSII (gray). (C, D) Ca-PSII S_3-minus-S_2 (black) and CD-PSII (gray). In B, CD-PSII was given one flash. CD-PSII is inactive in oxygen evolution but can form a modified S_2 state. In D, CD-PSII was given three flashes. CD-PSII is inactive in oxygen evolution and cannot reach the S_0 state.

Figure 2.8 shows the effect of exchanging Ca-PSII samples into $D_2{}^{16}O$ buffer (pD 7.5) as a function of flash number (Figure 2.8, A-D). Compared to our previous report,[24] information concerning the entire S-state cycle has now been obtained. Exchange into

$D_2{}^{16}O$ results in a decrease of intensity of all bands between 3,000-2,800 cm^{-1} on each transition (Figure 2.8, A-D), due to a shift of these bands into the solvent $D_2{}^{16}O$ region. Note that Figure 2.8 omits the 2,600-2,200 cm^{-1} region, corresponding the solvent O-D stretching band, and that baseline correction gives rise to the sloping background (see Figure 2.2, for an example of the uncorrected data). This $D_2{}^{16}O$ exchange experiment assigns these bands to normal modes, which involve displacement of exchangeable protons.

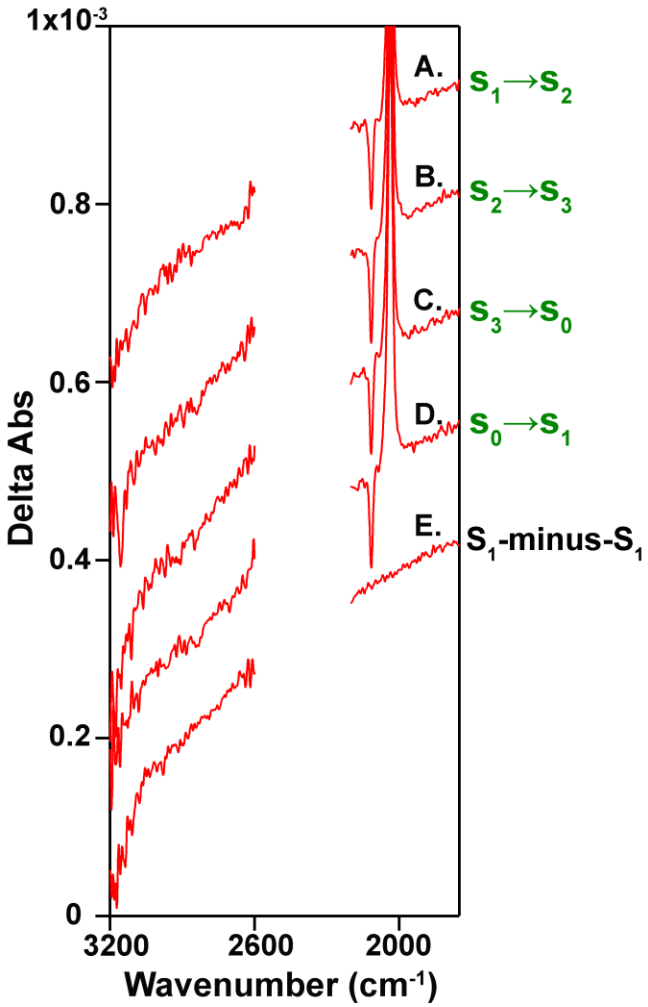

Figure 2.8 RIFT-IR spectra (3,200-1,750 cm^{-1} region) of Ca-PSII samples associated with the entire S-state cycle at pL 7.5 and 263 K. Measurements were performed in $D_2{}^{16}O$ buffer at pD 7.5. The O-D stretching region is off scale and was omitted for

clarity. (A) S_2-minus-S_1 spectrum; (B) S_3-minus-S_2 spectrum; (C) S_0-minus-S_3 spectrum and (D) S_1-minus-S_0 spectrum. (E) Data obtained from the S_1-minus-S_1 spectrum. Each spectrum is an average of 3-5 loops obtained on 3 different samples.

To test the hypothesis that vibrational modes of water are detected, samples were exchanged into $H_2{}^{18}O$ buffer (pH 7.5). Figure 2.4 presents a comparison of the 3,200-1,750 cm^{-1} regions, derived from Ca-PSII samples in $H_2{}^{16}O$ (Figure 2.4A-D, black) and $H_2{}^{18}O$ (Figure 2.4F-I, blue) as a function of flash number at 263 K. Figure 2.5, F-I shows that bands arising from $H_2{}^{18}O$ exchanged Ca-PSII (black) are decreased in intensity by removal of calcium (gray). In addition, Figure 2.4 demonstrates that ^{18}O isotope-sensitive bands are observed on each transition (also see expanded spectra in Figure 2.7). For example, after $H_2{}^{18}O$ exchange, the 3,100-2,800 cm^{-1} region of the S_2-minus-S_1 spectrum exhibits a broadened positive band, which can be modeled as two separate Gaussian peaks, centered at 2,848 and 2,661 cm^{-1} (Figure 2.6B). The former may arise from unexchanged PSII, with the latter band assigned to ^{18}O-exchanged PSII. The 2,661 cm^{-1} band corresponds to a 170 cm^{-1} downshift (black arrows), relative to the band observed in $H_2{}^{16}O$. This observation is consistent with the 140 cm^{-1} $H_2{}^{18}O$-induced downshift, which was reported for the analogous infrared band in the trapped cryogenic S_2 state (190 K, pH 6.0).[25] On the other hand, fitting the $H_2{}^{18}O$ data in Figure 2.6B as a single band predicts a frequency of 2,753 cm^{-1}. This analysis is consistent with a 77 cm^{-1} downshift (gray arrow) of the S_2 band as a result of $H_2{}^{18}O$ exchange.

Interestingly, the spectra associated with the S_3 to S_0 transition also exhibit ^{18}O-induced shifts for positive S_0 bands at 263 K. The positive 3,074 cm^{-1} band (Figure 2.6C) shifts to 3,016 cm^{-1} with $H_2{}^{18}O$ exchange (Figure 2.6D), assigning this band to a water normal mode. In addition, isotope exchange reveals a positive shoulder at ~2,950 cm^{-1},

which shifts to ~2,876 cm^{-1} (Figure 2.6C and D, black arrows). In the expanded view (Figure 2.6D) a broad positive band, centered at 2,590 cm^{-1} is also evident. This band does not exhibit a large ^{18}O-exchange induced shift. The $D_2{}^{16}O$ sensitivity of the band cannot be assessed due to overlap with the bulk solvent absorption. However, the band intensity may be sensitive to calcium-depletion (see Figure 2.7, C and D).

The effect of solvent isotope exchange on the mid-infrared region is also of interest. In this mid-infrared spectral region, vibrational bands from the peptide backbone and amino acid side chains are observed.[40-41] Figure 2.3 presents the 2,000-1,100 cm^{-1} regions of the Ca-PSII spectra in $H_2{}^{16}O$ (black), $D_2{}^{16}O$ (red), $H_2{}^{18}O$ (blue), as a function of flash number. $H_2{}^{18}O$ exchange has a small impact on the mid-infrared S state spectra, as evident in Figure 2.3, F-I. $D_2{}^{16}O$ exchange has a more pronounced effect on spectra acquired on the first flash (Figure 2.3, A-D). However, the spectra associated with the later S-state transitions are similar in $H_2{}^{16}O$ and $D_2{}^{16}O$ buffers. This is especially apparent in Figure 2.9, in which the double difference spectra, corresponding to $H_2{}^{16}O$-minus-$D_2{}^{16}O$, are presented (Figure 2.9).

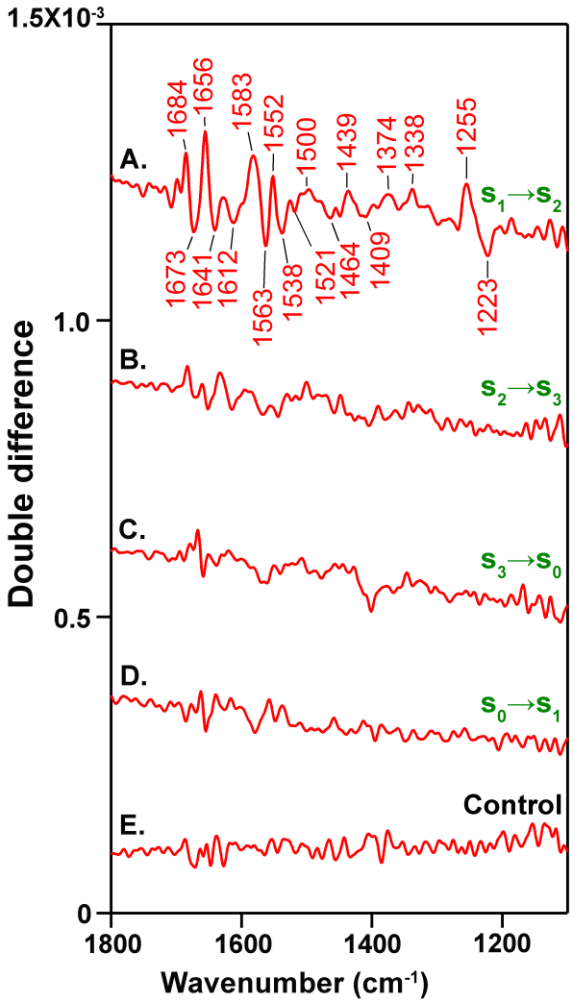

Figure 2.9 $H_2{}^{16}O$-minus-$D_2{}^{16}O$ double difference spectra (1,800-1,100 cm^{-1} region) derived from Ca-PSII. The spectra were recorded at 263 K and pL 7.5. In (A) S_1 to S_2 transition, (B) S_2 to S_3 transition, (C) S_3 to S_0 transition, and (D) S_0 to S_1 transition. In (E), a control double difference generated by subtracting one half of a data set from the other half with no additional correction factors.

The spectra discussed above were recorded at 263 K. RIFT-IR spectra of PSII were also recorded at 283 K. Figure 2.10 and Figure 2.11 present a comparison of spectra acquired at 263 K (A) and 283 K (B). For the S_1 to S_2 transition (Figure 2.10), the 283 K spectrum exhibited additional structure on the 2830 cm^{-1} band, but no significant change in center frequency. For the S_3 to S_0 transition (Figure 2.11), the 283 K spectrum exhibited less resolution near 3100 cm^{-1}, due to increased breadth of the solvent water peak.

However, the 3074 cm^{-1} peak was still observable as a shoulder in the 283 K S_3 to S_0 spectrum.

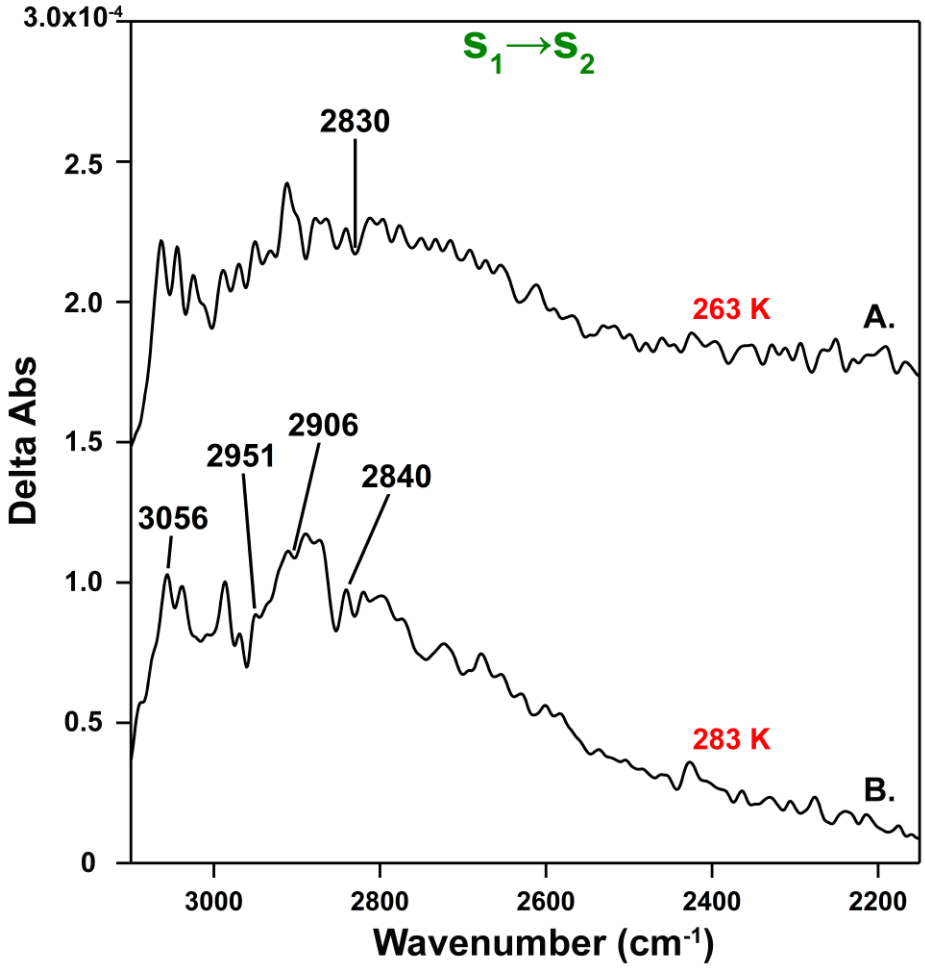

Figure 2.10 RIFT-IR spectrum (3,200-2,150 cm^{-1} region) of PSII-samples, associated with the S_1 to S_2 transition and acquired in $H_2{}^{16}O$ buffer, pL 7.5 at either (A) 263 K or (B) 283 K. Data in (A) reproduced from Fig. 2. The data were smoothed using a 17 point Savitzky–Golay algorithm. Each spectrum is an average of 3-5 data acquisition loops acquired from 12 different samples.

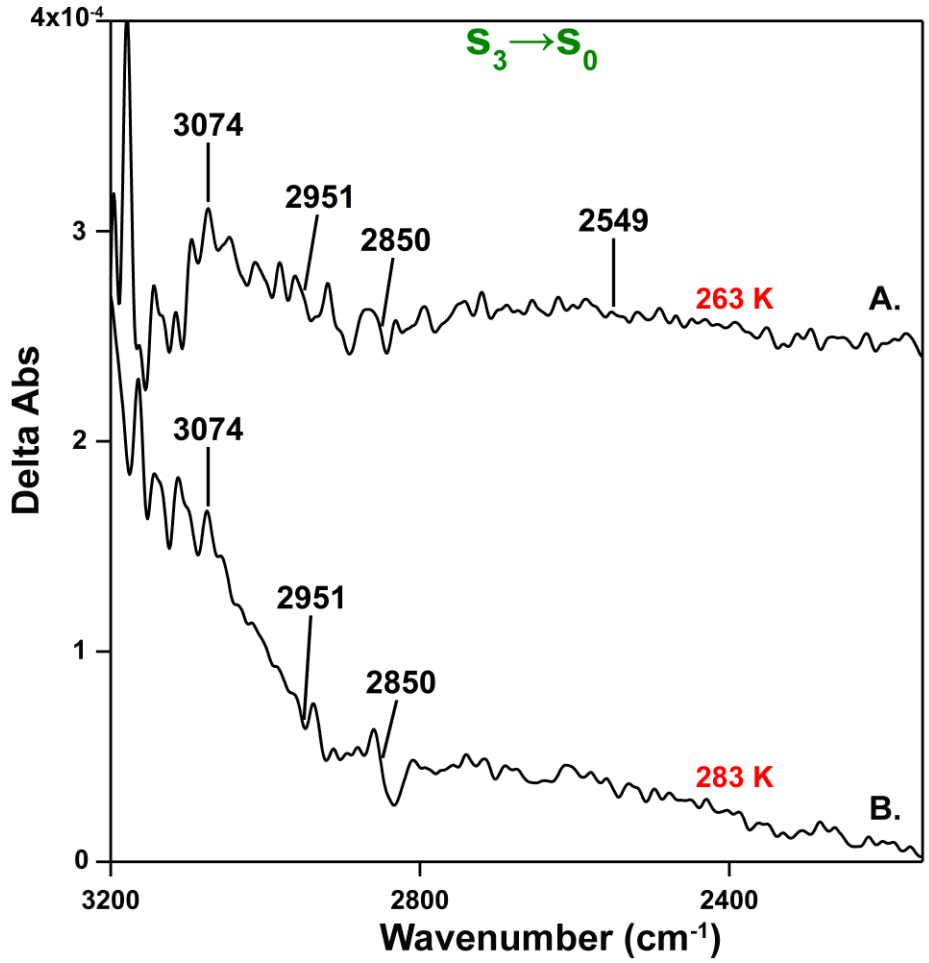

Figure 2.11 RIFT-IR spectrum (3,200-2,150 cm^{-1} region) of PSII-samples, associated with the S_3 to S_0 transition and acquired in $H_2{}^{16}O$ buffer, pL 7.5 at either (A) 263 K or (B) 283 K. Data in (A) reproduced from Fig. 2. The data were smoothed using a 17 point Savitzky–Golay algorithm. Each spectrum is an average of 3-5 data acquisition loops acquired from 12 different samples.

2.5 Discussion

We have used solvent isotope exchange and RIFT-IR spectroscopy to obtain new information concerning the mechanism of proton-coupled electron transfer in photosynthetic oxygen evolution. The S_3 to S_0 transition is the step in the S-state cycle,

during which oxygen is produced from the metatable S_4 state.[12] When the cycle resets to the S_0 state, at least one water molecule is known to bind in the OEC.[42] Thus, our observation of a unique positive band at 3,074 cm^{-1}, associated with this transition and attributable to the S_0 state, is significant. Calcium binds OEC water molecules,[8-9] and depletion of calcium is expected to disrupt the functional water network.[28] Therefore, the calcium sensitivity of the 3,074 cm^{-1} band supports its assignment to the internal hydrogen bonding network. The intensity of this band is sensitive to D_2O exchange, indicating that the normal mode involves displacement of a solvent-accessible, exchangeable proton. $H_2{}^{18}O$ exchange unambiguously assigns this band to a vibrational displacment of water; a 58 cm^{-1} downshift is observed. $H_2{}^{18}O$ exchange also identifies an overlapping positive S_0 band at approximately 2,950 cm^{-1}, which is associated with this transition.

Interestingly, the observed 3,074/2,950 cm^{-1} frequencies of the S_0 water bands are significantly downshifted compared to the O-H stretching mode expected for solvent water. Based on the literature, several possible explanations for the downshifted frequency are considered. First, downhifted water bands could arise from an OH stretching mode of strongly hydrogen-bonded water.[1, 43-44] However, formation of a water dimer in solid nitrogen matrix results in only a 100 cm^{-1} red shift, with absorption remaining in the 3,700-3,500 cm^{-1} region. In addition, only small $H_2{}^{18}O$ isotope shifts are expected in this case (<10 cm^{-1}).[45] In contrast, the 3,074 cm^{-1} band reported here is shifted >400 cm^{-1} from the absorption of liquid water and exhibits a much larger ^{18}O exchange-induced shift. Second, 3,074/2,950 cm^{-1} bands could correspond to a proton polarizability band, in which the positive charge is delocalized over a network of water molecules.[46-47] During the photocycle of bacteriorhodopsin, proton polarizability bands absorb at 3,000-2,700 cm^{-1}

and 1,500- 2,000 cm^{-1}.[46, 48] However, a proton polarizability band is not expected to exhibit a large $H_2{}^{18}O$ shift.[49] A third possibiltty is assignment to a small, protonated water cluster.[50-51] For example, in the gas phase, clusters of 5 to 8 water molecules were observed with hydronium stretching modes between 2,800 and 3,200 cm^{-1}.

We favor the assignment of the 3,074 cm^{-1} band to the stretching vibration of a protonated water cluster, due to the frequency, intensity, and the large (~58 cm^{-1}) ^{18}O exchange-induced shift. In this context, one explanation for the large isotope-associated shift is a change in the size of the internal water cluster changes in $H_2{}^{18}O$. Such a change could be due to its small change in viscosity relative to $H_2{}^{16}O$.[52] Previous work has shown that a change in gas water cluster size from 6 to 5 alters the frequency of the hydronium stretching band from 3,160 to 2,860 cm^{-1}.[50] The observation of an overlapping contribution at 2,950 cm^{-1} in the S_0-minus-S_3 spectrum may indicate that the size of the protonated water cluster is heterogeneous.

Assignment of these bands to a hydronium ion is consistent with the net transfer of a proton to internal water on the S_3 to S_0 transition. This proton may originate from a water or hydroxide ligand to the Mn_4CaO_5 cluster, which deprotonates with S state advancement. Alternatively, the proton may represent a Bohr proton, which is transferred to water as the result of electrostatic changes and pK_a shifts in amino acid residues at the catalytic site.

During the S_1 to S_2 transition, a positive 2830 cm^{-1} band, which is ^{18}O-isotope sensitive, is observed. Based on the large ^{18}O-induced shift, this positive band can also be assigned unambiguously to an exchangeable proton of water. The large ^{18}O-isotope shift is attributed to a change in cluster size, as discussed above. The observation of this band

is consistent with the hypothesis that protons are trapped on internal water on this transition. Temperature or preparation dependence may be observed, with substructure development at 283 K. In our reported work, we attributed this positive band to formation of a protonated water cluster, based on its intensity, frequency, and the effects of ammonia, calcium depletion, $D_2{}^{16}O$ exchange, and strontium substitution.[24, 30] A similar band has been observed in the bacterial reaction center.[53] Also, in bacteriorhodopsin, a band in the 3,000-2,000 cm^{-1} region was observed and assigned to the combined O-H stretching of a transiently formed, three water wire.[3] Note that, under our conditions, the S_2-minus-S_1 spectra provide no evidence for proton continua bands at 2,000 cm^{-1} region, which could be associated with the 2,830 cm^{-1} band. However, on the S_3 to S_0 transition, a proton continuum band may be observed at 2,590 cm^{-1}.

The 3,200-2,200 cm^{-1} region of the FT-IR spectrum has been described in previous PSII studies.[24,25,30,54-56] Table 1 provides a summary. In most reports (but see discussion of ref 54 below), a broad positive band has been assigned to the S_2 state. The first reports were presented in ref 24 and ref 30 with the detection of a 2,880 cm^{-1} band in oxygen-evolving plant PSII and with assignment of that band to a protonated water cluster in the S_2 state (Table 1). Our S_2 data reproduce those reported spectra, although with improved baselines.

Table 1 Summary of assignments in the 3200-1800 cm^{-1} region of the S_2-minus-S_1 RIFT-IR spectrum

Reference	PSII preparation	Temperature	pH	Position	^{18}O-shift	Assignment
Noguchi[54], 2002	*S. elongatus*	283 K	pH 6.0	3000 cm^{-1}	N.D.[a]	Proton polarizability band, S_2 State
Barry[24], 2013	Spinach[b,c,d]	263 and 283 K	pH 7.5	2880 cm^{-1}	N.D.	Protonated water cluster, S_2 state
Barry[30], 2013	Spinach[b,c]	263 K	pH 7.5	2880 cm^{-1}	N.D.	Protonated water cluster, S_2 state
Noguchi[55], 2014	*T. elongatus*, Tris-washed (inactive in oxygen evolution)	250 K	pH 6.5	Broad positive feature around 2800 cm^{-1}	N.D.	Protonated histidine in a putative $Y_Z^{\bullet}$-minus-Y_Z spectrum, but see ref;[5] proton polarizability band
	T. elongatus		N.S.[e]	Around 3000 cm^{-1}	No	S_2 state
	Spinach		N.S.	Around 3000 cm^{-1}	N.D.	S_2 state
Debus[56], 2014	*Synechocystis* sp. PCC 6803	273 K	pH 6.0	Centered at 3000 cm^{-1}	No	Proton polarizability band, S_2 state

Table 1 continued

Noguchi[57], 2016	Spinach	283 K	pH 6.0	Broad positive feature at 3200−2500 cm^{-1}	N.D.	OH bond of hydrogen bonded water, S_2 state
Barry[25], 2016a	Spinach[b,c,d]	190 K	pH 6.0 and 7.5	2900/2740 cm^{-1}, NaCl sensitive	Yes	Protonated water cluster, S_2 state
Barry[58], 2016b	Spinach[b,c]	263 and 283 K	pH 7.5	2830 cm^{-1} (at 263 and 283K)	Yes	Protonated water cluster, S_2 state
Noguchi[59], 2017	Spinach	283 K	pH 6.0	Around 2900 cm^{-1} (positive) and 2700 cm^{-1} (negative)	N.D.	Protonated histidine, S_2 state
Barry[60], 2017	Spinach[b]	283 K	pH 7.5	2830 cm^{-1}	Yes	Protonated water cluster, S_2 state
Barry[61], 2018	Spinach[b]	283 K	pH 7.5	2830 cm^{-1}	Yes	Protonated water cluster, S_2 state

[a] Not determined
[b] Oxygen-evolving PSII
[c] Calcium-depleted PSII
[d] Ammonia-treated PSII
[e] Not specified

In ref [55], the 3,200-2,200 cm^{-1} region was reported in cyanobacterial and spinach PSII (Table 1). A broad, light-induced 2,800 cm^{-1} band was assigned to a putative Y_Z

radical spectrum (but see ref 57 for alternate Y_Z assignments) in "Tris-washed" PSII, in which oxygen evolution is inactivated. Simultaneously, in ref 54, a broad band with a similar frequency was attributed to the S_2 state in untreated PSII. However, in untreated PSII, the lifetime of Y_Z radical is short, and the radical difference spectrum would not necessarily be detectable under S_2 conditions. In ref 56, the broad S_2 band was assigned to a water O-H stretching band, which is altered in frequency during the S_1 to S_2 transition. Such a band would be expected to show a ^{18}O solvent isotope shift; however, no $H_2{}^{18}O$ shift was detected for the broad S_2 band presented in ref 54. Table 1 summarizes this information. Note that attribution of the S_2 band, described here, to a hydrogen-bonded water is a less likely interpretation, compared to the protonated water cluster assignment. This is due to the large magnitude of the ^{18}O isotope effect and the substantial frequency downshift, relative to bulk water.

Ref [56] described the 3,200-2,200 cm^{-1} region derived from cyanobacterial PSII (Table 1). The 283 K S_2-minus-S_1 spectrum reported here is similar to the spectrum in ref 55. However, ref 55 reported no $H_2{}^{18}O$ solvent shift in this spectral region, and the broad positive spectral feature was assigned to a proton polarizability band in the S_2 state. The reason could be the use of dehydrated-rehydrated FT-IR samples, 283 K, or the different exchange method. A lower extent of exchange in internal, slowly exchanging regions of the samples may be inferred from data presented in ref 55. In the D_2O-exchanged PSII samples employed here, which are exchanged in solution and never dehydrated-rehydrated, the D_2O bulk solvent band is offscale at ~2,600 cm^{-1} on the 10^{-4} absorbance unit scale. In ref 55, absorbance at ~2,600 cm^{-1} was reported on scale at 10^{-5} absorbance units. The S_3 to S_0 spectrum in ref 55 was also reported to be insensitive to ^{18}O isotope exchange.

However, at higher temperature, the 3,074 cm^{-1} band is observed as a shoulder, as shown here at 283 K. These points are under further investigation.

In the latest report,[25] the 3,200-2,200 cm^{-1} region of the S_2-minus-S_1 spectrum was obtained from an oxygen-evolving plant PSII at 190 K (Table 1). A large, apparent ^{18}O solvent isotope effect on the frequency of a broad positive S_2 band was observed. The frequency of the band depended on the NaCl concentration (2,900 or 2,740 cm^{-1}). Those cryogenic experiments were used to assign the 190 K S_2 infrared band to an internal, $n(H_2O)H_3O^+$ cluster. The S_3 state is not accessible at 190 K. Those latest results support the conclusions of this paper (Table 1).

To summarize, our experiments are consistent with the assignment of a S_2 band at 2,830 cm^{-1} and S_0 bands at 3,074/2950 cm^{-1} to the hydronium cores of protonated, internal water clusters in the OEC. For gas phase water clusters with sizes of 4-8, an increase in H_3O^+ stretching frequency was associated with an increase in cluster size.[50] Comparison of the S_0 3,074 cm^{-1} frequency with the S_2 2,830 cm^{-1} frequency suggests that the proton in the S_0 state may be trapped on a larger cluster of water molecules in some population of centers (illustrated in Figure 2.1C and D).

Literature reports on protonated gas phase clusters[50] have reported that some protonated water cluster sizes are associated with vibrational bands in the 1,800-1,100 cm^{-1} region. Under our current experimental conditions, ^{18}O solvent exchange had only a minor effect on the mid-infrared regions of the S state spectra. This result suggests that the cluster sizes in the S_0 and S_2 states may be 4 or 6-8, giving rise to vibrational bands below 1,100 cm^{-1}, which are not accessible in our experiment. Alternatively, strong

absorbance from the protein may obscure the contributions of cationic water in this region. Similarly, only minor changes were observed in this region for bacteriorhodopsin in an ^{18}O-exchange study.[49]

$D_2{}^{16}O$ exchange was observed to shift the broad positive and negative bands in the 3,100-2,800 cm^{-1} region on each transition, but the effect of $D_2{}^{16}O$ exchange in the mid-infrared region (1,800-1,100 cm^{-1}) was most significant for the S_1 to S_2 transition. Frequency shifts and intensity changes are observed in amide I (1,650 cm^{-1}), II (1,550 cm^{-1}) and III (1,400 to 1,200 cm^{-1}) bands.[40] We have previously reported that the majority of bands in the S_1 to S_2 spectrum shift when strontium is substituted for calcium and when PSII is ammonia-treated. This sensitivity supports assignment of this spectrum to the donor side and to OEC amide bands.[30,58] Protein amide vibrational bands are altered by $D_2{}^{16}O$ exchange when the amide bands arise from hydrogen-bonded and solvent-accessible portions of the protein.[40] Therefore, a possible explanation of these D_2O data is that the S_1 to S_2 transition alters peptide backbone contributions in exchangeable regions of the protein, and other transitions do not. In bacteriohodopsin, the extent of deuterium exchange depended on the extent of solvent exposure, with solvent-exposed regions displaying greater susceptibility to exchange compared to buried alpha helical regions.[59]

Terminal water ligand and hydroxide ligand deprotonation reactions are proposed to accompany electron transfer and the S-state transitions[60,61] but the mechanism by which these chemical protons are transferred to the lumenal surface is not known.[23] The PSII X-ray structures[8-9] reveal a polarizable network of hydrogen bonds, involving chloride, calcium, water, and amino acid side chains (Fig. 7), which could be used in proton transfer. Based on sensitivity to calcium removal, the cationic water clusters observed here are

concluded to be a component of this proton exit pathway. Taken together, these results provide evidence that water acts, not only as the substrate of photosystem II, but also as a transient proton acceptor and donor at multiple places in the S state cycle. The connection between these trapped protons and lumenal proton release is of interest and remains to be elucidated. This work provides new insight into photosynthetic water oxidation and is of relevance to proton-coupled electron transfer mechanisms in solar energy conversion and bioenergetics.

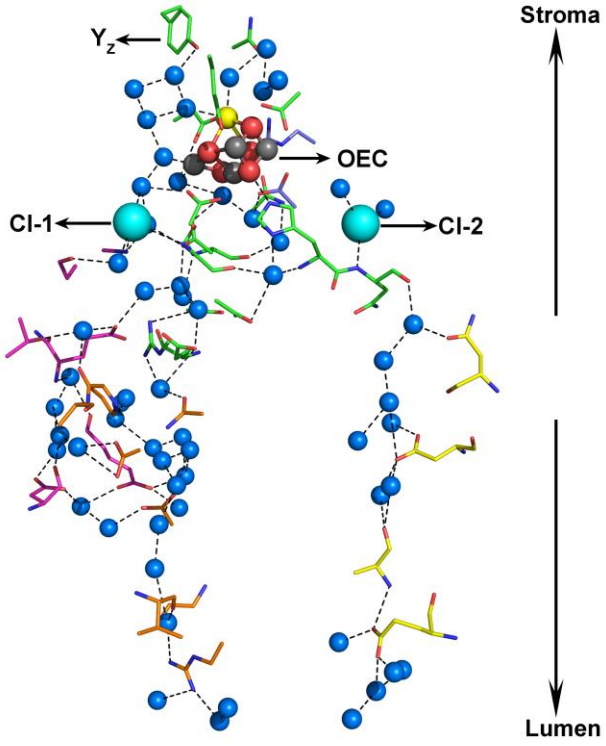

Figure 2.12 Putative proton exit pathway extending from the OEC to the lumen and involving the two chloride ions of cyanobacterial PSII (PDB ID: 4UB6).[9] The hydrogen-bonding network includes water molecules (blue spheres) and residues of PSII subunits: D1 (green), D2 (magenta), CP43 (yellow), CP47 (blue), psbO (orange) and psbV (wheat). Atoms: blue, nitrogen; cyan, chloride; red, oxygen; white, hydrogen.

2.6 References

1. Garczarek, F.; Gerwert, K. Functional Waters in Intraprotein Proton Transfer Monitored by Ftir Difference Spectroscopy. *Nature* **2006,** *439*, 109-112.

2. Freier, E.; Wolf, S.; Gerwert, K. Proton Transfer Via a Transient Linear Water-Molecule Chain in a Membrane Protein. *Proc. Natl. Acad. Sci. U.S.A.* **2011,** *108*, 11435-11439.

3. Wolf, S.; Freier, E.; Cui, Q.; Gerwert, K. Infrared Spectral Marker Bands Characterizing a Transient Water Wire inside a Hydrophobic Membrane Protein. *J. Chem. Phys.* **2014,** *141*, 22D524.

4. Silverman, D. N.; McKenna, R. Solvent-Mediated Proton Transfer in Catalysis by Carbonic Anhydrase. *Acc. Chem. Res.* **2007,** *40*, 669-675.

5. Seibold, S. A.; Mills, D. A.; Ferguson-Miller, S.; Cukier, R. I. Water Chain Formation and Possible Proton Pumping Routes in *Rhodobacter Sphaeroides* Cytochrome *C* Oxidase: A Molecular Dynamics Comparison of the Wild Type and R481k Mutant. *Biochemistry* **2005,** *44*, 10475-10485.

6. Dau, H.; Zaharieva, I.; Haumann, M. Recent Developments in Research on Water Oxidation by Photosystem Ii. *Curr. Opin. Chem. Biol.* **2012,** *16*, 3-10.

7. Cox, N.; Pantazis, D. A.; Neese, F.; Lubitz, W. Biological Water Oxidation. *Acc. Chem. Res.* **2013,** *46*, 1588-1596.

8. Umena, Y.; Kawakami, K.; Shen, J.-R.; Kamiya, N. Crystal Structure of Oxygen-Evolving Photosystem Ii at a Resolution of 1.9 Å. *Nature* **2011,** *473*, 55-60.

9. Suga, M.; Akita, F.; Hirata, K.; Ueno, G.; Murakami, H.; Nakajima, Y.; Shimizu, T.; Yamashita, K.; Yamamoto, M.; Ago, H., et al. Native Structure of Photosystem Ii at 1.95 Å Resolution Viewed by Femtosecond X-Ray Pulses. *Nature* **2015,** *517*, 99-103.

10. Wei, X.; Su, X.; Cao, P.; Liu, X.; Chang, W.; Li, M.; Zhang, X.; Liu, Z. Structure of Spinach Photosystem Ii–Lhcii Supercomplex at 3.2 Å Resolution. *Nature* **2016,** *534*, 69-74.

11. Barry, B. A. Proton Coupled Electron Transfer and Redox Active Tyrosines in Photosystem Ii. *J. Photochem. Photobiol., B* **2011,** *104*, 60-71.

12. Kok, B.; Forbush, B.; McGloin, M. Cooperation of Charges in Photosynthetic O_2 Evolution-I. A Linear Four Step Mechanism. *Photochem. Photobiol.* **1970,** *11*, 457-75.

13. Dekker, J. P.; Van Gorkom, H. J.; Brok, M.; Ouwehand, L. Optical Characterization of Photosystem Ii Electron Donors. *Biochim. Biophys. Acta* **1984,** *764*, 301-309.

14. Gerken, S.; Brettel, K.; Schlodder, E.; Witt, H. Optical Characterization of the Immediate Electron Donor to Chlorophyll a^{+Ii} in O_2-Evolving Photosystem Ii Complexes Tyrosine as Possible Electron Carrier between Chlorophyll A_{ii} and the Water-Oxidizing Manganese Complex. *FEBS Lett.* **1988,** *237*, 69-75.

15. Gatt, P.; Petrie, S.; Stranger, R.; Pace, R. J. Rationalizing the 1.9 Å Crystal Structure of Photosystem Ii—a Remarkable Jahn–Teller Balancing Act Induced by a Single Proton Transfer. *Angew. Chem. Int. Ed.* **2012,** *51*, 12025-12028.

16. Yocum, C. F. The Calcium and Chloride Requirements of the O_2 Evolving Complex. *Coord. Chem. Rev.* **2008,** *252*, 296-305.

17. Bricker, T. M.; Roose, J. L.; Fagerlund, R. D.; Frankel, L. K.; Eaton-Rye, J. J. The Extrinsic Proteins of Photosystem Ii. *Biochim. Biophys. Acta* **2012,** *1817*, 121-142.

18. Roose, J. L.; Frankel, L. K.; Mummadisetti, M. P.; Bricker, T. M. The Extrinsic Proteins of Photosystem Ii: Update. *Planta* **2016,** *243*, 889-908.

19. Krishtalik, L. I. Energetics of Multielectron Reactions - Photosynthetic Oxygen Evolution. *Biochim. Biophys. Acta* **1986,** *849*, 162-171.

20. Junge, W.; Haumann, M.; Ahlbrink, R.; Mulkidjanian, A.; Clausen, J. Electrostatics and Proton Transfer in Photosynthetic Water Oxidation. *Philos. Trans. R. Soc., B* **2002,** *357*, 1407-1418.

21. Dau, H.; Haumann, M. Eight Steps Preceding O–O Bond Formation in Oxygenic Photosynthesis—a Basic Reaction Cycle of the Photosystem Ii Manganese Complex. *Biochim. Biophys. Acta* **2007,** *1767*, 472-483.

22. Dilbeck, P. L.; Hwang, H. J.; Zaharieva, I.; Gerencser, L.; Dau, H.; Burnap, R. L. The D1-D61n Mutation in *Synechocystis* Sp. Pcc 6803 Allows the Observation of Ph-Sensitive Intermediates in the Formation and Release of O_2 from Photosystem Ii. *Biochemistry* **2012,** *51*, 1079-1091.

23. Ho, F. M. Structural and Mechanistic Investigations of Photosystem Ii through Computational Methods. *Biochim. Biophys. Acta* **2012,** *1817*, 106-120.

24. Polander, B. C.; Barry, B. A. Detection of an Intermediary, Protonated Water Cluster in Photosynthetic Oxygen Evolution. *Proc. Natl. Acad. Sci. U.S.A.* **2013,** *110*, 10634-9.

25. Guo, Z.; Barry, B. A. Cryogenic Trapping and Isotope Editing Identify a Protonated Water Cluster as an Intermediate in the Photosynthetic Oxygen-Evolving Reaction. *J. Phys. Chem. B* **2016,** *120*, 8794-8808.

26. Berthold, D. A.; Babcock, G. T.; Yocum, C. F. A Highly Resolved, Oxygen-Evolving Photosystem Ii Preparation from Spinach Thylakoid Membranes: Epr and Electron-Transport Properties. *FEBS Lett.* **1981,** *134*, 231-234.

27. Mishra, R. K.; Ghanotakis, D. F. Selective Extraction of Cp 26 and Cp 29 Proteins without Affecting the Binding of the Extrinsic Proteins (33, 23 and 17 Kda) and the Dcmu Sensitivity of a Photosystem Ii Core Complex. *Photosynth. Res.* **1994,** *42*, 37-42.

28. Polander, B. C.; Barry, B. A. Calcium and the Hydrogen-Bonded Water Network in the Photosynthetic Oxygen-Evolving Complex. *J. Phys. Chem. Lett.* **2013,** *4*, 786-791.

29. Barry, B. A. Tyrosyl Radicals in Photosystem Ii. *Methods Enzymol.* **1995,** *258*, 303-319.

30. Polander, B. C.; Barry, B. A. Calcium, Strontium, and Protein Dynamics During the S_2 to S_3 Transition in the Photosynthetic Oxygen-Evolving Cycle. *J. Phys. Chem. Lett.* **2013,** *4*, 3356-3362.

31. Ghanotakis, D. F.; Babcock, G. T.; Yocum, C. F. Calcium Reconstitutes High Rates of Oxygen Evolution in Polypeptide Depleted Photosystem Ii Preparations. *FEBS Lett.* **1984,** *167*, 127-130.

32. Noguchi, T.; Sugiura, M. Flash-Induced Fourier Transform Infrared Detection of the Structural Changes During the S-State Cycle of the Oxygen-Evolving Complex in Photosystem Ii. *Biochemistry* **2001,** *40*, 1497-1502.

33. Hillier, W.; Babcock, G. T. S-State Dependent Fourier Transform Infrared Difference Spectra for the Photosystem Ii Oxygen Evolving Complex. *Biochemistry* **2001,** *40*, 1503-1509.

34. Barry, B. A.; Cooper, I. B.; De Riso, A.; Brewer, S. H.; Vu, D. M.; Dyer, R. B. Time-Resolved Vibrational Spectroscopy Detects Protein-Based Intermediates in the Photosynthetic Oxygen-Evolving Cycle. *Proc. Natl. Acad. Sci. U.S.A.* **2006,** *103*, 7288-7291.

35. De Riso, A.; Jenson, D. L.; Barry, B. A. Calcium Exchange and Structural Changes During the Photosynthetic Oxygen Evolving Cycle. *Biophys. J.* **2006,** *91*, 1999-2008.

36. Miqyass, M.; van Gorkom, H. J.; Yocum, C. The Psii Calcium Site Revisited. *Photosynth. Res.* **2007,** *92*, 275-287.

37. Goodin, D. B.; Yachandra, V. K.; Britt, R. D.; Sauer, K.; Klein, M. P. The State of Manganese in the Photosynthetic Apparatus. 3. Light-Induced Changes in X-Ray Absorption (K-Edge) Energies of Manganese in Photosynthetic Membranes. *Biochim. Biophys. Acta* **1984,** *767*, 209-216.

38. de Wijn, R.; van Gorkom, H. J. Kinetics of Electron Transfer from Q_a to Q_b in Photosystem Ii. *Biochemistry* **2001,** *40*, 11912-11922.

39. Cox, N.; Retegan, M.; Neese, F.; Pantazis, D. A.; Boussac, A.; Lubitz, W. Electronic Structure of the Oxygen-Evolving Complex in Photosystem Ii Prior to Oo Bond Formation. *Science* **2014,** *345*, 804-808.

40. Krimm, S.; Bandekar, J. Vibrational Spectroscopy and Conformation of Peptides, Polypeptides, and Proteins. *Adv. Protein Chem.* **1986,** *38*, 181-367.

41. Barth, A. The Infrared Absorption of Amino Acid Side Chains. *Prog. Biophys. Mol. Biol.* **2000,** *74*, 141-173.

42. Hendry, G.; Wydrzynski, T. ^{18}o Isotope Exchange Measurements Reveal That Calcium Is Involved in the Binding of One Substrate-Water Molecule to the Oxygen-Evolving Complex in Photosystem Ii. *Biochemistry* **2003,** *42*, 6209-6217.

43. Fredin, L.; Nelander, B.; Ribbegård, G. Infrared Spectrum of the Water Dimer in Solid Nitrogen. I. Assignment and Force Constant Calculations. *J. Chem. Phys.* **1977,** *66*, 4065-4072.

44. Perchard, J. Anharmonicity and Hydrogen Bonding: Ii–a near Infrared Study of Water Trapped in Nitrogen Matrix. *Chem. Phys.* **2001,** *266*, 109-124.

45. Kandori, H.; Shichida, Y. Direct Observation of the Bridged Water Stretching Vibrations inside a Protein. *J. Am. Chem. Soc.* **2000,** *122*, 11745-11746.

46. Zundel, G. Hydrogen-Bonded Chains with Large Proton Polarizability as Charge Conductors in Proteins Bacteriorhodopsin and the F_0 Subunit of *E. Coli*. *J. Mol. Struct.* **1994,** *322*, 33-42.

47. Garczarek, F.; Wang, J.; El-Sayed, M. A.; Gerwert, K. The Assignment of the Different Infrared Continuum Absorbance Changes Observed in the 3000–1800-Cm^{-1} Region During the Bacteriorhodopsin Photocycle. *Biophys. J.* **2004,** *87*, 2676-2682.

48. Wang, J.; El-Sayed, M. A. Proton Polarizability of Hydrogen-Bonded Network and Its Role in Proton Transfer in Bacteriorhodopsin. *J. Phys. Chem. A* **2000,** *104*, 4333-4337.

49. Lórenz-Fonfría, V. A.; Furutani, Y.; Kandori, H. Active Internal Waters in the Bacteriorhodopsin Photocycle. A Comparative Study of the L and M Intermediates at Room and Cryogenic Temperatures by Infrared Spectroscopy. *Biochemistry* **2008,** *47*, 4071-4081.

50. Headrick, J. M.; Diken, E. G.; Walters, R. S.; Hammer, N. I.; Christie, R. A.; Cui, J.; Myshakin, E. M.; Duncan, M. A.; Johnson, M. A.; Jordan, K. D. Spectral Signatures of Hydrated Proton Vibrations in Water Clusters. *Science* **2005,** *308*, 1765-1769.

51. Wang, H.; Agmon, N. Protonated Water Dimer on Benzene: Standing Eigen or Crouching Zundel? *J. Phys. Chem. B* **2015,** *119*, 2658-2667.

52. Horita, J.; Cole, D. R., *Aqueous Systems at Elevated Temperatures and Pressures: Physical Chemistry in Water, Steam and Hydrothermal Solutions*, Fernandez-Prini, R.; Harvey, A. H.; Palmer, D. A., Eds. Elsevier: Amsterdam, 2004, pp 277-319.

53. Hermes, S.; Stachnik, J. M.; Onidas, D.; Remy, A.; Hofmann, E.; Gerwert, K. Proton Uptake in the Reaction Center Mutant L210dn from *Rhodobacter Sphaeroides* Via Protonated Water Molecules. *Biochemistry* **2006,** *45*, 13741-13749.

54. Noguchi, T.; Sugiura, M. Ftir Detection of Water Reactions During the Flash-Induced S-State Cycle of the Photosynthetic Water-Oxidizing Complex. *Biochemistry* **2002,** *41*, 15706-15712.

55. Nakamura, S.; Nagao, R.; Takahashi, R.; Noguchi, T. Fourier Transform Infrared Detection of a Polarizable Proton Trapped between Photooxidized Tyrosine Yz and a Coupled Histidine in Photosystem Ii: Relevance to the Proton Transfer Mechanism of Water Oxidation. *Biochemistry* **2014,** *53*, 3131-3144.

56. Debus, R. J. Evidence from Ftir Difference Spectroscopy That D1-Asp61 Influences the Water Reactions of the Oxygen-Evolving Mn_4cao_5 Cluster of Photosystem Ii. *Biochemistry* **2014,** *53*, 2941-2955.

57. Nakamura, S.; Ota, K.; Shibuya, Y.; Noguchi, T. Role of a Water Network around the Mn_4cao_5 Cluster in Photosynthetic Water Oxidation: A Fourier Transform Infrared Spectroscopy and Quantum Mechanics/Molecular Mechanics Calculation Study. *Biochemistry* **2016,** *55*, 597-607.

58. Brahmachari, U.; Barry, B. A. Dynamics of Proton Transfer to Internal Water During the Photosynthetic Oxygen-Evolving Cycle. *J. Phys. Chem. B* **2016,** *120*, 11464-11473.

59. Nakamura, S.; Noguchi, T. Infrared Determination of the Protonation State of a Key Histidine Residue in the Photosynthetic Water Oxidizing Center. *J. Am. Chem. Soc.* **2017,** *139*, 9364–9375.

60. Brahmachari, U.; Gonthier, J. F.; Sherrill, C. D.; Barry, B. A. Chloride Maintains a Protonated Internal Water Network in the Photosynthetic Oxygen Evolving Complex. *J. Phys. Chem. B* **2017,** *121*, 10327-10337.

61. Brahmachari, U.; Guo, Z.; Konecny, S. E.; Obi, E. N. C.; Barry, B. A. Engineering Proton Transfer in Photosynthetic Oxygen Evolution: Chloride, Nitrate, and Trehalose Reorganize a Hydrogen-Bonding Network. *J Phys Chem B* **2018,** *122*, 6702-6711.

CHAPTER 3. CHLORIDE MAINTAINS A PROTONATED INTERNAL WATER NETWORK IN THE PHOTOSYNTHETIC OXYGEN EVOLVING COMPLEX

Reprinted with permission from *The Journal of Physical Chemistry B*

Brahmachari, U.; Gonthier, J. F.; Sherrill, C. D.; and Barry, B. A. Chloride Maintains a Protonated Internal Water Network in the Photosynthetic Oxygen Evolving Complex. *J. Phys. Chem. B* **2017,** *121*, 10327-10337.

3.1 Abstract

In photosystem II (PSII), water oxidation occurs at a Mn_4CaO_5 cluster and results in production of molecular oxygen. The Mn_4CaO_5 cluster cycles among five oxidation states, called S_n states. As a result, protons are released at the metal cluster and transferred through a 35 Å hydrogen-bonding network to the lumen. At 283 K, an infrared band at 2830 cm^{-1} is assigned an internal solvated hydronium ion via $H_2{}^{18}O$ solvent exchange. This result is similar to a previous report at 263 K. Computations on an OEC model predict that chloride stabilizes this hydronium ion on a network of nine water molecules. In this model, a H_3O^+ stretching mode at 2738 cm^{-1} is predicted to shift to higher frequency with bromide and to lower frequency with nitrate substitution. The calculated frequencies were compared to S_2-minus-S_1 RIFT-IR spectra acquired from chloride-, bromide-, or nitrate-containing PSII samples, which were active in oxygen evolution. As predicted, the frequency of the 2830 cm^{-1} band shifted to higher energy with bromide and to lower energy with nitrate substitution. These results support the conclusion that an internal hydronium ion and chloride play a direct role in an internal proton transfer event during the S_1 to S_2 transition.

3.2 Introduction

Water plays a vital role in proton transfer because of its ability to act as both an acid and a base. The mechanism by which water functions in proton transfer has been the subject of extensive investigation.[1-4] The behavior of water molecules involved in proton transfer in bulk solution is distinct from that in proteins. Extensive hydrogen bonding networks involving internal water molecules and amino acid side chains enable proteins to

shuttle protons effectively. This kind of active water participation in proton transfer has been reported in bacteriorhodopsin,[5-7] cytochrome c oxidase,[8] and carbonic anhydrase.[9]

PSII is a transmembrane multisubunit protein, which comprises several membrane-spanning subunits and three extrinsic subunits located in the lumen.[10-12] PSII oxidizes water to generate oxygen by sequential light-induced oxidation at its catalytic core, a Mn_4CaO_5 cluster (Figure 3.1A), commonly referred to as the oxygen evolving complex (OEC).[13-14] Oxygen evolution follows an oscillatory pattern with period four.[15] The overall reaction is the production of one molecule of oxygen, along with four electrons and four protons from two water molecules. Absorption of light induces charge separation among the redox-active cofactors in PSII, which ultimately results in the oxidation of the OEC. Photoinduced charge separation leads to oxidation of the dimeric chlorophyll donor, P_{680} and reduction of a plastoquinone molecule, Q_A, the terminal acceptor. Reduction of P_{680}^+ occurs via the redox-active tyrosine, Y_Z (Y161 of D1 polypeptide).[16] The neutral tyrosyl radical, $Y_Z^\bullet$, is a powerful oxidant and oxidizes the OEC.[17] Four such oxidations of the OEC takes place via $Y_Z^\bullet$, and these oxidation reactions result in oxygen production.[18] Each of these OEC oxidation states is called a S_n state, where n refers to the number of oxidizing equivalents stored on the OEC (Figure 3.1B). In dark-adapted PSII, the OEC primarily exists in the S_1 state. A single flash oxidizes S_1 to the S_2 state.[13, 19] The second flash oxidizes the metal cluster to the S_3 state, and the third flash converts the S_3 state to the S_0 state via the metastable S_4 state.[15] Substrate water oxidation accompanies this transition, and the OEC is restored to its most reduced (S_0) state. A fourth flash resets the OEC back to the S_1 state.

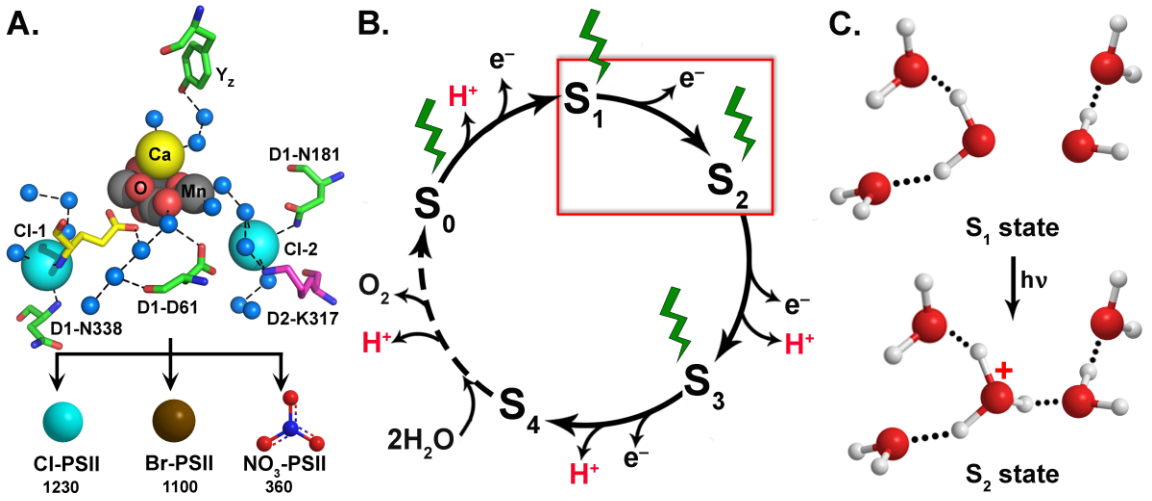

Figure 3.1 (A) Chloride ions and amino acid residues located near the OEC. The structure was derived from cyanobacterial PSII. Water molecules involved in the predicted hydrogen-bonding network are blue spheres (PDB ID: 4UB6[10]). Amino acids are shown as sticks, and hydrogen-bonding interactions are dashed lines. Residues from the PSII subunits, D1, D2 and CP43, are green, magenta and yellow, respectively. Mn_4CaO_5 cluster: calcium, yellow; chloride, cyan; manganese, gray; oxygen, red. Oxygen evolution rates, in μmol O_2/(mg Chl.hr)$^{-1}$, measured from Cl-PSII, Br-PSII and NO_3-PSII, are shown below the representations of each ion. (B) S-state cycle[15] of photosynthetic water oxidation; the cycle is induced in PSII using laser flashes. The S_1 to S_2 transition is described in the present study. (C) Illustration of a cationic cluster of five water molecules, proposed to be formed during the S_1 to S_2 transition. Color of atoms: red, oxygen; white, hydrogen.

In addition to a four-electron oxidation, the oxygen-evolving reaction also results in the release of four protons to the lumen. On progressing from S_0 to S_1, S_1 to S_2, S_2 to S_3 and from S_3 back to S_0, a 1:0:1:2 stoichiometry of proton release to the lumen has been measured experimentally in sucrose-containing buffers (Figure 3.1B).[20-21] Thus, the S_1 to S_2 transition is distinct from the rest of the S-state cycle, because no proton release to the lumen has been detected, when sucrose is the cryoprotectant.

For approximately 50 years, it has been known that chloride plays a facilitating role in photosynthetic water oxidation.[22] However, chloride's exact role in the mechanism has been the subject of debate.[23-27] Using radioisotope labeling and spinach PSII preparations,

chloride was reported to have one high affinity binding site per reaction center.[24] In plants, chloride affinity was modulated by the extrinsic subunits, PsbP and PsbQ.[28-31] Intact PSII, retaining these subunits, exhibited high chloride affinity, while removal of the PsbP and PsbQ subunits lowered chloride affinity (reviewed in ref[22]). In the 1.95 Å crystal structure of cyanobacterial PSII,[10] two chloride ions, Cl-1 and Cl-2, were resolved at 6.6 and 7.5 Å from the OEC, respectively (Figure 3.1A). The cyanobacterial PSII structure exhibits a third chloride, located ~25 Å away from the OEC.[10] The third chloride was not identified in a recently published plant PSII structure.[12] Chloride is required kinetically only for the latter two S-state transitions (S_2 to S_3 and S_3 to S_0).[25] Some chloride analogs support oxygen evolution activity in the series, $Cl^- > Br^- >> NO_3^- > NO_2^- > I^-$.[32]

Chloride is an uncommon cofactor in biology. In halorhodopsin, light energy is used to pump chloride ions across membranes.[33] Haloperoxidases use chloride and other halides as substrates but not as cofactors.[34] Besides PSII, only two other enzymes, α-amylase[35] and angiotensin-converting enzyme (ACE)[36-37] are presently known to require chloride as a cofactor.[38] Therefore, the role of chloride in photosynthetic oxygen evolution is unusual and is an important, fundamental question in biological chemistry.

In PSII, chloride has been proposed to facilitate efficient proton transfer to the lumen.[24, 39-43] In the present study, we have investigated whether chloride plays a role during the S_1 to S_2 transition using a novel infrared band derived from a hydronium ion. Previously, our group reported this broad, absorptive, infrared band at ~2830 cm^{-1}, produced in the S_2 state at 263 K (reviewed in ref [44]). This band was assigned to W_n^+, a protonated water cluster, which was proposed to be a trapped intermediate on the internal, proton transfer pathway[45-48] (Figure 3.1C). Here, we monitor the frequency and amplitude

of this S_2 band in chloride, bromide, and nitrate-containing PSII samples, using reaction-induced FTIR (RIFT-IR) spectroscopy at 283 K. All three preparations are active in oxygen evolution. We report $H_2{}^{18}O$ solvent exchange shifts in the $W_n{}^+$ band at this temperature. We also find that the $W_n{}^+$ band is sensitive to bromide and nitrate substitution. The results of the study are compared to quantum mechanical calculations on a small model of the OEC, which contains nine water molecules and stabilizes a hydronium ion near a chloride, bromide, or nitrate ion. When experimental bands are compared to the computed vibrational frequencies, the predicted frequencies and the direction of the anion exchange-induced shifts are well correlated. This study provides new information concerning the role of chloride in proton transfer, and the results suggest that chloride functions in proton transfer via formation and stabilization of $W_n{}^+$ on the lumenal exit pathway during the S_1 to S_2 transition. While not required kinetically during this transition, chloride could play a role in the creation and maintenance of an essential water network. The presence of this network during the non-rate limiting S_1 to S_2 transition may be important in mediating chloride effects on latter transitions.

3.3 Materials and Methods

3.3.1 PSII sample preparation.

Commercially available spinach was used to prepare PSII samples. Treatment with the detergent, Triton X-100, yielded PSII-enriched membrane particles, called BBY membranes.[49] A second round of detergent treatment was carried out using 0.4% octylthioglucoside (OTG) to further purify PSII (OTG-PSII). Removal of the light-harvesting complexes, LHCII, CP24, CP26 and CP29, was achieved by treatment with 10

mM $MgCl_2$.[50] PSII samples obtained following these treatments were suspended into a buffer containing 0.4 M sucrose, 50 mM 2-(N-morpholino)ethanesulfonic acid (MES)-NaOH, pH 6, and 15 mM NaCl and stored at -70°C.

3.3.2 pH 7.5 anion substitution

Anion substitution with either bromide or nitrate was performed using a treatment at pH 7.5, designed to remove extrinsic subunits and increase accessibility to the chloride site. Chloride-substituted controls were also generated using the same procedure. To this end, PSII samples were washed twice with 0.4 M sucrose, 50 mM 2-[4-(2-hydroxyethyl)piperazin-1-yl]ethanesulfonic acid (HEPES)-NaOH, pH 7.5, and 15 mM NaCl, NaBr or $NaNO_3$ depending on the anion being exchanged. Removal of PsbP and PsbQ occurs at pH 7.5[46, 51] and increases access to the chloride site. PSII samples containing chloride, bromide and nitrate ions will be referred to as Cl-PSII, Br-PSII and NO_3-PSII, respectively. Samples were aliquoted and frozen at -70°C. Oxygen evolution activities are reported below (see below).

3.3.3 Sulfate treatment (chloride depletion).

As an additional method, chloride depletion using sulfate treatment was performed using literature protocols.[25, 52] Briefly, isolated OTG-PSII samples were treated with a buffer containing 400 mM sucrose, 50 mM HEPES-NaOH, pH 7.5 and 50 mM Na_2SO_4. The chlorophyll concentration was maintained at 0.2 mg/mL, and the sample was incubated on ice for 15 minutes with shaking in the dark. Subsequently, the sample was pelleted through centrifugation (50,000 x *g*, 10 minutes, 4°C) and resuspended in chloride-free buffer

containing 400 mM sucrose and 50 mM HEPES-NaOH, pH 7.5. This sample will be referred to as Cl-depleted PSII. Aliquots were frozen and stored at -70°C.

3.3.4 Oxygen evolution assays, methods.

PSII samples were assayed for oxygen evolution activity using a Clark-type oxygen electrode.[53] In these assays, freshly prepared 1 mM potassium ferricyanide ($K_3[Fe(CN)_6]$) and recrystallized 0.5 mM 2,6-dichlorobenzoquinone were used as external electron acceptors. For pH 6.0 measurements, the assay buffer contained 0.4 M sucrose, 50 mM MES-NaOH, pH 6.0 and 15 mM NaCl. For pH 7.5 measurements, the assay buffer used for Cl-PSII, Br-PSII and NO_3-PSII contained 0.4 M sucrose, 50 mM HEPES-NaOH, pH 7.5 and 15 mM NaCl, NaBr, and $NaNO_3$, respectively. The anion concentrations were kept constant at 155 mM by addition from a 3 M buffered stock of the corresponding sodium salt. Calcium concentrations were maintained at 20 mM by addition from 3 M buffered stocks. The calcium salt of the exchanged anion was used to make the calcium stock. For Cl-depleted PSII samples, the assay buffer contained 400 mM sucrose and 50 mM HEPES-NaOH, pH 7.5.

3.3.5 Oxygen evolution activities, results derived from pH 7.5 treated PSII.

At pH 6.0, isolated PSII gave oxygen evolution rates of 1,260 ± 130 μmol O_2 (mg Chl-h)$^{-1}$. After the pH 7.5 treatment, Cl-PSII samples exhibited oxygen evolution rates of 1,230 ± 120 μmol O_2 (mg Chl-h)$^{-1}$. Br-PSII samples had rates of 1,100 ± 70 μmol O_2 (mg Chl-h)$^{-1}$. NO_3-PSII had oxygen evolution rates of 360 ± 90 μmol O_2 (mg Chl-h)$^{-1}$. Thus, the rates of oxygen evolution derived from Br-PSII and NO_3-PSII samples were 89% and 29%, respectively of the Cl-PSII controls. This result is in agreement with literature reports

derived from studies of BBY membranes.[32] Addition of 155 mM chloride to NO_3-PSII samples restored the rates to 1,350 ± 70 μmol O_2 (mg Chl-h)$^{-1}$ demonstrating that the effects of nitrate substitution were reversible. Note the recovery of oxygen evolution in the presence of chloride, in which 98% of the activity was reconstituted.

3.3.6 Oxygen evolution assays, results derived from sulfate-treated PSII.

When assayed without exogenous calcium and chloride, Cl-depleted PSII exhibited oxygen evolution rates of 80 ± 40 μmol O_2 (mg Chl-h)$^{-1}$. This preparation is judged to be inactive in oxygen evolution. Addition either of 155 mM chloride or 10 mM calcium (using $Ca(OH)_2$) to Cl-depleted PSII yielded oxygen evolution rates only of 570 ± 30 μmol O_2 (mg Chl-h)$^{-1}$ and 51 μmol O_2 (mg Chl-h)$^{-1}$, respectively. Simultaneous addition of 155 mM chloride and 20 mM calcium to Cl-depleted PSII caused the activity to increase to 1010 ± 40 μmol O_2 (mg Chl-h)$^{-1}$. Hence, the oxygen evolving activity of sulfate-treated OTG-PSII was recovered by addition of chloride and calcium, but not recovered by addition of chloride alone. This is distinct from previous reports using sulfate-treated BBY membranes and is attributed to a preparation-specific effect.[32, 52, 54]

3.3.7 RIFT-IR experiments.

Samples for RIFT-IR experiments were prepared by thawing Cl-PSII, Br-PSII, NO_3-PSII and Cl-depleted samples, followed by a final resuspension/centrifugation in the respective buffer being used. To generate Cl-PSII, Br-PSII, and $^{14}NO_3$-PSII, 20 mM calcium and 155 mM of chloride, bromide or nitrate, were added. To generate $^{15}NO_3$-PSII, the final resuspension was performed in buffer containing 20 mM $Ca(^{15}NO_3)_2$ and 155 mM $Na^{15}NO_3$. Cl-depleted samples were resuspended in chloride free buffer containg 400 mM

sucrose and 50 mM HEPES-NaOH, pH 7.5. Freshly prepared 15 mM ferricyanide was added to each sample from a 100 mM stock prepared in the respective buffer. Samples in $H_2{}^{18}O$ were prepared by performing the final resuspension of Cl-PSII samples in $H_2{}^{18}O$ buffer containing 400 mM sucrose, 50 mM HEPES-NaOH, pH 7.5, 155 mM chloride and 20 mM calcium. For $H_2{}^{18}O$ experiments, the ferricyanide stock (1 M) was prepared in $H_2{}^{16}O$ buffer and added to the sample. All samples were then pelleted by centrifugation (50,000 x *g*, 10 minutes, 4°C). We have previously reported the observation of the ~2800 cm^{-1} band in the S_2 state at 283 K in pH 7.5 buffer.[45] While a similar band has also been reported at 190 K using pH 6,[46] in this 283 K study we continued to use pH 7.5 in order to build on previous results at this temperature.

RIFT-IR experiments were performed using literature protocols[48, 55-56] at pH 7.5 and 283 K. After being pelleted through centrifugation, the PSII sample was spread between two CaF_2 (25 x 2 mm) windows. The sample was concentrated with nitrogen gas to give an absorbance ratio of 2.3-3.3 between the O-H stretch (3370 cm^{-1}) and amide II (1550 cm^{-1}). A small piece of parafilm was wedged between the two sample windows to maintain a fixed path length and to reduce contributions from interference fringes. The windows were sealed with high vacuum grease and wrapped with parafilm to prevent sample dehydration during the experiment.

A Bruker IFS 66v/S instrument was used. Data acquisition was performed with the following parameters:[3,4] 4 cm^{-1} for $H_2{}^{18}O$ measurements and corresponding $H_2{}^{16}O$ controls and 8 cm^{-1} spectral resolution for all other measurements and their controls; Happ-Genzel apodization function; 60 kHz mirror speed; four levels of zero filling; and Mertz phase correction. PSII samples were subjected to a single saturated preflash from a 532 nm Nd-

YAG laser (at 40 mJ/cm^2 power density). The preflash was followed by 20 min of dark adaptation. The spectrometer's internal HeNe laser was blocked by a germanium window. Immediately after the dark adaptation, the sample was subjected to eight consecutive actinic, 532 nm flashes. Each laser flash was preceded and followed by 5 s of rapid scan data collection, except for the $H_2{}^{18}O$ measurements (and corresponding $H_2{}^{16}O$ controls) in which data were acquired for 15 s. One such series of eight flashes comprised a single loop of data collection. After the first loop, the sample was dark adapted for 15 minutes. Following this, the entire loop of data collection, including the dark adaptation, was repeated four times, except for the $H_2{}^{18}O$ measurements (and corresponding $H_2{}^{16}O$ controls), in which loops were repeated nine times. Hence, the total wait time in between loops was 35 minutes. This dark adaptation or wait time is sufficient to synchronize all anion-replaced preparations back to the S_1 state, even in anion-substituted preparations.[32] The difference, RIFT-IR spectra (S_2-minus-S_1) were obtained by ratioing the single channel data obtained before and after the actinic laser flash.

The absorption spectrum of each RIFT-IR sample was collected against an open beam background, and the intensity of the amide II band were determined. These amide II intensities were used to normalize the RIFT-IR data to an absorbance of 0.5. This procedure accounts for differences in sample thickness and path length between samples. The RIFT-IR spectra were plotted using IGOR (Wavemetrics, Lake Oswego, OR) software.

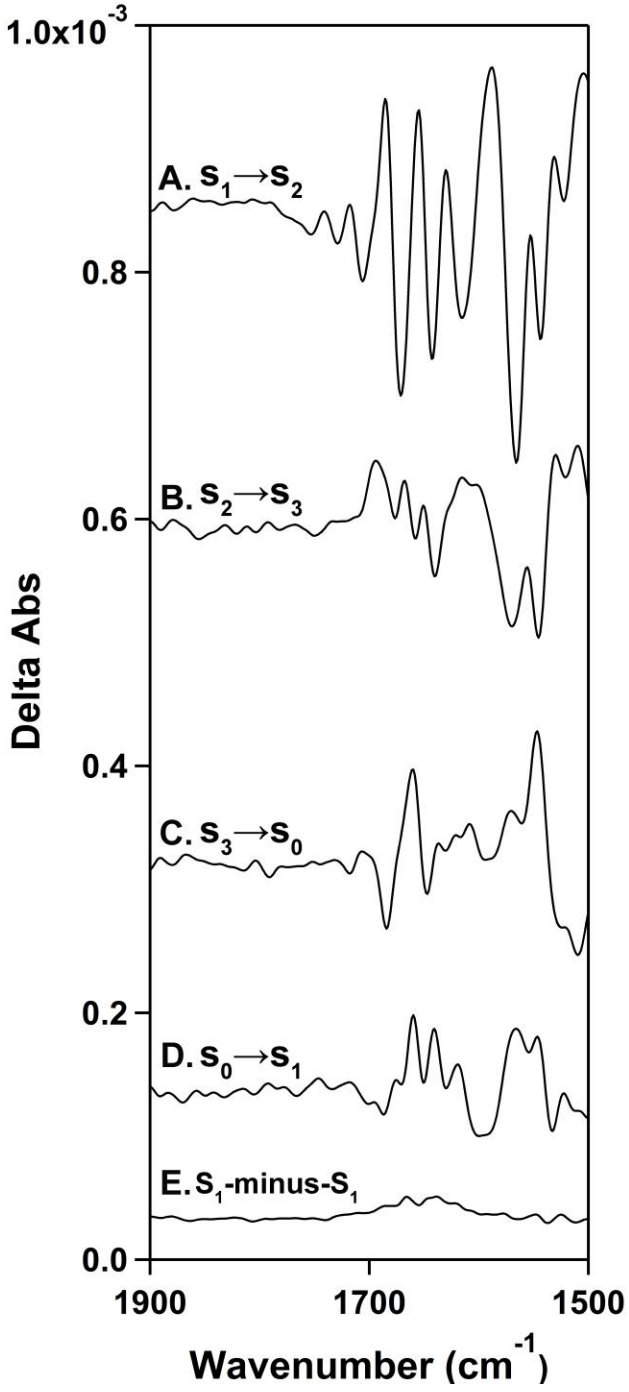

Figure 3.2 RIFT-IR difference spectra (1900-1500 cm^{-1} region) of Cl-PSII samples accompanying the entire S-state cycle at pH 7.5 and 283 K. (A) S_2-minus-S_1 spectrum; (B) S_3-minus-S_2 spectrum; (C) S_0-minus-S_3 spectrum; and (D) S_1-minus-S_0 spectrum. (E) Data obtained from the S_1-minus-S_1 spectra of Cl-PSII samples. Each spectrum is an average of 5 loops of data collected using 12 different samples. (E) was collected as background from those 12 samples with three times the amount of data averaging

used for (A-D). A 17-point smoothing has been applied to the data using the Savitzky–Golay algorithm.

This RIFT-IR method has been employed in the literature to probe conformational changes coupled to the S-state progression of the OEC.[48, 55, 57] The 5 s and 15 s time scale of the current experiments is similar to literature reports[55] and is expected to reflect donor side dynamics. As expected, S state dependent spectral changes are observed in the mid-infrared region of these data, as shown in Figure 3.2, A-E. In Figure 3.2, Cl-PSII samples (283 K, pH 7.5), in the dark-adapted S_1 state, were subjected to four sequential laser flashes to advance the reaction centers to the S_2, S_3, S_0 and finally back to the S_1 state. Difference spectra were generated by subtracting the initial from the final state. The bands observed each of the transitions are consistent with literature reports[48, 55, 57] and thereby reflect successful S-state advancement (Figure 3.3). In particular, the spectra are similar to those previously reported from our group on chloride-reconstituted BBY membranes,[52] but with improved signal to noise ratio due to the use of the additional OTG purification step. In Figure 3.3, the entire 4000-1000 cm^{-1} of Cl-PSII is shown. The data in Figure 3.3 exhibit an overall signal-to-noise ratio of 8, when the band amplitude at 2830 cm^{-1} is compared to peak-to-peak noise at 2220 cm^{-1}.

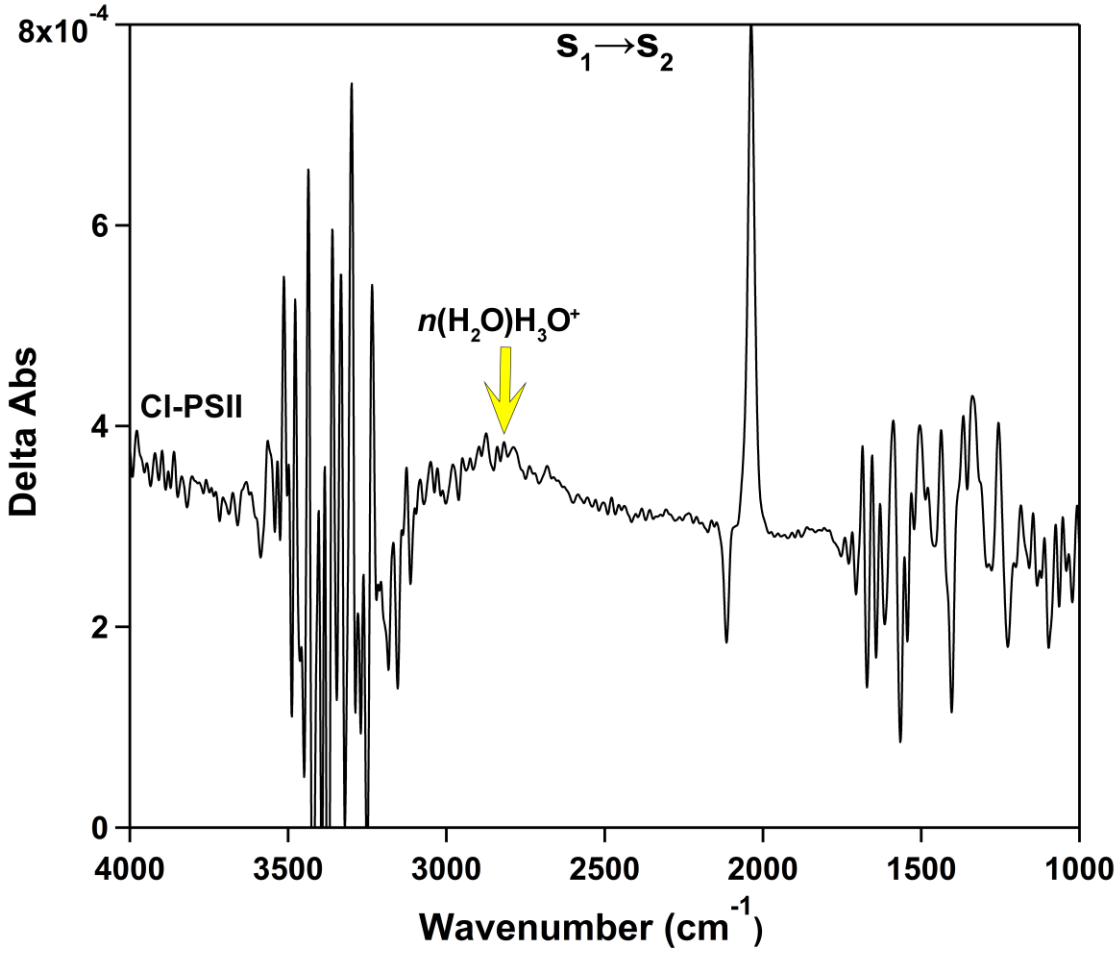

Figure 3.3 RIFT-IR spectrum in the 4000-1000 cm^{-1} region associated with the S_1 to S_2 transition. Data acquired using Cl-PSII samples at 283 K in pH 7.5 buffer. The data were smoothed using a 17 point Savitzky–Golay algorithm. Each spectrum is an average of 60 data sets: 5 data acquisition loops acquired from 12 different samples.

3.3.8 Theoretical methods.

To simulate the geometry and the vibrational spectrum of the protonated water cluster, the most relevant elements of the PSII environment were included. The protein structure 3ARC[11] was extracted from the RCSB PDB database[58]. Hydrogen atoms were added to the structure through the webportal of the WHAT IF software.[59] Exploratory computations indicated that the water close to Cl679 (in 3ARC[11]) is a suitable proton accepting site,

whereas other water molecules initially tested did not yield a hydronium ion upon geometry optimization, the proton moving instead either to the OEC or to D1-D61.

Vibrational frequency computations are much more expensive than simple geometry optimizations, and so we employed a truncated model system. However, the most relevant structural motifs from the protein were retained. The Mn atom from the Mn_4CaO_5 cluster closest to the protonated water, namely Mn4 was included. The full coordination sphere of Mn4 was included as well, i.e., the two water molecules HOH999 and HOH1000 (in their deprotonated state), the μ-oxo O5 and O4, and the amino acids D1-D170 and D1-E333. Because the μ-oxo oxygen lacked their interacting partners, their valence was completed by adding one hydrogen atom on each of them. To correctly model the main features of the electrostatic environment, the calcium ion (Ca1) was also retained. The amino acids D1-A344 and D1-E189 served as calcium ligands. The chloride ion and D2-K317, which stabilizes Cl^-, were both included. D1-D61 has been proposed to be on the proton exit pathway and was also included.[10-11, 60] Six other surrounding water molecules were included in addition to the protonated water. The oxidation state of OEC in the S_2 state is still discussed.[10, 19] In the current model, we considered the oxidation states of Mn1-Mn4 to be (III, IV, IV, IV). The Mn4 retained in our small cluster model is attributed a +IV oxidation state, and our model is thus relevant to the charge on the S_2 state of the OEC.[13-14, 61] A center with a single positive charge was used to efficiently represent the electrostatic influence of the remainder of the metal-oxo complex on the water cluster; computationally, a lithium ion was used for this purpose. We verified the accuracy of this model by comparing its electrostatic potential to the one of the crystal structures of the OEC complex (Table 2). At the position of the protonated water cluster, the average

absolute percent difference between the two is 5.5 ± 8.1 %, which is acceptable given the corresponding computational savings (Table 2).

Table 2 ESP computed at the 10 nuclear positions of hydronium and its two coordinated water molecules for the single charge, no charge, OEC_{frozen} and $OEC_{crystal}$ models. Statistics are based on percent differences with respect to the single charge model. All values in atomic units.

ESP computed at	Single charge	No charge	OEC_{frozen}	$OEC_{crystal}$
point 1	-2.38E-01	-3.31E-01	-2.40E-01	-2.29E-01
point 2	-2.44E-01	-3.32E-01	-2.40E-01	-1.79E-01
point 3	-2.20E-01	-2.97E-01	-2.26E-01	-2.16E-01
point 4	-2.17E-01	-2.95E-01	-2.20E-01	-2.05E-01
point 5	-2.69E-01	-3.46E-01	-2.76E-01	-2.69E-01
point 6	-2.72E-01	-3.67E-01	-2.82E-01	-2.71E-01
point 7	-2.73E-01	-3.41E-01	-2.78E-01	-2.67E-01
point 8	-2.10E-01	-2.90E-01	-2.19E-01	-2.10E-01
point 9	-2.28E-01	-3.01E-01	-2.32E-01	-2.20E-01
point 10	-2.12E-01	-3.00E-01	-2.12E-01	-1.90E-01
average abs. percent diff.	**0 %**	**34.5 %**	**2.1 %**	**5.5 %**
std. deviation	**0**	**4.9**	**1.3**	**8.1**
maximum abs. percent difference	0 %	41.4 %	4.3 %	26.7 %
minimum abs. percent difference	0 %	24.8 %	0.01 %	0.01 %

There are two isomers of the S_2 state. Previous modeling[61] has predicted that the +III oxidation state is preferred for Mn4 when O5 is coordinated to it, whereas +IV is preferred when O5 is closer to the other Mn atoms. In the 3ARC crystal structure, O5 is quite distant from Mn4 and thus we chose the corresponding +IV oxidation state for this manganese ion. Our analysis agrees with reference [43] where the +IV state is found to be preferred.

The initial system is represented in Figure 3.4. The lithium ion and the amino acids were treated by Molecular Mechanics (MM) except for the functional groups ($–COO^-$ or $–NH_3^+$) directly interacting with Mn, Cl^- or the network of hydrogen-bonded water molecules and the $–CH_2–$ fragment nearest to these functional groups. Note again that the lithium ion is only used to provide a positive charge, representing the effect of the remainder of the metal-oxo complex, and at the MM level it is actually a gaussian-smeared point charge. Some MM atoms have incomplete valence because the peptide chain in the protein was truncated. Their spatial coordinates were frozen to their X-ray structure values in all geometry optimizations. All non-MM atoms are treated together as the quantum mechanical (QM) system, and all following computations were performed with Q-Chem.[62]

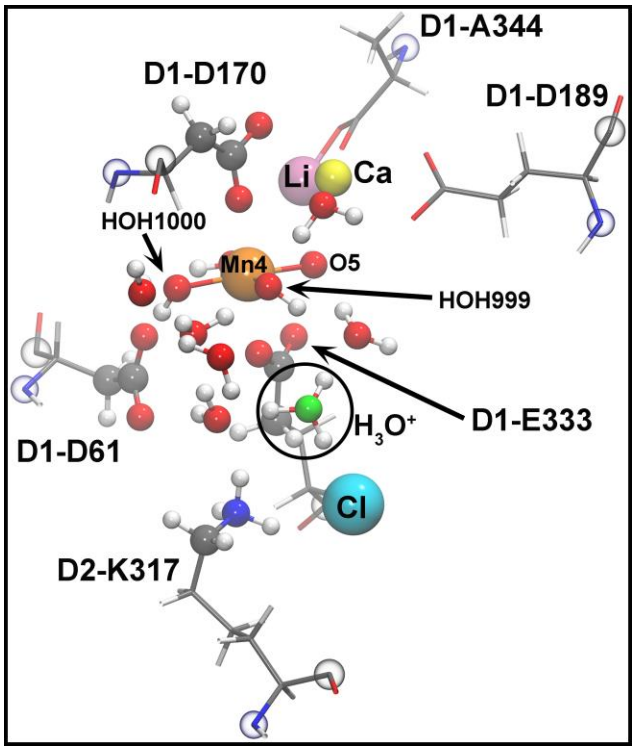

Figure 3.4 Initial QM/MM model of the protonated water cluster and its environment. QM atoms represented as balls and sticks, MM atoms as sticks only, with the exception of Li, which was treated with MM but is represented as a sphere for convenience. The translucent atoms have incomplete valence and their coordinates

are frozen to their X-ray structure value. The water bearing the extra proton has been encircled and the oxygen changed to green. C in gray, N in blue, O in red, H in white, Mn in orange, Ca in yellow, Li in pink and Cl in cyan.

To avoid the costly computation of vibrational frequencies at the QM/MM level, which is only available by finite difference in Q-Chem 4.3, it is desirable to retain only the minimal functional groups from the amino acids and to treat the system fully quantum mechanically. For this purpose, we followed several steps. First, the QM system was frozen and only the MM atoms were optimized using the AMBER99[63] force field. In a second step, a QM/MM optimization was performed, where the QM and MM systems are described above and in Figure 3.4. At first, constraints were applied to the protonated water molecule to avoid spurious effects in a geometry far from equilibrium. As the geometric gradient became smaller, the constraints on water were released, and only those on the backbone atoms with incomplete valences were kept. In the third step, the amino acids were truncated and capped with H atoms as represented in Figure 3.5. The positions of the capping hydrogens were relaxed by optimizing them with all other atoms frozen. In the final step, the capping hydrogens and their connected atoms, represented with translucent spheres on Figure 3.5, were frozen while all other atoms were reoptimized. The QM system was treated by B3LYP-D3[64-66]/6-31G*[67-69] and a Lebedev grid[70] with 50 radial points and 194 angular points.

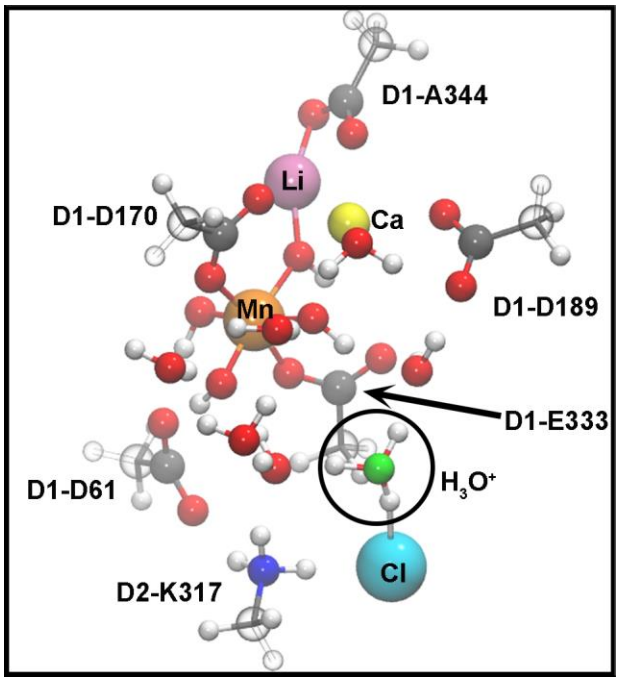

Figure 3.5 Final QM model of the protonated water cluster and its environment. The translucent atoms coordinates are frozen for all optimizations. The predicted protonated cluster is shown inside the circle with the oxygen in green. Color of atoms: carbon, gray; nitrogen, blue; oxygen, red; hydrogen, white; manganese, orange; calcium, yellow; lithium, pink; and chloride in cyan.

Vibrational frequencies and intensities were computed at the optimized geometry with the partial Hessian capability of Q-Chem.[71-72] The partial Hessian computation excludes all atoms that were frozen in the optimization, since their geometric gradient is non-vanishing and the associated second derivatives cannot be identified with vibrational frequencies. The chloride ion was replaced successively by bromide and nitrate, the geometry reoptimized with B3LYP-D3/6-31G*, and the frequencies recomputed. All geometries were verified to be minima on the potential energy surface by the absence of imaginary frequencies. This also indicates that the small (50,194) grid chosen for the computations yields reasonable results.

3.4 Results

In this study, we test the proposal that chloride is directly involved in regulating proton transfer reactions in PSII through the stabilization of hydronium ions in the internal, proton transfer pathway. Reaction-induced FT-IR (RIFT-IR) spectroscopy is used to study the effect of anion exchange on a 2830 cm^{-1} band in the S_2 state. Quantum mechanical (QM) calculations on a small OEC model are used to interpret the experimental results and to propose a role for chloride during the S_1 to S_2 transition.

Figure 3.6 presents the 3200-1750 cm^{-1} region of the RIFT-IR S_1 to S_2 spectrum derived from PSII samples at pH 7.5 (for mid-infrared region, see Figure 3.2). Figure 3.6, A and B are reproduced from previous work (see ref[46]) and were acquired at 263 K. In Figure 3.6A, a broad positive infrared band centered at 2830 cm^{-1} is observed and is assigned to the S_2 state.[46] A band with similar frequency has been attributed to the S_2 state in other types of samples, for example, PSII maintained at pH 6.0 and pH 7.5 and at 190 K[46] and 263 K.[45, 47-48] This S_2 infrared band was assigned to W_n^+, an internal protonated cluster of five water molecules (see Table 1 for an experimental overview).[45-48] An example of the $H_2{}^{18}O$ solvent isotope shift at 263 K is presented in Figure 3.6B, in which a large ^{18}O induced shift in frequency is observed, compared to Figure 3.6A. This large $H_2{}^{18}O$ shift was attributed previously to a reorganized, protonated water cluster of different size at this temperature (Figure 3.6A and B).[46] See also Table 1, which summarizes results from other groups on this topic. A reported failure to observe the $H_2{}^{18}O$ solvent isotope shift in two cases in the literature may have been due to lack of efficient exchange.

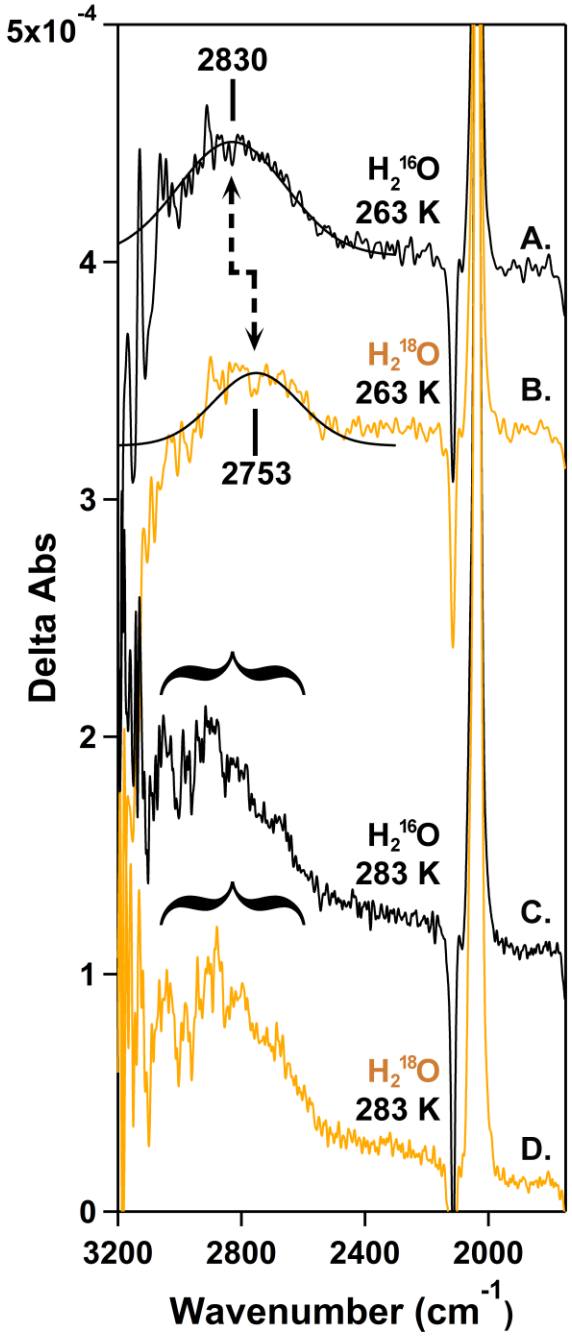

Figure 3.6 $H_2{}^{18}O$ solvent exchange effects on a PSII infrared band as a function of temperature. RIFT-IR difference spectra (3200-1750 cm^{-1} region) are associated with the S_1 to S_2 transition at pH 7.5. S_2-minus-S_1 spectra were recorded either at (A-B) 263 K or (C-D) 283 K. Samples: (A) PSII in $H_2{}^{16}O$ buffer; (B) PSII in $H_2{}^{18}O$ buffer; (C) Cl-PSII in $H_2{}^{16}O$ buffer; and (D) Cl-PSII in $H_2{}^{18}O$ buffer. Each spectrum is an average of (A, B) 5 and (C, D) 10 data acquisition loops acquired from (A) 12, (B) 11, (C) 16 and (D) 15 different samples. The data in (A, B) are reproduced from ref[47]. In (A) and (B), Gaussian fits are shown as superimposed solid lines. Data were fit with

IGOR (Wavemetrics, Lake Oswego, OR) software. Spectra in (A, B) were acquired at 8 cm^{-1} resolution; spectra in (C, D) were acquired at 4 cm^{-1} resolution.

Figure 3.6C and D present the S_2-minus-S_1 spectrum obtained from Cl-PSII at 283 K and pH 7.5. At 283 K, a large apparent ^{18}O shift is not apparent, and this result is attributed to inability to trap a reorganized species at this temperature (Figure 3.6C and D). However, with 4 cm^{-1} spectral resolution, additional sharp bands are resolved in the 2830 cm^{-1} region, and small $H_2{}^{18}O$-induced isotope shifts, expected as ~10 cm^{-1}, are indeed observed in these bands (Figure 3.6C and D, brackets). The coupling that occurs between hydronium, water, and amino acid side chains complicates a simple interpretation of the isotope shifts at this temperature. Note that coupling of H_3O^+ bands with amino acid vibrational bands may rationalize ^{15}N shifts reported previously in the literature in this region (Table 1 and ref. [44]). The observation of this $H_2{}^{18}O$ shift in Cl-PSII at 283 K unambiguously supports assignment of the 2830 cm^{-1} band to water. The low frequency of this water band, which is downshifted significantly from that of bulk water, supports assignment to a hydronium ion. The sensitivity to calcium depletion and ammonia treatment, previously reported (Table 1), supports assignment to an internal hydronium ion.

Figure 3.7A shows that depletion of chloride through sulfate treatment leads to a reduction in the intensity of the 2830 cm^{-1} band (Figure 3.7B, green). Accompanying dramatic decreases in intensity in the mid-infrared region were also observed (compare Figure 3.7C and Figure 3.7D, green). Compared to previous mid-infrared report in the literature,[26,40,72] the intensity change in the mid-infrared region in Figure 3.7 is more extensive, consistent with more effective chloride depletion in this type of preparation and with this method.

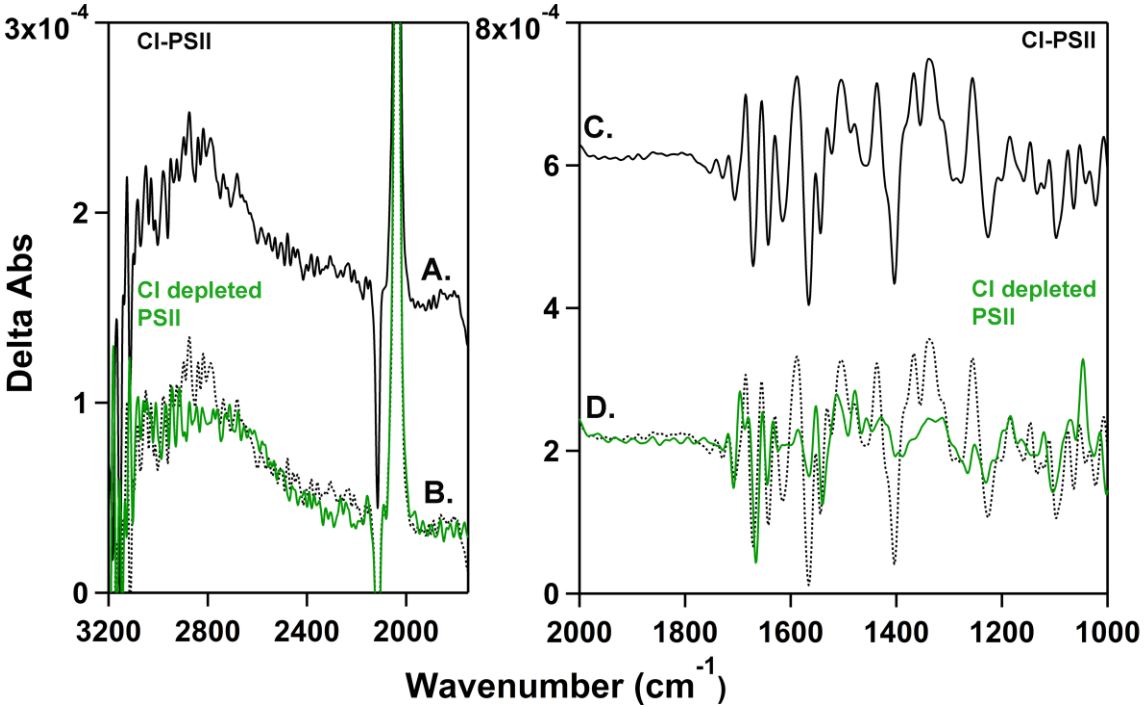

Figure 3.7 RIFT-IR spectrum of the (A) 3200-1750 cm^{-1} region and (B) 2000-1000 cm^{-1} region associated with the S_1 to S_2 transition. Data acquired using either (A, C) Cl-PSII or (B, D) Cl-depleted PSII (green) samples at 283 K in pH 7.5 buffer. In (B, D), the Cl-PSII spectrum from (A, C) has been overlaid for comparison (black dotted line). The data were smoothed using a 17 point Savitzky–Golay algorithm. Each spectrum is an average of 5 data acquisition loops acquired from (A) 12 and (B) 11 different samples.

To test for a possible role of chloride in maintaining W_n^+, anion exchange with two other activating anions, bromide and nitrate, was performed, and the results are summarized in Figure 3.8.

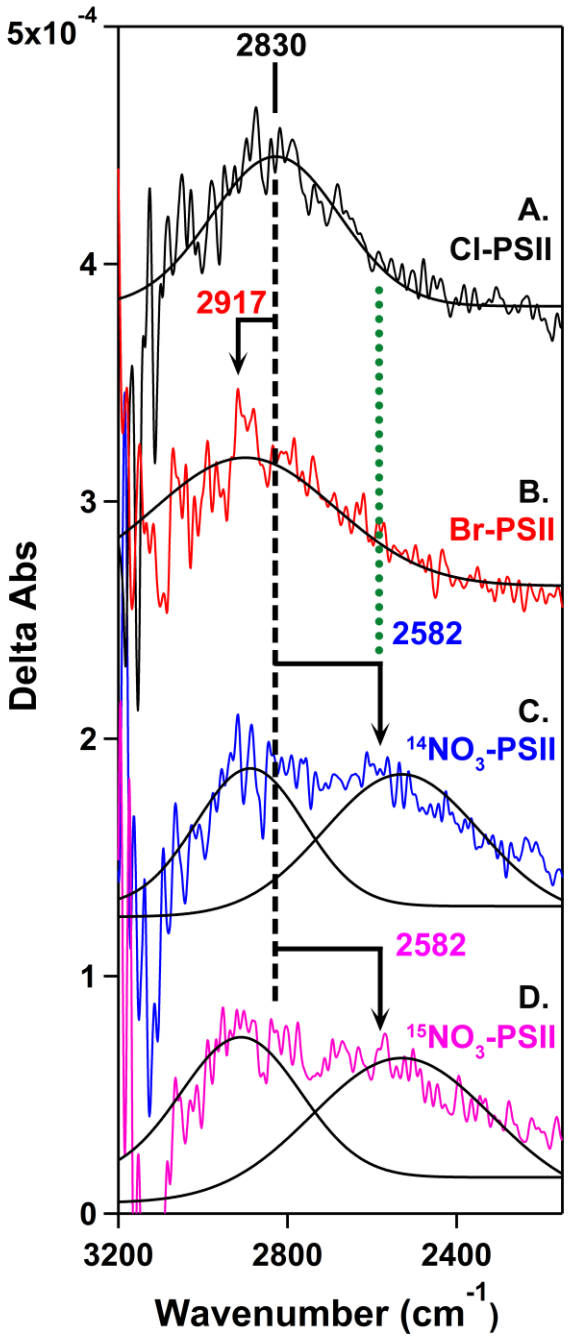

Figure 3.8 Anion substitution effects on a PSII infrared band at 283 K. RIFT-IR difference spectra (3200-2150 cm^{-1} region) are associated with the S_1 to S_2 transition at pH 7.5. S_2-minus-S_1 spectra derived from samples: (A, black) Cl-PSII; (B, red) Br-PSII; (C, blue) $^{14}NO_3$-PSII; and (D, pink) $^{15}NO_3$-PSII. Each spectrum is an average of 5 data acquisition loops acquired from (A) 12, (B) 10, and (C and D) 8 different samples. A 17-point smoothing has been applied to the data using the Savitzky–Golay algorithm. Gaussian functions are shown superimposed as solid lines. Data were fit with IGOR (Wavemetrics, Lake Oswego, OR) software.

In Figure 3.8B (red), C (blue) and D (pink), the 3200-2150 cm^{-1} regions acquired from Br-PSII, $^{14}NO_3$-PSII and $^{15}NO_3$-PSII samples are presented. Figure 3.8A shows the analogous band in Cl-PSII samples. Bromide exchange (Figure 3.8B, red) upshifts the 2830 cm^{-1} band by 87 cm^{-1}, to 2917 cm^{-1} in Br-PSII. In $^{14}NO_3$-PSII (Figure 3.8C, blue), part of the 2830 cm^{-1} band shifts down, with a new positive band appearing at ~2582 cm^{-1}. As shown in Figure 3.8D, pink, data obtained in $Na^{15}NO_3$-containing buffer are indistinguishable from the $^{14}NO_3$-PSII data. Hence, vibrational modes of the nitrate anion that involve significant nitrogen displacement do not contribute to this spectral region. Note that the literature contains reports of anion replacement and depletion in "salt washed" PSII and BBY membranes.[26,40,72] However, the 2800 cm^{-1} region was not reported in those previous studies.

To interpret our experimental results, QM calculations on a model of the OEC were conducted (Figure 3.5). The model comprised seven free water molecules, manganese, calcium, chloride and additional stabilizing ligands as detailed above. A hydronium ion was found to be stabilized in close proximity to the chloride. Chloride was computationally substituted by bromide and nitrate, and the geometry of the model was allowed to relax. The anion substitutions did not affect significantly the structure of the hydronium ion or the positions of water molecules in the model.

The final geometry optimized structure with chloride (Figure 3.5) was used to compute vibrational frequencies (Figure 3.9). A relevant portion of the predicted infrared spectrum is shown in Figure 3.9.

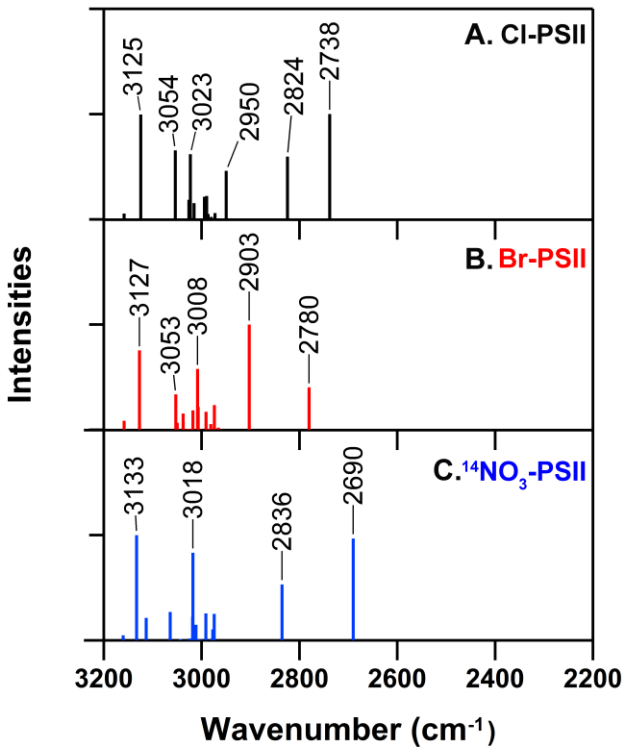

Figure 3.9 Computed IR spectrum (3200-2200 cm^{-1} region) of the geometry optimized model in Fig. 2 containing either (A) chloride, (B) bromide, or (C) nitrate. The normalized intensities are plotted along the Y-axis.

Normal mode descriptions of the 2738, 2824, and 3125 cm^{-1} infrared bands are given in Figure 3.10, A-C. Bands at 2738 (WS_I) and 2824 cm^{-1} (WS_{II}) correspond mainly to stretching modes of the hydronium ion (Figure 3.9A). This result is in agreement with previous experimental and theoretical studies of gas phase, protonated water clusters.[73] The representative 3125 cm^{-1} normal mode is distinct from WS_I and WS_{II} in that this mode mainly involves atomic displacements of free OH groups and OH groups bound to metal ions.

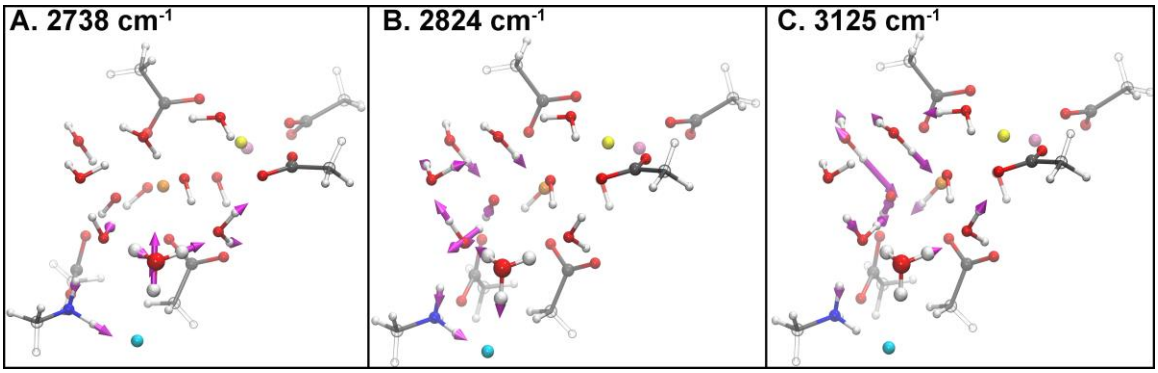

Figure 3.10 Normal mode analysis of the Cl-PSII model for (A) 2738 cm^{-1} (B) 2824 cm^{-1} and (C) 3125 cm^{-1}. Atomic displacements are displayed as purple arrows. Color of atoms: carbon, gray; nitrogen, blue; oxygen, red; hydrogen, white; manganese, orange; calcium, yellow; lithium, pink; and chloride, cyan.

Bromide was substituted for chloride in the model, and the geometry was reoptimized. The recalculated hydronium stretching frequencies shift due to bromide substitution (Figure 3.9B). The 2824 cm^{-1} (WS_{II}) band is predicted to downshift by 44 cm^{-1} to 2780 cm^{-1}, while the 2738 cm^{-1} (WS_{I}) band upshifts in frequency by 165 cm^{-1} (Figure 3.9B). When the predicted relative intensities are considered, the overall expectation derived from the bromide-substituted model is a shift of bands in the 2700-2800 cm^{-1} region to higher wavenumber. With nitrate substitution in the computational model, two bands are predicted at 2690 cm^{-1} and 2836 cm^{-1}. When compared to the chloride model, the 2738 cm^{-1} (WS_{I}) band downshifts by 48 cm^{-1} to give an intense 2690 cm^{-1} band, whereas the 2824 cm^{-1} (WS_{II}) band upshifts by 12 cm^{-1} to give a less intense 2836 cm^{-1} band. The overall prediction, considering frequency and intensity and based on this nitrate-substituted model, is a spectral downshift of the hydronium stretching mode.

For the bromide model, the 2780, 2903 and 3127 cm^{-1} normal modes are shown in Figure 3.11, A-C.

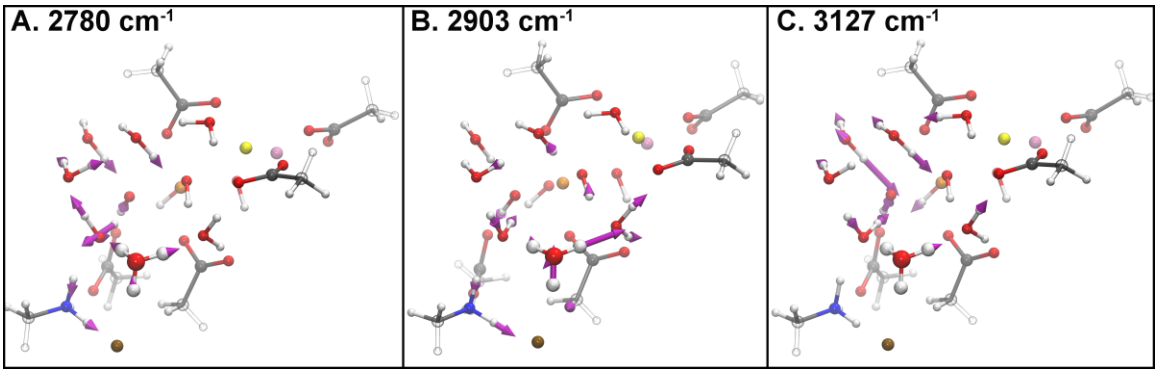

Figure 3.11 Normal mode analysis of the Br-PSII model for (A) 2780 cm^{-1} (B) 2903 cm^{-1} and (C) 3127 cm^{-1}. Atomic displacements are displayed as purple arrows. Color of atoms: carbon, gray; nitrogen, blue; oxygen, red; hydrogen, white; manganese, orange; calcium, yellow; lithium, pink; and bromide, brown.

Figure 3.12, A-C, presents the atomic displacements giving rise to the corresponding 2690, 2836 and 3133 cm^{-1} vibrational modes in NO_3-PSII. In all the models, the extra proton is stabilized as H_3O^+ on the water closest to the anion. As predicted for the chloride-substituted model, the WS_I and WS_{II} modes are localized mainly on the hydronium group in the bromide and nitrate-containing model. The representative >3100 cm^{-1} bands have very little contribution from the hydronium ion in any of the three models and are not as sensitive to anion substitution as WS_I and WS_{II} (Figure 3.10, Figure 3.11, and Figure 3.12).

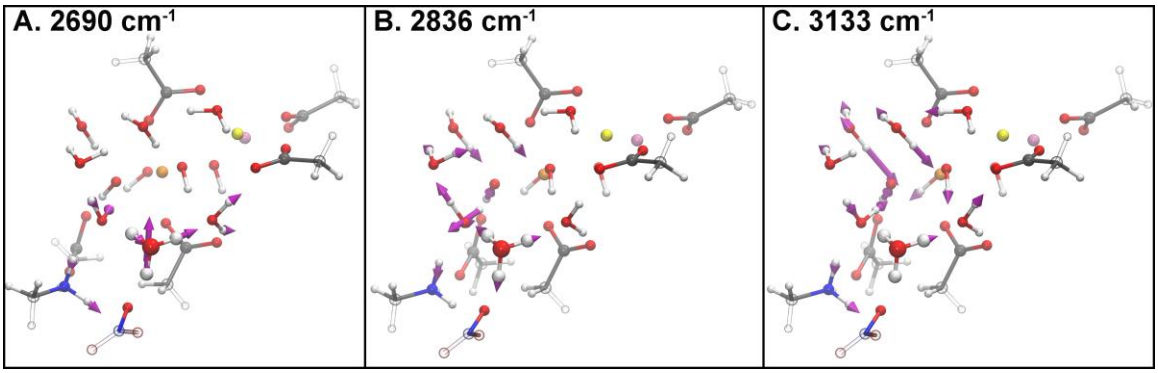

Figure 3.12 Normal mode analysis of the NO_3-PSII model for (A) 2690 cm^{-1} (B) 2836 cm^{-1} and (C) 3133 cm^{-1}. Atomic displacements are displayed as purple arrows. Color of atoms: carbon, gray; nitrogen, blue; oxygen, red; hydrogen, white; manganese, orange; calcium, yellow; and lithium, pink.

Comparing these predictions to PSII derived spectra, the frequency and intensity observed for W_n^+ in Cl-PSII is consistent with an assignment to WS_I/WS_{II} mode(s) of H_3O^+. In PSII, exchange of bromide induced a ~90 cm^{-1} upshift in the W_n^+ 2830 cm^{-1} band, and nitrate substitution induced a 250 cm^{-1} downshift in the W_n^+ band. Thus, the observed frequencies and directions of anion-induced shifts, are consistent with the theoretical predictions derived from the OEC model. While the direction of the shift matches the theoretical prediction, the magnitudes are different, especially for nitrate. This difference could be due to long-range electrostatic interactions and to geometric constraints on nitrate conformation induced by OEC amino acids, which are not included in our small model.

3.5 Discussion

We have used RIFT-IR spectroscopy and quantum mechanical calculations to investigate the role of chloride in PSII proton transfer. Theoretical treatment of a minimal OEC model predicts stabilization of a hydronium ion near the chloride ion. The bromide

and nitrate substituted analogs also stabilize the hydronium ion *in silico*. In the chloride model, normal mode analysis predicts two infrared bands at 2738 and 2824 cm^{-1}, which originate from localized stretching vibrations of the hydronium group. This prediction is in excellent agreement with the experimental data and ^{18}O isotope exchange data, which assign bands with significant absorption at 2830 cm^{-1} to a small, protonated water cluster in the S_2 state. Previous assignments of this band have been discussed extensively[45-48] and have been summarized in Table 1. At 263 K, a large $H_2{}^{18}O$ solvent exchange effect is observed for the 2830 cm^{-1} band. This large, apparent isotope shift may be due to heterogeneity in cluster size at this temperature, caused by the change in viscosity of $H_2{}^{18}O$.[47] At higher temperature, as employed here at 283 K, small isotope shifts in sharp spectral features are observed, consistent with the expected isotope shift due to ^{18}O exchange of 10 cm^{-1}.[74]

In PSII, we report that anion exchange with activating bromide and nitrate anions shifts the 2830 cm^{-1} band. In the case of bromide, the direction and magnitude of the anion exchange-induced shift agrees when theory and experiment are compared. An upshift of ~50-150 cm^{-1} is predicted while a 90 cm^{-1} upshift is observed in the bromide-substitution experiment. After nitrate exchange, a new downshifted band is observed at 2582 cm^{-1}, which corresponds to a downshift of 250 cm^{-1}. This is in qualitative agreement with the theoretically predicted downshift, however the magnitude of the theoretical, predicted shift, 48 cm^{-1}, is smaller. The structure employed for the OEC is a small model, designed to develop intuition concerning the contributions of the hydronium ion species. The model may not yet include all pertinent influences on the nitrate-supported hydronium ion. Note that the charge on the model is relevant to the S_2 state and that electronic structure

calculations on large OEC models have been reported previously.[75-77] However, these computationally more demanding models have not yet explicitly considered water protonation during the S_1 to S_2 transition.

To rationalize the direction of the frequency shifts, observed with different anions, we considered the size and basicity of the anions. The ionic radii of chloride, bromide, and nitrate are similar at 184, 196, and 189 pm.[78-79] Hence, substitution of bromide or nitrate for chloride should not be sterically disruptive. The proton-accepting ability of these conjugate bases can be assessed based on the pK_a values of their corresponding acids, HCl, HBr, and HNO_3. HNO_3 (pK_a -1.4) is the weakest acid, followed by HCl (pK_a -7) and then HBr (pK_a -9), which is the strongest acid.[79] Therefore, nitrate is the strongest conjugate base in the series and has a strong, stabilizing interaction with the neighboring hydronium ion. The observed effect on the spectrum is analogous to the influence of strengthening hydrogen bonds, i.e., a downshifting of vibrational bands. The opposite effect on spectral bands is observed in bromide, which is the weakest base in the series. Because of its larger size and weaker affinity for the proton, bromide causes the proton to be weakly bound to the neighboring water molecule, thereby causing an upshift of the infrared bands relative to chloride. In addition to the direction of the observed shifts, the magnitudes can also be rationalized by the difference in the pK_a values of the acids. Chloride and bromide are much closer in pK_a compared to nitrate. Hence, the magnitude of the anion-induced shift is much larger for the nitrate substitution, compared to the bromide substitution.

The experimentally observed 2830 cm^{-1} band in the S_2 state is quite broad, and this can be due to several contributing factors. First, inhomogeneous broadening could play a major role. Observed frequencies are dependent on the size, shape and environment of the

contributing hydronium ions. The spectrum is a superposition of contributions from hydronium ions in similar but not identical environments. Second, besides the 2738 and 2824 cm^{-1} bands arising from vibrations of the hydronium ion, there are additional bands in the 3200-2700 cm^{-1} region predicted in the anion-substituted spectra by the small OEC model. For example, in the Cl-PSII calculated spectrum, there are predicted bands at 2950, 3023, 3054, and 3125 cm^{-1}. These bands contain contributions from N-H stretches of K317, O-H stretches of free water molecules, and Mn-bound hydroxides. It is possible that these underlying vibrations contribute to the overall broad infrared band that is experimentally observed. The observation that chloride depletion does not completely eliminate the 2830 cm^{-1} band lends credence to this idea.

By structural analogy with two other chloride-dependent enzymes, α-amylase and ACE, it has been proposed that chloride exerts its effect on PSII activity by a conformational gating mechanism, which tunes the pK_a of acidic residues involved in the proton transfer pathway.[80] For example, chloride has been proposed to prevent a salt bridge formation between the side chains of D1-D61 and D2-K317. D1-D61 is a part of the putative proton exit pathway. Chloride is proposed to make D1-D61 an efficient proton acceptor by regulating its pK_a and/or correctly positioning the aspartate side chain (Figure 3.1 and Figure 2.12). Theoretical[43, 81] and mutagenesis studies in cyanobacterial PSII[41-42] have provided support for this idea. For example, in a recent computational study, the effects of chloride depletion on the generation of the S_2 state was investigated.[43] It was concluded that in the absence of chloride, the deprotonation of a Mn-bound water becomes unfavorable. In another study, the role of D1-D61 was investigated in detail in cyanobacteria (Table 1).[82] The broad ~2800 cm^{-1} band was found to be eliminated in the

D1-D61A mutant. This observation implies a role of D1-D61 in maintaining and stabilizing the network required for proton transfer. The results reported in the current study are consistent with these existing proposals in the literature.

In our work, we show that, in addition to this putative role for chloride in conformational gating, chloride plays a direct role maintaining internal proton transfer networks, which involve water in PSII. Although chloride is not required kinetically for the S_1 to S_2 transition,[25, 32] chloride may play a structural role during this transition, which is not rate limiting. Our results are consistent with a mechanism in which chloride stabilizes a S_2 proton transfer intermediate during photosynthetic water oxidation.

3.6 Conclusions

Water functions as both a substrate and catalyst for proton transfer during photosynthetic oxygen evolution. Based on our experimental results, the intermediary protonated cluster of water molecules, W_n^+, formed during the S_1 to S_2 transition, is proposed to be near the chloride ion (Figure 3.1C and Figure 2.12). This conclusion is based on the significant shifts observed in the vibrational spectrum after anion exchange and depletion in PSII. Our theoretical model predicts that all three anions, chloride, bromide, and nitrate, stabilize a protonated water cluster. This finding provides a rationalization of activity retention in all three anion-substituted PSII samples. Our work provides the first evidence for the involvement of the chloride ion in regulating proton transfer by internal water networks in photosystem II.

3.7 References

1. Schuster, P.; Zundel, G.; Sandorfy, C., *Hydrogen Bond; Recent Developments in Theory and Experiments*, North-Holland Publishing Company: Amsterdam, Holland, 1976.

2. Knight, C.; Voth, G. A. The Curious Case of the Hydrated Proton. *Acc. Chem. Res.* **2011,** *45*, 101-109.

3. Kulig, W.; Agmon, N. A 'Clusters-in-Liquid'method for Calculating Infrared Spectra Identifies the Proton-Transfer Mode in Acidic Aqueous Solutions. *Nat. Chem.* **2013,** *5*, 29-35.

4. Mohammed, O. F.; Pines, D.; Dreyer, J.; Pines, E.; Nibbering, E. T. Sequential Proton Transfer through Water Bridges in Acid-Base Reactions. *Science* **2005,** *310*, 83-86.

5. Garczarek, F.; Gerwert, K. Functional Waters in Intraprotein Proton Transfer Monitored by Ftir Difference Spectroscopy. *Nature* **2006,** *439*, 109-112.

6. Freier, E.; Wolf, S.; Gerwert, K. Proton Transfer Via a Transient Linear Water-Molecule Chain in a Membrane Protein. *Proc. Natl. Acad. Sci. U.S.A.* **2011,** *108*, 11435-11439.

7. Lórenz-Fonfría, V. A.; Furutani, Y.; Kandori, H. Active Internal Waters in the Bacteriorhodopsin Photocycle. A Comparative Study of the L and M Intermediates at Room and Cryogenic Temperatures by Infrared Spectroscopy. *Biochemistry* **2008,** *47*, 4071-4081.

8. Seibold, S. A.; Mills, D. A.; Ferguson-Miller, S.; Cukier, R. I. Water Chain Formation and Possible Proton Pumping Routes in *Rhodobacter Sphaeroides* Cytochrome *C* Oxidase: A Molecular Dynamics Comparison of the Wild Type and R481k Mutant. *Biochemistry* **2005,** *44*, 10475-10485.

9. Silverman, D. N.; McKenna, R. Solvent-Mediated Proton Transfer in Catalysis by Carbonic Anhydrase. *Acc. Chem. Res.* **2007,** *40*, 669-675.

10. Suga, M.; Akita, F.; Hirata, K.; Ueno, G.; Murakami, H.; Nakajima, Y.; Shimizu, T.; Yamashita, K.; Yamamoto, M.; Ago, H., et al. Native Structure of Photosystem Ii at 1.95 Å Resolution Viewed by Femtosecond X-Ray Pulses. *Nature* **2015,** *517*, 99-103.

11. Umena, Y.; Kawakami, K.; Shen, J.-R.; Kamiya, N. Crystal Structure of Oxygen-Evolving Photosystem Ii at a Resolution of 1.9 Å. *Nature* **2011,** *473*, 55-60.

12. Wei, X.; Su, X.; Cao, P.; Liu, X.; Chang, W.; Li, M.; Zhang, X.; Liu, Z. Structure of Spinach Photosystem Ii–Lhcii Supercomplex at 3.2 Å Resolution. *Nature* **2016,** *534*, 69-74.

13. Dau, H.; Zaharieva, I.; Haumann, M. Recent Developments in Research on Water Oxidation by Photosystem Ii. *Curr. Opin. Chem. Biol.* **2012,** *16*, 3-10.

14. Cox, N.; Pantazis, D. A.; Neese, F.; Lubitz, W. Biological Water Oxidation. *Acc. Chem. Res.* **2013,** *46*, 1588-1596.

15. Kok, B.; Forbush, B.; McGloin, M. Cooperation of Charges in Photosynthetic O_2 Evolution-I. A Linear Four Step Mechanism. *Photochem. Photobiol.* **1970,** *11*, 457-75.

16. Barry, B. A. Proton Coupled Electron Transfer and Redox Active Tyrosines in Photosystem Ii. *J. Photochem. Photobiol., B* **2011,** *104*, 60-71.

17. Renger, G.; Renger, T. Photosystem Ii: The Machinery of Photosynthetic Water Splitting. *Photosynth. Res.* **2008,** *98*, 53-80.

18. Gerken, S.; Brettel, K.; Schlodder, E.; Witt, H. Optical Characterization of the Immediate Electron Donor to Chlorophyll a^{+Ii} in O_2-Evolving Photosystem Ii Complexes Tyrosine as Possible Electron Carrier between Chlorophyll A_{ii} and the Water-Oxidizing Manganese Complex. *FEBS Lett.* **1988,** *237*, 69-75.

19. Petrie, S.; Pace, R. J.; Stranger, R. Resolving the Differences between the 1.9 Å and 1.95 Å Crystal Structures of Photosystem Ii: A Single Proton Relocation Defines Two Tautomeric Forms of the Water-Oxidizing Complex. *Angew. Chem. Int. Ed.* **2015,** *54*, 7120-7124.

20. Bao, H.; Dilbeck, P. L.; Burnap, R. L. Proton Transport Facilitating Water-Oxidation: The Role of Second Sphere Ligands Surrounding the Catalytic Metal Cluster. *Photosynth. Res.* **2013,** *116*, 215-229.

21. Haumann, M.; Hundelt, M.; Jahns, P.; Chroni, S.; Bögershausen, O.; Ghanotakis, D.; Junge, W. Proton Release from Water Oxidation by Photosystemii: Similar

Stoichiometries Are Stabilized in Thylakoids and Psii Core Particles by Glycerol. *FEBS Lett.* **1997,** *410*, 243-248.

22. Yocum, C. F. The Calcium and Chloride Requirements of the O_2 Evolving Complex. *Coord. Chem. Rev.* **2008,** *252*, 296-305.

23. Sandusky, P. O.; Yocum, C. F. The Chloride Requirement for Photosynthetic Oxygen Evolution. Analysis of the Effects of Chloride and Other Anions on Amine Inhibition of the Oxygen-Evolving Complex. *Biochim. Biophys. Acta* **1984,** *766*, 603-611.

24. Lindberg, K.; Vänngård, T.; Andréasson, L.-E. Studies of the Slowly Exchanging Chloride in Photosystem Ii of Higher Plants. *Photosynth. Res.* **1993,** *38*, 401-408.

25. Wincencjusz, H.; van Gorkom, H. J.; Yocum, C. F. The Photosynthetic Oxygen Evolving Complex Requires Chloride for Its Redox State S2→ S3 and S3→ S0 Transitions but Not for S0→ S1 or S1→ S2 Transitions. *Biochemistry* **1997,** *36*, 3663-3670.

26. Hasegawa, K.; Kimura, Y.; Ono, T.-a. Chloride Cofactor in the Photosynthetic Oxygen-Evolving Complex Studied by Fourier Transform Infrared Spectroscopy. *Biochemistry* **2002,** *41*, 13839-13850.

27. Baranov, S.; Haddy, A. An Enzyme Kinetics Study of the Ph Dependence of Chloride Activation of Oxygen Evolution in Photosystem Ii. *Photosynth. Res.* **2016**, 1-16.

28. Lindberg, K.; Andréasson, L.-E. A One-Site, Two-State Model for the Binding of Anions in Photosystem Ii. *Biochemistry* **1996,** *35*, 14259-14267.

29. Homann, P. H. Chloride Relations of Photosystem Ii Membrane Preparations Depleted of, and Resupplied with, Their 17 and 23 Kda Extrinsic Polypeptides. *Photosynth. Res.* **1988,** *15*, 205-220.

30. Bricker, T. M.; Roose, J. L.; Fagerlund, R. D.; Frankel, L. K.; Eaton-Rye, J. J. The Extrinsic Proteins of Photosystem Ii. *Biochimica et Biophysica Acta, Bioenergetics* **2012,** *1817*, 121-142.

31. Roose, J. L.; Frankel, L. K.; Mummadisetti, M. P.; Bricker, T. M. The Extrinsic Proteins of Photosystem Ii: Update. *Planta* **2016**, 1-20.

32. Wincencjusz, H.; Yocum, C. F.; Van Gorkom, H. J. Activating Anions That Replace Cl-in the O2-Evolving Complex of Photosystem Ii Slow the Kinetics of the Terminal Step in Water Oxidation and Destabilize the S2 and S3 States. *Biochemistry* **1999,** *38*, 3719-3725.

33. Lanyi, J. K. Halorhodopsin: A Light-Driven Chloride Ion Pump. *Annual review of biophysics and biophysical chemistry* **1986,** *15*, 11-28.

34. Morrison, M.; Schonbaum, G. R. Peroxidase-Catalyzed Halogenation. *Annu. Rev. Biochem* **1976,** *45*, 861-888.

35. Feller, G.; le Bussy, O.; Houssier, C.; Gerday, C. Structural and Functional Aspects of Chloride Binding to Alteromonas Haloplanctis A-Amylase. *J. Biol. Chem.* **1996,** *271*, 23836-23841.

36. Skeggs, L. T.; Marsh, W. H.; Kahn, J. R.; Shumway, N. P. The Existence of Two Forms of Hypertensin. *J. Exp. Med.* **1954,** *99*, 275-282.

37. Wei, L.; Alhenc-Gelas, F.; Corvol, P.; Clauser, E. The Two Homologous Domains of Human Angiotensin I-Converting Enzyme Are Both Catalytically Active. *J. Biol. Chem.* **1991,** *266*, 9002-9008.

38. Coleman, W. J. Chloride Binding Proteins: Mechanistic Implications for the Oxygen-Evolving Complex of Photosystem Ii. *Photosynth. Res.* **1990,** *23*, 1-27.

39. Lindberg, K.; Wydrzynski, T.; Vänngård, T.; Andréasson, L.-E. Slow Release of Chloride from ^{36}cl-Labeled Photosystem Ii Membranes. *FEBS Lett.* **1990,** *264*, 153-155.

40. Cooper, I. B.; Barry, B. A. Azide as a Probe of Proton Transfer Reactions in Photosynthetic Oxygen Evolution. *Biophys. J.* **2008,** *95*, 5843-5850.

41. Suzuki, H.; Yu, J.; Kobayashi, T.; Nakanishi, H.; Nixon, P. J.; Noguchi, T. Functional Roles of D2-Lys317 and the Interacting Chloride Ion in the Water Oxidation Reaction of Photosystem Ii as Revealed by Fourier Transform Infrared Analysis. *Biochemistry* **2013,** *52*, 4748–4757.

42. Pokhrel, R.; Service, R. J.; Debus, R. J.; Brudvig, G. W. Mutation of Lysine 317 in the D2 Subunit of Photosystem Ii Alters Chloride Binding and Proton Transport. *Biochemistry* **2013,** *52*, 4758-4773.

43. Amin, M.; Pokhrel, R.; Brudvig, G. W.; Badawi, A.; Obayya, S. Effect of Chloride Depletion on the Magnetic Properties and the Redox Leveling of the Oxygen-Evolving Complex in Photosystem Ii. *J. Phys. Chem. B* **2016,** *120*, 4243-4248.

44. Barry, B. A.; Brahmachari, U.; Guo, Z. Tracking Reactive Water and Hydrogen-Bonding Networks in Photosynthetic Oxygen Evolution. *Acc. Chem. Res.* **2017,** *50*, 1937-1945.

45. Polander, B. C.; Barry, B. A. Detection of an Intermediary, Protonated Water Cluster in Photosynthetic Oxygen Evolution. *Proc. Natl. Acad. Sci. U.S.A.* **2013,** *110*, 10634-9.

46. Guo, Z.; Barry, B. A. Cryogenic Trapping and Isotope Editing Identify a Protonated Water Cluster as an Intermediate in the Photosynthetic Oxygen-Evolving Reaction. *J. Phys. Chem. B* **2016,** *120*, 8794-8808.

47. Brahmachari, U.; Barry, B. A. Dynamics of Proton Transfer to Internal Water During the Photosynthetic Oxygen-Evolving Cycle. *J. Phys. Chem. B* **2016,** *120*, 11464-11473.

48. Polander, B. C.; Barry, B. A. Calcium, Strontium, and Protein Dynamics During the S_2 to S_3 Transition in the Photosynthetic Oxygen-Evolving Cycle. *J. Phys. Chem. Lett.* **2013,** *4*, 3356-3362.

49. Berthold, D. A.; Babcock, G. T.; Yocum, C. F. A Highly Resolved, Oxygen-Evolving Photosystem Ii Preparation from Spinach Thylakoid Membranes: Epr and Electron-Transport Properties. *FEBS Lett.* **1981,** *134*, 231-234.

50. Mishra, R. K.; Ghanotakis, D. F. Selective Extraction of Cp 26 and Cp 29 Proteins without Affecting the Binding of the Extrinsic Proteins (33, 23 and 17 Kda) and the Dcmu Sensitivity of a Photosystem Ii Core Complex. *Photosynth. Res.* **1994,** *42*, 37-42.

51. Guo, Z.; Barry, B. A. Calcium, Ammonia, Redox-Active Tyrosine Yz, and Proton-Coupled Electron Transfer in the Photosynthetic Oxygen-Evolving Complex. *J. Phys. Chem. B* **2017,** *121*, 3987-3996.

52. Cooper, I. B.; Barry, B. A. Perturbations at the Chloride Site During the Photosynthetic Oxygen-Evolving Cycle. *Photosynth. Res.* **2007,** *92*, 345-356.

53. Barry, B. A. Tyrosyl Radicals in Photosystem Ii. *Methods Enzymol.* **1995,** *258*, 303-319.

54. Wincencjusz, H.; Yocum, C. F.; van Gorkom, H. J. S-State Dependence of Chloride Binding Affinities and Exchange Dynamics in the Intact and Polypeptide-Depleted O2 Evolving Complex of Photosystem Ii. *Biochemistry* **1998,** *37*, 8595-8604.

55. Noguchi, T.; Sugiura, M. Flash-Induced Fourier Transform Infrared Detection of the Structural Changes During the S-State Cycle of the Oxygen-Evolving Complex in Photosystem Ii. *Biochemistry* **2001,** *40*, 1497-1502.

56. Polander, B. C.; Barry, B. A. Calcium and the Hydrogen-Bonded Water Network in the Photosynthetic Oxygen-Evolving Complex. *J. Phys. Chem. Lett.* **2013,** *4*, 786-791.

57. Hillier, W.; Babcock, G. T. S-State Dependent Fourier Transform Infrared Difference Spectra for the Photosystem Ii Oxygen Evolving Complex. *Biochemistry* **2001,** *40*, 1503-1509.

58. Berman, H. M.; Westbrook, J.; Feng, Z.; Gilliland, G.; Bhat, T. N.; Weissig, H.; Shindyalov, I. N.; Bourne, P. E. The Protein Data Bank. *Nucleic Acids Res.* **2000,** *28*, 235-242.

59. Vriend, G. What If: A Molecular Modeling and Drug Design Program. *Journal of molecular graphics* **1990,** *8*, 52-56.

60. Dilbeck, P. L.; Hwang, H. J.; Zaharieva, I.; Gerencser, L.; Dau, H.; Burnap, R. L. The D1-D61n Mutation in *Synechocystis* Sp. Pcc 6803 Allows the Observation of Ph-Sensitive Intermediates in the Formation and Release of O_2 from Photosystem Ii. *Biochemistry* **2012,** *51*, 1079-1091.

61. Siegbahn, P. E. Water Oxidation Energy Diagrams for Photosystem Ii for Different Protonation States, and the Effect of Removing Calcium. *Phys. Chem. Chem. Phys.* **2014,** *16*, 11893-11900.

62. Shao, Y.; Gan, Z.; Epifanovsky, E.; Gilbert, A. T. B.; Wormit, M.; Kussmann, J.; Lange, A. W.; Behn, A.; Deng, J.; Feng, X., et al. Advances in Molecular Quantum Chemistry Contained in the Q-Chem 4 Program Package. *Mol. Phys.* **2015,** *113*, 184-215.

63. Wang, J.; Cieplak, P.; Kollman, P. A. How Well Does a Restrained Electrostatic Potential (Resp) Model Perform in Calculating Conformational Energies of Organic and Biological Molecules? *J. Comput. Chem.* **2000,** *21*, 1049-1074.

64. Becke, A. D. Density-Functional Thermochemistry. Iii. The Role of Exact Exchange. *J. Chem. Phys.* **1993,** *98*, 5648-5652.

65. Lee, C.; Yang, W.; Parr, R. G. Development of the Colle-Salvetti Correlation-Energy Formula into a Functional of the Electron Density. *Physical Review B* **1988,** *37*, 785-789.

66. Grimme, S.; Antony, J.; Ehrlich, S.; Krieg, H. A Consistent and Accurate Ab Initio Parametrization of Density Functional Dispersion Correction (Dft-D) for the 94 Elements H-Pu. *J. Chem. Phys.* **2010,** *132*, 154104.

67. Francl, M. M.; Pietro, W. J.; Hehre, W. J.; Binkley, J. S.; Gordon, M. S.; DeFrees, D. J.; Pople, J. A. Self-Consistent Molecular Orbital Methods. Xxiii. A Polarization-Type Basis Set for Second-Row Elements. *J. Chem. Phys.* **1982,** *77*, 3654-3665.

68. Hariharan, P. C.; Pople, J. A. The Influence of Polarization Functions on Molecular Orbital Hydrogenation Energies. *Theoretica chimica acta* **1973,** *28*, 213-222.

69. Hehre, W. J.; Ditchfield, R.; Pople, J. A. Self—Consistent Molecular Orbital Methods. Xii. Further Extensions of Gaussian—Type Basis Sets for Use in Molecular Orbital Studies of Organic Molecules. *J. Chem. Phys.* **1972,** *56*, 2257-2261.

70. Lebedev, V. Values of the Nodes and Weights of Ninth to Seventeenth Order Gauss-Markov Quadrature Formulae Invariant under the Octahedron Group with Inversion. *USSR Computational Mathematics and Mathematical Physics* **1975,** *15*, 44-51.

71. Besley, N. A.; Metcalf, K. A. Computation of the Amide I Band of Polypeptides and Proteins Using a Partial Hessian Approach. *J. Chem. Phys.* **2007,** *126*, 035101.

72. Besley, N. A.; Bryan, J. A. Partial Hessian Vibrational Analysis of Organic Molecules Adsorbed on Si (100). *J. Phys. Chem. C* **2008,** *112*, 4308-4314.

73. Headrick, J. M.; Diken, E. G.; Walters, R. S.; Hammer, N. I.; Christie, R. A.; Cui, J.; Myshakin, E. M.; Duncan, M. A.; Johnson, M. A.; Jordan, K. D. Spectral Signatures of Hydrated Proton Vibrations in Water Clusters. *Science* **2005,** *308*, 1765-1769.

74. Kandori, H.; Shichida, Y. Direct Observation of the Bridged Water Stretching Vibrations inside a Protein. *J. Am. Chem. Soc.* **2000,** *122*, 11745-11746.

75. Sproviero, E. M.; Gascon, J. A.; McEvoy, J. P.; Brudvig, G. W.; Batista, V. S. Quantum Mechanics/Molecular Mechanics Study of the Catalytic Cycle of Water Splitting in Photosystem Ii. *J. Am. Chem. Soc.* **2008,** *130*, 3428-3442.

76. Siegbahn, P. E. Water Oxidation Mechanism in Photosystem Ii, Including Oxidations, Proton Release Pathways, O—O Bond Formation and O_2 Release. *Biochim. Biophys. Acta* **2013,** *1827*, 1003-1019.

77. Nakamura, S.; Ota, K.; Shibuya, Y.; Noguchi, T. Role of a Water Network around the Mn_4cao_5 Cluster in Photosynthetic Water Oxidation: A Fourier Transform Infrared Spectroscopy and Quantum Mechanics/Molecular Mechanics Calculation Study. *Biochemistry* **2016,** *55*, 597-607.

78. Addison, C. C.; Logan, N., *Advances in Inorganic Chemistry and Radiochemistry*, Emeléus, H. J.; Sharpe, A. G., Eds. Academic Press: New York, 1964; Vol. 6, pp 71-142.

79. Greenwood, N. N.; Earnshaw, A., *Chemistry of the Elements (Second Edition)*. Butterworth-Heinemann: Oxford, 1997, http://dx.doi.org/10.1016/B978-0-7506-3365-9.50023-7p 789-887.

80. Pokhrel, R.; McConnell, I. L.; Brudvig, G. W. Chloride Regulation of Enzyme Turnover: Application to the Role of Chloride in Photosystem Ii. *Biochemistry* **2011,** *50*, 2725-2734.

81. Rivalta, I.; Amin, M.; Luber, S.; Vassiliev, S.; Pokhrel, R.; Umena, Y.; Kawakami, K.; Shen, J.-R.; Kamiya, N.; Bruce, D. Structural–Functional Role of Chloride in Photosystem Ii. *Biochemistry* **2011,** *50*, 6312-6315.

82. Debus, R. J. Evidence from Ftir Difference Spectroscopy That D1-Asp61 Influences the Water Reactions of the Oxygen-Evolving Mn_4cao_5 Cluster of Photosystem Ii. *Biochemistry* **2014,** *53*, 2941-2955.

CHAPTER 4. ENGINEERING PROTON TRANSFER IN PHOTOSYNTHETIC OXYGEN EVOLUTION: CHLORIDE, NITRATE AND TREHALOSE REORGANIZE A HYDROGEN-BONDING NETWORK

Reprinted with permission from *The Journal of Physical Chemistry B*

Brahmachari, U.; Guo, Z.; Konecny, S.; Obi, C.; and Barry, B. A. Engineering Proton Transfer in Photosynthetic Oxygen Evolution: Chloride, Nitrate, and Trehalose Reorganize a Hydrogen-Bonding Network. *J. Phys. Chem. B* **2018,** *122*, 6702-6711.

4.1 Abstract

Photosystem II oxidizes water at a Mn_4CaO_5 cluster. Oxygen evolution is accompanied by proton release through a 35 Å hydrogen-bonding network to the lumen. The mechanism of this proton transfer reaction is not known, but the reaction is dependent on chloride. Here, vibrational spectroscopy defines the functional properties of the proton-transfer network using chloride, bromide, and nitrate as perturbative agents. As assessed by peptide C=O frequencies, bromide substitution yields a spectral Stark shift, due to its increase in ionic radius. Nitrate substitution leads to more complex spectral changes, consistent with an overall increase in hydrogen bonding interactions with the peptide backbone. The effects are similar to spectral changes previously documented in site-directed mutations in a putative lumenal pathway. Importantly, the effects of nitrate are reversed by the osmolyte, trehalose. Trehalose is known to alter hydrogen-bonding interactions in proteins. Trehalose addition also reverses a shift in an internal hydronium ion signal, consistent with an alteration in its pK_a value and a change in the basicity of bound nitrate. The spectra provide evidence that the proton transfer pathway contains peptide carbonyl groups, internal water, a hydronium ion, and amino acid side chains. These experiments also show that the proton transfer pathway functionally adapts to changes in electric field, pK_a, and hydrogen bonding and thereby optimizes proton transfer to the lumen.

4.2 Introduction

Photosynthetic oxygen evolution by green plants and cyanobacteria is directly responsible for sustaining aerobic life on earth.[1] The mechanism of the water oxidation reaction, which generates molecular oxygen, is not yet fully understood. The site of oxygen

evolution is the multisubunit membrane protein, photosystem II (PSII). Several transmembrane subunits, along with three extrinsic subunits, comprise PSII. [2-4] The integral membrane-spanning subunits are D1, D2, CP47 and CP43. Oxygen evolution follows a period four oscillatory pattern.[5] At its catalytic core, PSII contains a Mn_4CaO_5 cluster (Figure 4.1), referred to as the oxygen-evolving complex (OEC). Stepwise, photoinduced oxidation of the OEC causes it to sample a series of oxidation states called the S_n states (Figure 4.1B), where n corresponds to the number of accumulated oxidizing equivalents (n=0-4).[5] These oxidation reactions are driven by charge separation involving redox active cofactors after light absorption. Oxidation of the dimeric chlorophyll donor, P_{680}, initiates the oxidation of the redox active tyrosine Y_Z (D1-Y161).[6] The powerful oxidant $Y_Z^{\bullet}$ is thereby generated, which subsequently oxidizes the OEC.[7-8] This oxidation reaction is repeated four times and leads to the generation of molecular oxygen.[9] After dark adaptation, the S_1 state is predominant. With each flash, the cycle advances to the next S-state. After reaching the S_3, state, the OEC reverts to its most reduced S_0 state by oxidizing water. This transition occurs through the metastable S_4 state.[5] Four flashes are therefore required to reset the OEC back to the S_1 state.

The S_1 to S_2 transition corresponds to a manganese oxidation reaction.[9] Figure 4.1B illustrates the S state cycle of proton release in sucrose-containing buffers. Four protons are released over one full S-state cycle, but the pattern of this release is not symmetrical. The S_0 to S_1 and S_2 to S_3 transitions are accompanied by the release of one proton, and the S_3 to S_0 transition is associated with the release of two protons. However, the S_1 to S_2 transition is not associated with proton release in sucrose buffers.[10] On this transition,

recent evidence suggests that an internal hydronium ion is formed and is stabilized on the proton transfer network.[11]

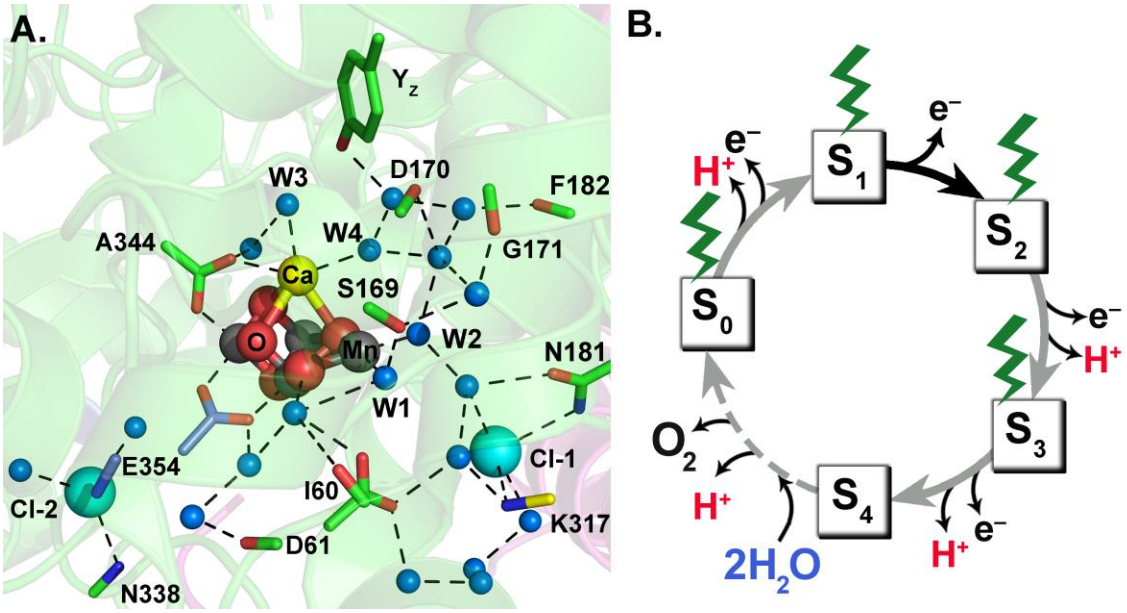

Figure 4.1 (A) Hydrogen-bonding network extending from the OEC to the chloride ions. The figure was created using the cyanobacterial PSII X-ray structure (PDB ID: 4UB6[2]). Blue spheres represent water molecules involved in the predicted hydrogen-bonding network. Chloride ions are represented as cyan spheres. Amino acid residues are shown as sticks, and hydrogen-bonding interactions are represented by dashed lines. Residues from the PSII subunits, D1, D2, and CP43 are green, yellow, and blue, respectively. Mn_4CaO_5 cluster: calcium, yellow; manganese, gray; oxygen, red. (B) S-state cycle[5] leading to photosynthetic water oxidation; the step-wise oxidation is achieved in PSII using laser flashes. The current study describes the S_1 to S_2 transition.

Chloride ions are required for optimal oxygen evolution activity.[12] The mechanism by which this anion exerts its influence on oxygen evolution is still under investigation. Two chloride ions, Cl-1 and Cl-2, are located 6.6 and 7.5 Å away from the OEC, respectively[2] (Figure 4.1A). A third chloride ion, ~25 Å away from the metal cluster, is evident in the cyanobacterial PSII structure, but is not assigned in a recently published plant PSII structure.[4] Recently, a nitrate-substituted cyanobacterial PSII structure has been

published but is not available yet for detailed analysis.[13] The S_2 to S_3 and S_3 to S_0 transitions exhibit a kinetic requirement for chloride.[14] Other monovalent ions have been tested for their ability to replace chloride and sustain oxygen evolution. The observed activation followed the series: $Cl^- > Br^- >> NO_3^- > NO_2^- > I^-$.[15]

There are very few examples of proteins that employ chloride as a cofactor in biology. Two other enzymes, α-amylase[16] and angiotensin-converting enzyme (ACE),[17] utilize chloride as a cofactor. One of the proposed roles for the chloride ion in PSII is as a regulator of proton transfer reactions. Studies comparing PSII to these enzymes have suggested that chloride requirement arises from a conformational gating mechanism, where chloride maintains the pK_a of residues involved in proton transfer.[18] Several theoretical[19-20] and experimental studies[13, 21-22] have provided support for this mechanism.

Previously, we have shown the effect of chloride substitution on the internal hydronium ion, which is detected as a 2830 cm^{-1} infrared band observed during the S_1 to S_2 transition.[11,23] This band has been proposed to arise from an internal, protonated water cluster, designated W_n^+.[24-26] Anion substitutions shifted the band in directions predicted by quantum mechanical calculations on a small model of the OEC. Based on these observations, we proposed that chloride stabilizes W_n^+, a trapped and intermediary, protonated water cluster on the internal proton exit pathway on this transition.[11] Although chloride has been reported to have no kinetic effect on this transition,[15] structural effects associated with stabilization of the hydronium cation may be of consequence on latter transitions.

In the present study, we employ reaction-induced FT-IR (RIFT-IR) spectroscopy

to investigate the mechanism of proton transfer and charge storage, and the role of chloride and activating anions in these processes. The stabilizing network is predicted to include peptide carbonyl groups, amino acid side chains, and water molecules. Therefore, infrared detectable amide C=O and W_n^+ vibrational frequencies can be used as markers for changes in the network.[27-29] We show that bromide and nitrate have significant effects on the infrared spectrum. Importantly, the enzyme is active in oxygen evolution in each case. Interestingly, the addition of trehalose, an osmolyte that increases hydrogen-bonding interactions, reverses the effects of nitrate. The trehalose effect implies that internal water molecules play important roles in proton storage and transfer. This study also provides evidence that chloride and other effective anions tune electrostatics and pK_a values in the proton transfer network. Remarkably, the results indicate that the network is robust and remains functional in spite of these changes in electrostatic and hydrogen bonding interactions. This attribute may be important in optimizing proton transfer to the lumen under a diverse set of physiological conditions.

4.3 Materials and Methods

PSII was isolated from market spinach. Membrane fragments enriched in PSII content, called BBY membranes, were obtained through Triton X-100 treatment.[30] Octylthioglucoside (OTG) was used to further purify PSII.[31] The PSII samples thus obtained (OTG-PSII) were suspended into 0.4 M sucrose, 50 mM 2-(N-morpholino)ethanesulfonic acid (MES)-NaOH, pH 6.0, and 15 mM NaCl buffer and stored at -70^{o}C.

Substitution of bromide and nitrate ions for chloride was accomplished by washing OTG-PSII three times with buffer containing 0.4 M sucrose, 50 mM 2-[4-(2-

hydroxyethyl)piperazin-1-yl]ethanesulfonic acid (HEPES)-NaOH, pH 7.5, and 15 mM sodium salt of the anion being exchanged. To generate nitrate- and bromide-substituted PSII (referred to as NO_3-PSII and Br-PSII, respectively), we used 15 mM $NaNO_3$ and NaBr, respectively. The chloride control, referred to as Cl-PSII, was obtained by using 15 mM NaCl in the same buffer as the other anions. To exchange NO_3-PSII into trehalose buffer, the third wash was performed with buffer containing 0.4 M trehalose, 50 mM HEPES-NaOH, pH 7.5, and 15 mM $NaNO_3$. Samples were aliquoted and frozen at -70^{o}C. Using literature protocols, chloride depletion was performed using sulfate treatment. See Supporting Information for more detail.[14, 32] Chloride-depleted, sulfate-treated PSII samples will be referred to as Cl-depleted PSII. Samples were frozen and stored at -70^{o}C after aliquoting.

Oxygen evolution assays were performed using a Clark-type electrode with freshly prepared 1 mM potassium ferricyanide ($K_3[Fe(CN)_6]$) and recrystallized 0.5 mM 2,6-dichlorobenzoquinone as external electron acceptors.[11] See Supporting Information for oxygen evolution rates and more detail concerning the measurements and characterization of the preparations. Samples for RIFT-IR experiments were prepared by performing the final pH 7.5 wash in the respective buffer. For Cl-PSII, Br-PSII, $^{14}NO_3$-PSII, and $^{15}NO_3$-PSII samples, the buffer contained 155 mM chloride, bromide, ^{14}N-nitrate, and ^{15}N-nitrate as well as 20 mM calcium from the corresponding calcium salt. For Cl-depleted samples, the final wash was performed in chloride-free buffer containing 0.4 M sucrose, 50 mM HEPES-NaOH, pH 7.5 and 10 mM $Ca(OH)_2$. A 100 mM buffered stock of ferricyanide was used to add 15 mM ferricyanide to all RIFT-IR samples. The only exception was Cl-PSII samples in $H_2{}^{18}O$ containing buffer. In that case, 15 mM ferricyanide was added to

RIFT-IR samples from a 1 M stock prepared in $H_2{}^{16}O$ buffer. All samples were subsequently pelleted by centrifugation (50,000 x *g*, 10 minutes, 4°C).

Literature protocols were used to perform RIFT-IR experiments at 283 K and pH 7.5.[28-29] The pellet obtained after centrifugation was spread between two CaF_2 windows (25 x 2 mm). The sample was then stabilized with a stream of nitrogen gas to yield a ratio of 2.3-3.3 between the O-H stretch (3370 cm^{-1}) and amide II (1550 cm^{-1}) bands. The sample was never dehydrated. Nitrogen treatment has only a small effect on the concentration of sucrose, trehalose, chloride and other anions. To estimate the magnitude of the concentration increase, gravimetric methods were used to measure sample weight before and after treatment with the nitrogen gas. In this experiment, the increase in analyte concentration due to nitrogen treatment was estimated as no more than 25%. To maintain a fixed path and prevent the appearance of interference fringes, a small piece of parafilm was wedged between the two windows. Silicone grease was applied to the edges of the windows, which were then sealed with parafilm to prevent sample dehydration during the experiment.

RIFT-IR experiments were performed using a Bruker IFS 66v/S instrument. Data acquisition parameters were: spectral resolution of 4 cm^{-1} for Cl-PSII samples in $H_2{}^{18}O$ buffer and corresponding $H_2{}^{16}O$ controls and 8 cm^{-1} for all other samples; Happ-Genzel apodization function; 60 kHz mirror speed; four levels of zero filling; and Mertz phase correction. A single saturated preflash from a 532 nm Nd-YAG laser (at 40 mJ/cm^2 power density) was applied to the PSII sample. The sample was then dark adapted for 20 minutes. A germanium window was used to block the internal HeNe laser of the FT-IR spectrometer. Following the dark adaptation, the sample was subjected to eight 532 nm actinic flashes.

Rapid scan data was collected for 5 seconds before and after each flash. One series of eight such flashes constituted one data collection loop. The first loop was followed by 15 minutes of dark adaptation after which the entire data collection loop, including the preflash and 20 minutes dark adaptation, was repeated four times. This protocol allows sufficient time to reset the sample to the S_1 state between loops. The difference spectra were generated by ratioing the single channel data preceding and following each actinic laser flash. Using the absorption spectrum (scans ratioed to background) of each sample, the intensity of the amide II band was determined. Using these intensities, the RIFT-IR difference spectra were normalized to an absorbance of 0.5. This step ensured that differences in path length and sample thickness were accounted for among all the difference spectra. The RIFT-IR difference spectra were then plotted and analyzed using IGOR (Wavemetrics, Lake Oswego, OR) software.

4.4 Results

Figure 4.2 presents the effects of anion exchange on the S_2-minus-S_1 RIFT-IR difference spectrum in the 1800-1200 cm^{-1} region as derived from Cl-PSII (A), Br-PSII (B), and NO_3-PSII (C) samples. The spectrum acquired from Cl-PSII samples (Figure 4.2) is similar to earlier reports from our laboratory, in which spectra were derived from PSII samples at 263 K.[26, 29] Distinctive bands in the three amide regions (amide I: 1650 cm^{-1}; amide II: 1550 cm^{-1}; amide III: 1400-1200 cm^{-1}) are observed. The frequencies and intensities of these bands are expected to be sensitive to intramolecular and intermolecular hydrogen bonding and will serve as probes of the environment around the chloride ion.

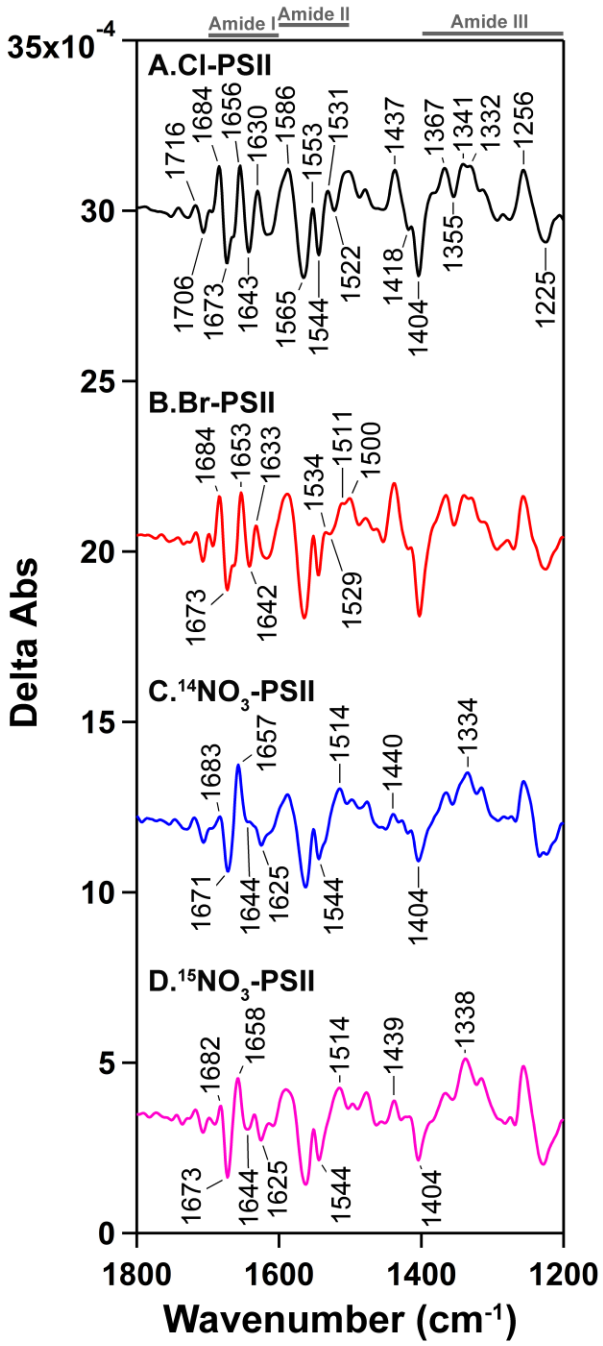

Figure 4.2 Effects of anion substitution on PSII at pH 7.5 and 283 K (1800-1200 cm^{-1} region). The S_2-minus-S_1 spectra were derived from (A, black) Cl-PSII; (B, red) Br-PSII; (C, blue) $^{14}NO_3$-PSII; and (D, pink) $^{15}NO_3$-PSII. Each spectrum contains the average of 5 data acquisition loops obtained from (A) 15, (B) 10, and (C and D) 8 different samples.

Figure 4.2B presents the S_2-minus-S_1 spectrum derived from Br-PSII samples. The spectrum is similar to the Cl-PSII spectrum (overlaid in Figure 4.3A). This similarity is easily rationalized because bromide is an activating anion and supports oxygen evolution at 89% of the chloride control. However, the chloride-minus-bromide double difference spectrum (Figure 4.4A) does identify spectral changes. Interestingly, a second derivative-shaped band is observed with frequencies of (+)1658, (-)1649, and (+)1628 cm^{-1}. Upon examining the overlaid data, this spectral feature can be attributed to a ~4 cm^{-1}, bromide-induced downshift of a derivative band at 1656/1643 cm^{-1} (Figure 4.3, inset). Spectral shifts observed in the remainder of the mid-infrared are of similar magnitude. Note that this altered spectrum is associated with enzymatic turnover through the bromide-substituted pathway.

In Figure 4.2C, the $^{14}NO_3$-PSII spectrum associated with the S_1 to S_2 transition is presented. Significant changes are evident when comparing these data to the Cl-PSII or Br-PSII spectra (overlaid in Figure 4.3). Complex changes are observed in the amide I (1650 cm^{-1}), amide II (1550 cm^{-1}), and amide III (1400-1200 cm^{-1}) regions. In particular, a 1630 cm^{-1} band, observed in Cl-PSII, is eliminated in NO_3-PSII. The analogous band is observed in Br-PSII at 1633 cm^{-1}. In addition, nitrate substitution alters a band at 1531(+)/1522(-) cm^{-1} and in the 1390-1330 cm^{-1} region. Note that when $^{14}NO_3$-PSII and $^{15}NO_3$-PSII are compared, no significant spectral changes are observed (Figure 4.2D). On the other hand, the chloride-minus-nitrate double difference spectrum, generated using the $^{14}NO_3$-PSII and $^{15}NO_3$-PSII data (Figure 4.4, B and C) does show significant spectral perturbations, as described above. These nitrate-altered spectra are also associated with light-induced turnover, although at lower steady state levels (29%) compared to Cl-PSII.

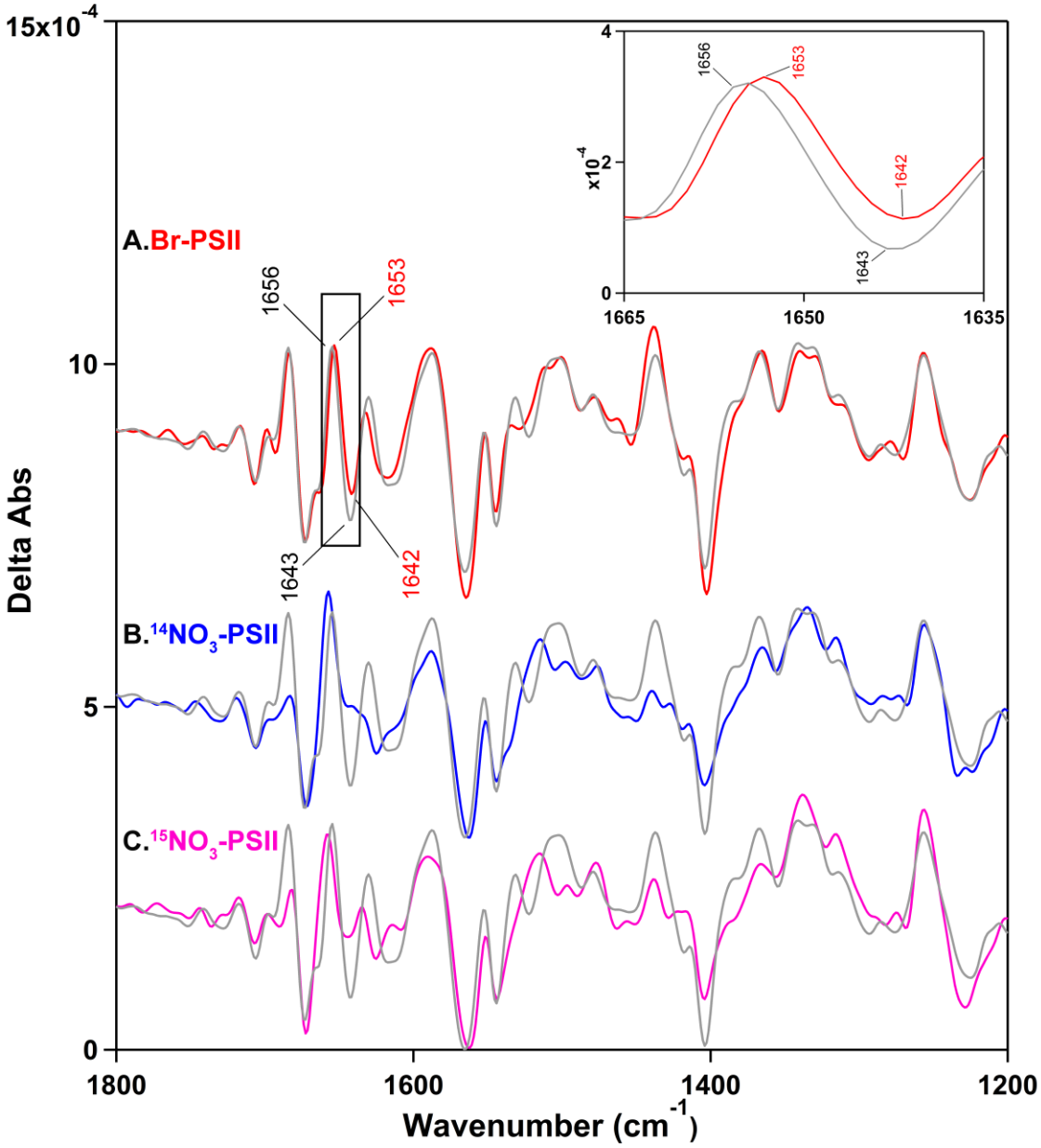

Figure 4.3 Overlay of RIFT-IR spectra (1800-1200 cm^{-1} region) associated with the S_1 to S_2 transition and effects of anion substitution at pH 7.5 and 283 K. Samples: in (A, B, C, gray) Cl-PSII; in (A, red) Br-PSII; in (B, blue) $^{14}NO_3$-PSII; and in (C, pink) $^{15}NO_3$-PSII. Inset: Br-PSII spectrum (red) overlaid with Cl-PSII spectrum (gray) in the 1665-1635 cm^{-1} region.

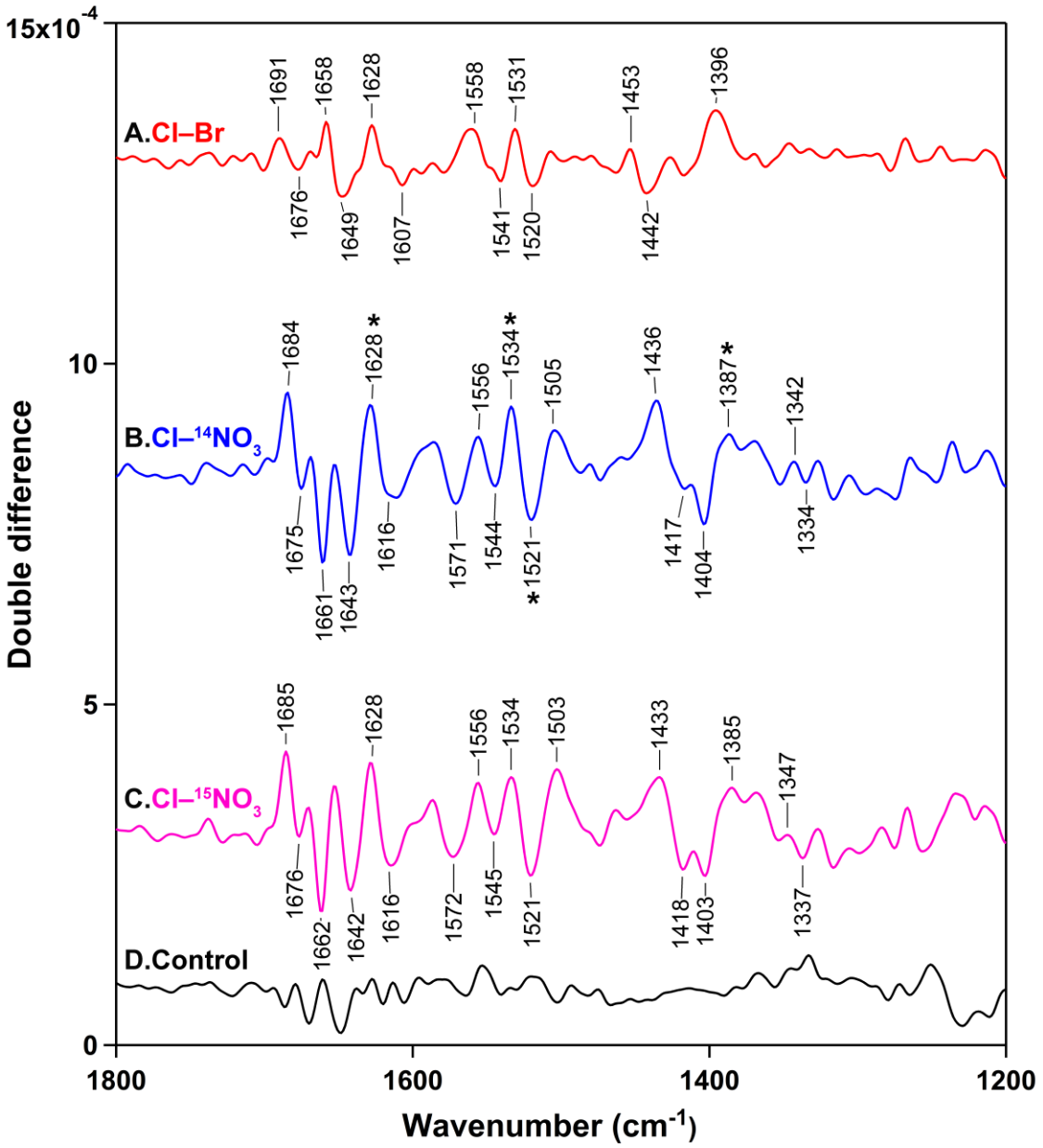

Figure 4.4 RIFT-IR double difference spectra (1800-1200 cm^{-1} region) showing the effects of anion substitution on PSII at pH 7.5 and 283 K. Double difference spectrum associated with the S_1 to S_2 transition for (A) Cl-minus-Br PSII; (B) Cl-minus-$^{14}NO_3$ PSII; and (C) Cl-minus-$^{15}NO_3$ PSII. (D) represents a control double difference generated by subtracting one half of the Cl-PSII data set from the other half and dividing by $\sqrt{2}$.

In the 1650 cm^{-1} region of the RIFT-IR spectrum, spectral bands arising from C=O groups of the protein are expected to make a major contribution to the spectrum. These

contributions can arise due to changes in hydrogen bonding and electrostatic interactions. However, a direct, overlapping contribution from water is also possible in this region. To test the assignment of the 1630 cm^{-1} band, which is altered by nitrate treatment, we employed $H_2{}^{18}O$ solvent exchange. Figure 4.5 presents the Cl-PSII spectrum in the 1800-1600 cm^{-1} region, recorded using 4 cm^{-1} resolution. In Figure 4.5B, Cl-PSII was exchanged into $H_2{}^{18}O$-containing buffer. In this region, bands from water are expected to originate from O-H bending modes and usually appear ~1650 cm^{-1}. As shown using the red asterisk in Figure 4.5, the 1630 cm^{-1} band is not altered by $H_2{}^{18}O$ exchange. This observation supports the assignment of this band to the peptide backbone and not to a water bending mode.

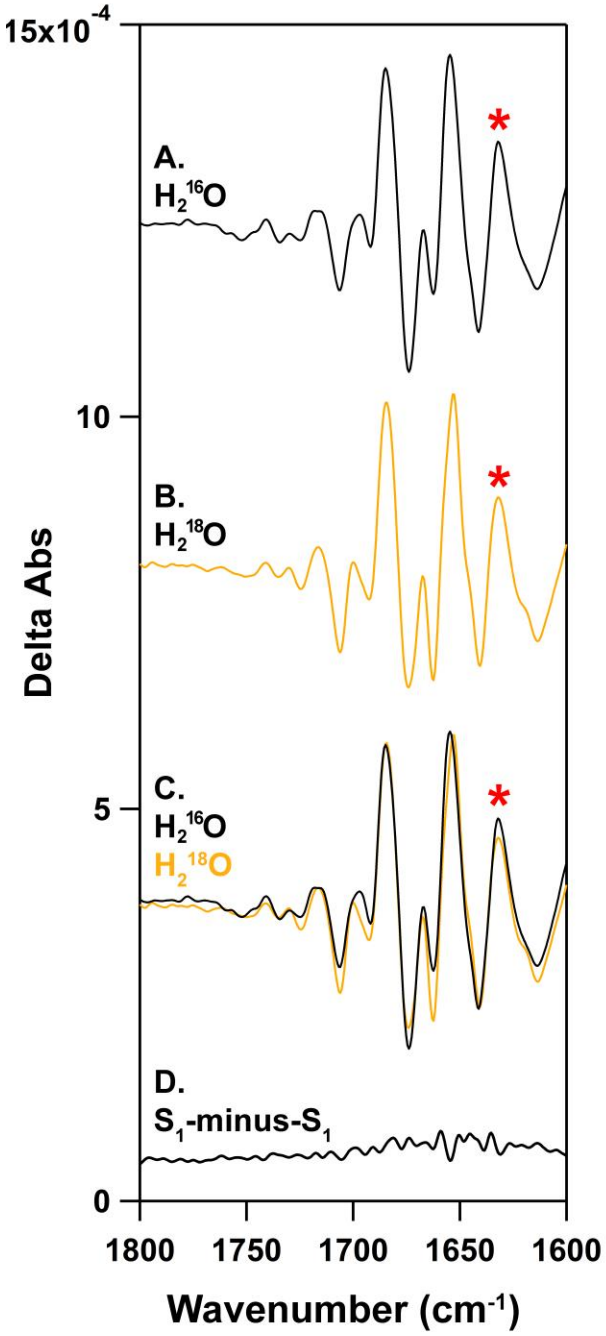

Figure 4.5 RIFT-IR spectra associated with $H_2{}^{18}O$ solvent exchange in Cl-PSII at pH 7.5 and 283 K (1800-1600 cm^{-1} region). The S_2-minus-S_1 difference spectra are derived from: (A) Cl-PSII in $H_2{}^{16}O$ buffer; (B) Cl-PSII in $H_2{}^{18}O$ buffer; and (C) overlay of data shown in (A) and (B). (D) represents the baseline before the first flash, as derived from the Cl-PSII samples. The red asterisk indicates the position of the 1630 cm^{-1} band. Each spectrum is an average of 10 data acquisition loops acquired from (A) 16, and (B) 15 different samples. Spectra were acquired at 4 cm^{-1} resolution.

To summarize, nitrate substitution induces amide band intensity changes; this effect is consistent with a perturbation of the OEC hydrogen-bonding network due to nitrate binding at the chloride site. Nitrate is an extended, planar molecule with many possible hydrogen-bonding interactions with its environment, when compared either to chloride or bromide. To test this idea, we used the cryoprotectant, trehalose, which is known to restore hydrogen-bonding networks in proteins.[33] Trehalose has been shown previously to reverse ammonia-induced changes in the OEC hydrogen-bonding network.[28] Figure 4.6 compares the amide I (A-D) and amide II (E-H) regions of NO_3-PSII in trehalose (Figure 4.6, C and G) and sucrose buffer (Figure 4.6, B and 4F). The 1630 cm^{-1} amide I signal, which was eliminated by nitrate substitution in sucrose, is partially restored when NO_3-PSII is suspended in trehalose-containing buffer (compare Figure 4.6, A and C). The 1531(+)/1522(-) cm^{-1} differential feature is also partially restored. In the absence of nitrate, trehalose has only a minor effect on the mid-infrared region of the spectrum, as previously reported.[28] Significantly, trehalose-induced changes in the 1630 cm^{-1}, 1531/1522 cm^{-1}, and amide III bands are specific to the use of nitrate-treated PSII and are not observed in the chloride-treated control (Figure 4.7).

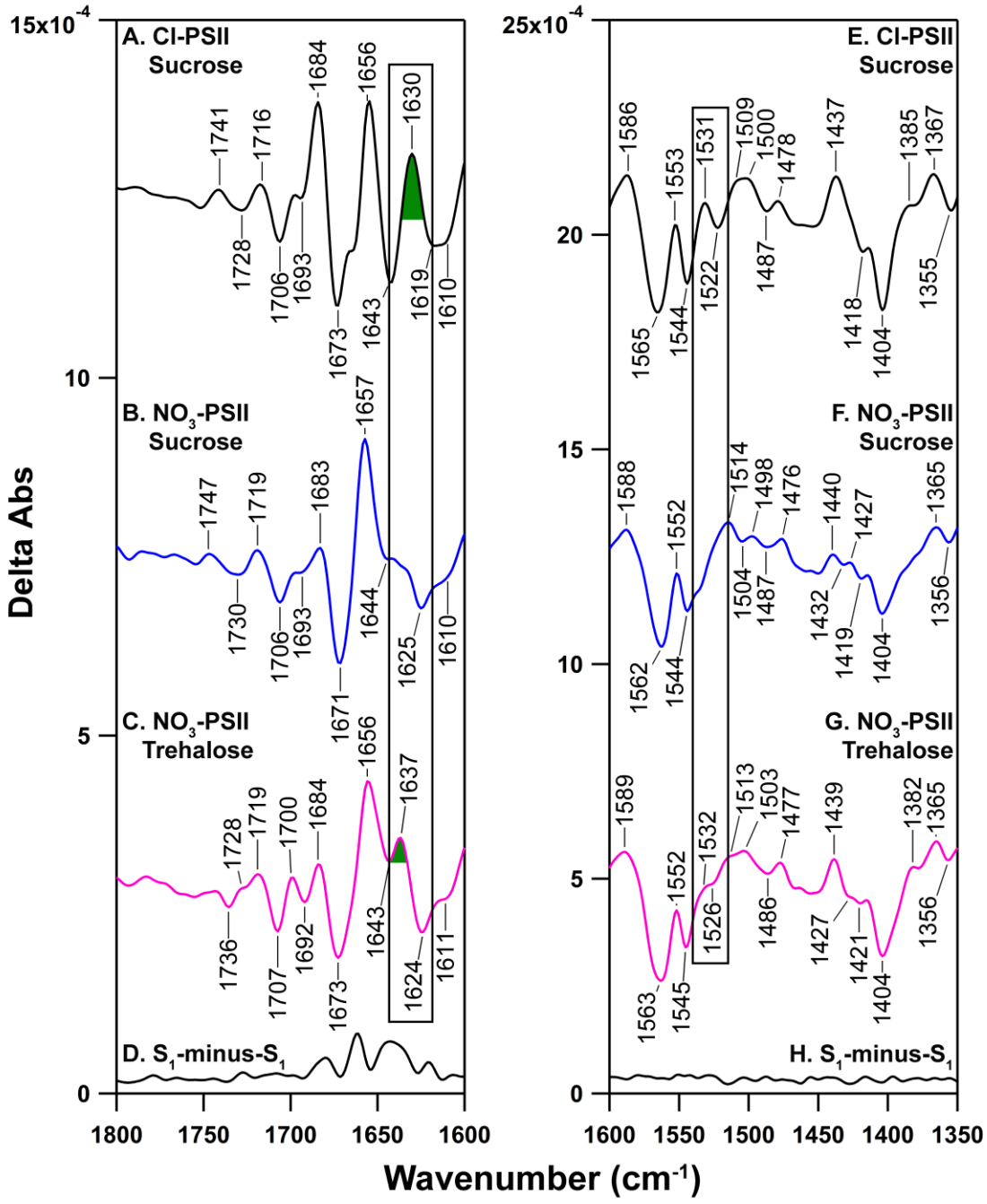

Figure 4.6 Trehalose-induced changes during the S_1 to S_2 transition in nitrate-substituted PSII at pH 7.5 and 283 K. RIFT-IR difference spectrum in the (A-D) 1800-1600 cm^{-1}; and (E-H) 1600-1350 cm^{-1} region. S_2-minus-S_1 difference spectra generated from (A, E, black) Cl-PSII samples in sucrose-containing buffer; (B, F, blue) $^{14}NO_3$-PSII samples in sucrose-containing buffer; and (C, G, pink) $^{14}NO_3$-PSII samples in trehalose-containing buffer. (D, H, black) represents the baseline before the first flash derived from Cl-PSII samples. Spectra in (A, B, E and F) are reproduced from Figure 2. The boxed regions are discussed in the text.

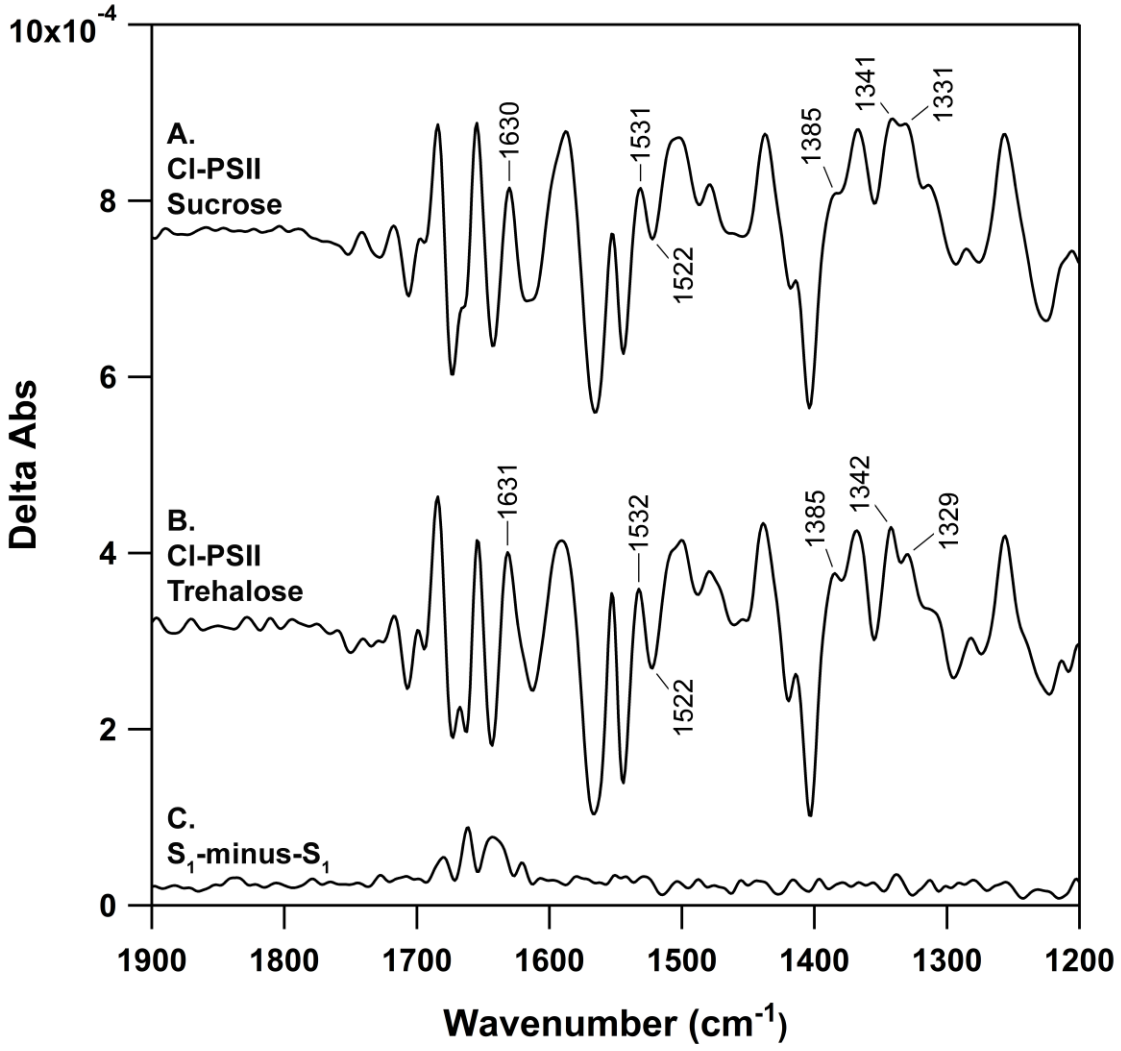

Figure 4.7 Trehalose and sucrose treatment of Cl-PSII and RIFT-IR spectra recorded at pH 7.5 and 283 K (1900-1200 cm^{-1}). S_2-minus-S_1 spectra are derived from Cl-PSII samples in (A) sucrose-containing buffer or (B) trehalose-containing buffer. In (C), the baseline before the first flash is shown. Each spectrum is an average of 5 data acquisition loops from (A) 15 and (B) 8 different samples.

We have recently reported the effect of anion exchange on a broad 2830 cm^{-1} band, assigned to the vibrations of a S_2 state, protonated water cluster, W_n^+.[11] Based on the anion-exchange induced shifts observed for the 2830 cm^{-1} band, we proposed that W_n^+ is influenced electrostatically by the chloride binding site(s). The 3200-2150 cm^{-1} region of Figure 4.6 is presented in Figure 4.8. As reported earlier,[11] the data exhibits a high signal-

to-noise ratio (~8), when comparing the 2830 cm^{-1} W_n^+ band to the peak-to-peak noise at 2220 cm^{-1}.

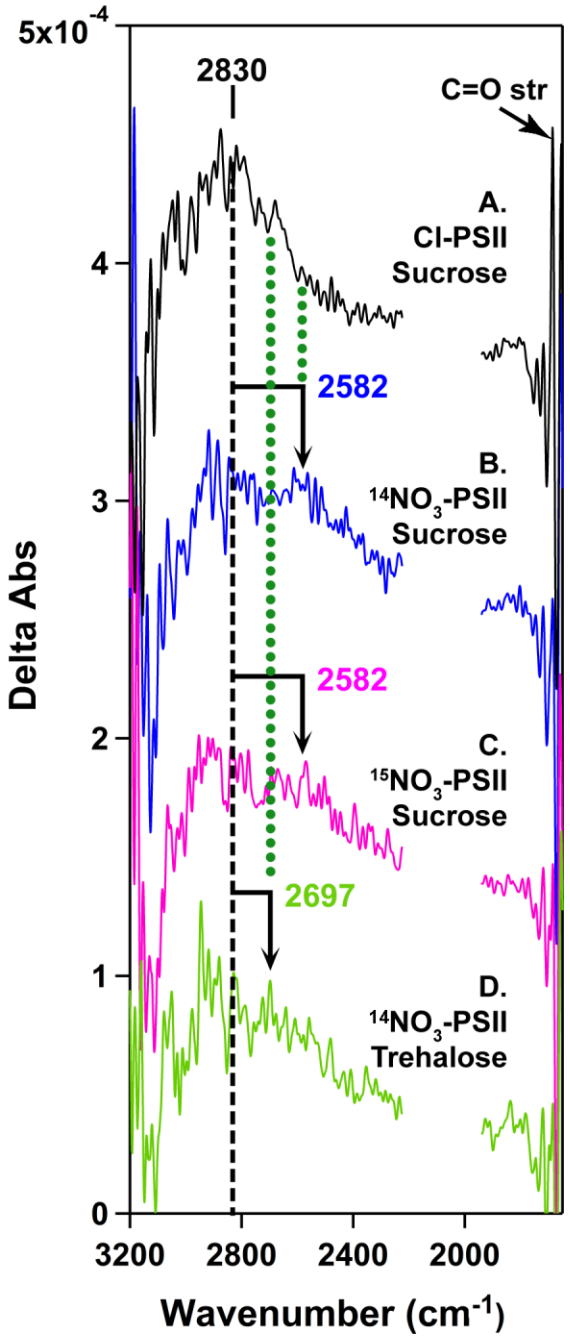

Figure 4.8 Effect of nitrate and trehalose on the W_n^+ infrared band at pH 7.5 and 283 K (3200-1650 cm^{-1} region). The S_2-minus-S_1 spectra are derived from samples: (A, black) Cl-PSII in sucrose-containing buffer; (B, blue) $^{14}NO_3$-PSII in sucrose-

containing buffer; (C, pink) $^{15}NO_3$-PSII in sucrose-containing buffer; and (D, green) $^{14}NO_3$-PSII in trehalose-containing buffer. Data were recorded at 8 cm^{-1} resolution. Each spectrum is an average of 5 data acquisition loops acquired from (A) 15, (B) 8, (C) 8, and (D) 9 different samples. A 17-point smoothing has been applied to the data using the Savitzky–Golay algorithm. Bands from ferricyanide and ferrocyanide have been removed for presentation purposes. The data in (B and C) are reproduced from ref[11].

In Figure 4.9, spectra were recorded from Cl-PSII in $H_2{}^{16}O$ (black) or $H_2{}^{18}O$ (yellow) buffer at 283 K. In previous work at 190 K or 263 K, a large ^{18}O downshift of the broad 2830 cm^{-1} band was observed.[25,26] This shift was previously attributed to a change in viscosity in $H_2{}^{18}O$ buffer at this temperature, which changes the size of the hydronium ion water shell. Figure 6 presents the results of $H_2{}^{18}O$ buffer exchange at 283 K. Spectra were acquired in $H_2{}^{16}O$ (Figure 4.9A) or $H_2{}^{18}O$ (Figure 4.9B); the data were divided into two pools and averaged to provide evidence of reproducibility of peak position and lineshape. In this context, the superposition of the $H_2{}^{16}O$ and $H_2{}^{18}O$ data (Figure 4.9C) provides evidence for complex solvent isotope shifts in the position of sharp spectral features and for alterations in the broad infrared lineshape of W_n^+. The effect is more subtle than the effects observed at lower temperature. Figure 4.9, inset presents spectra on an expanded scale to establish that 5-10 cm^{-1} $H_2{}^{18}O$-induced downshifts are observed in some of the sharp spectral features, which are superimposed on the broad band. As a negative control, one-half of the $H_2{}^{16}O$ data set is overlaid with the other half in Figure 4.9A. Peak position, lineshape, and many of the sharp spectral features reproduce in the sub-averages (Figure 4.9A). The reproducible positions and intensities of sharp spectral features are also evident in overlays of one half of the $H_2{}^{18}O$ data set with the other half (Figure 4.9B). By comparison, an overlay of $H_2{}^{18}O$ and $H_2{}^{16}O$ spectra exhibit solvent isotope-induced shifts (Figure 4.9C). The solvent isotope shifts, as well as the frequency

of the W_n^+ band,[24,25] are consistent with the assignment of the 2830 cm^{-1} signal to an internal, protonated water cluster (see discussion in ref[11, 26] and Table 1).

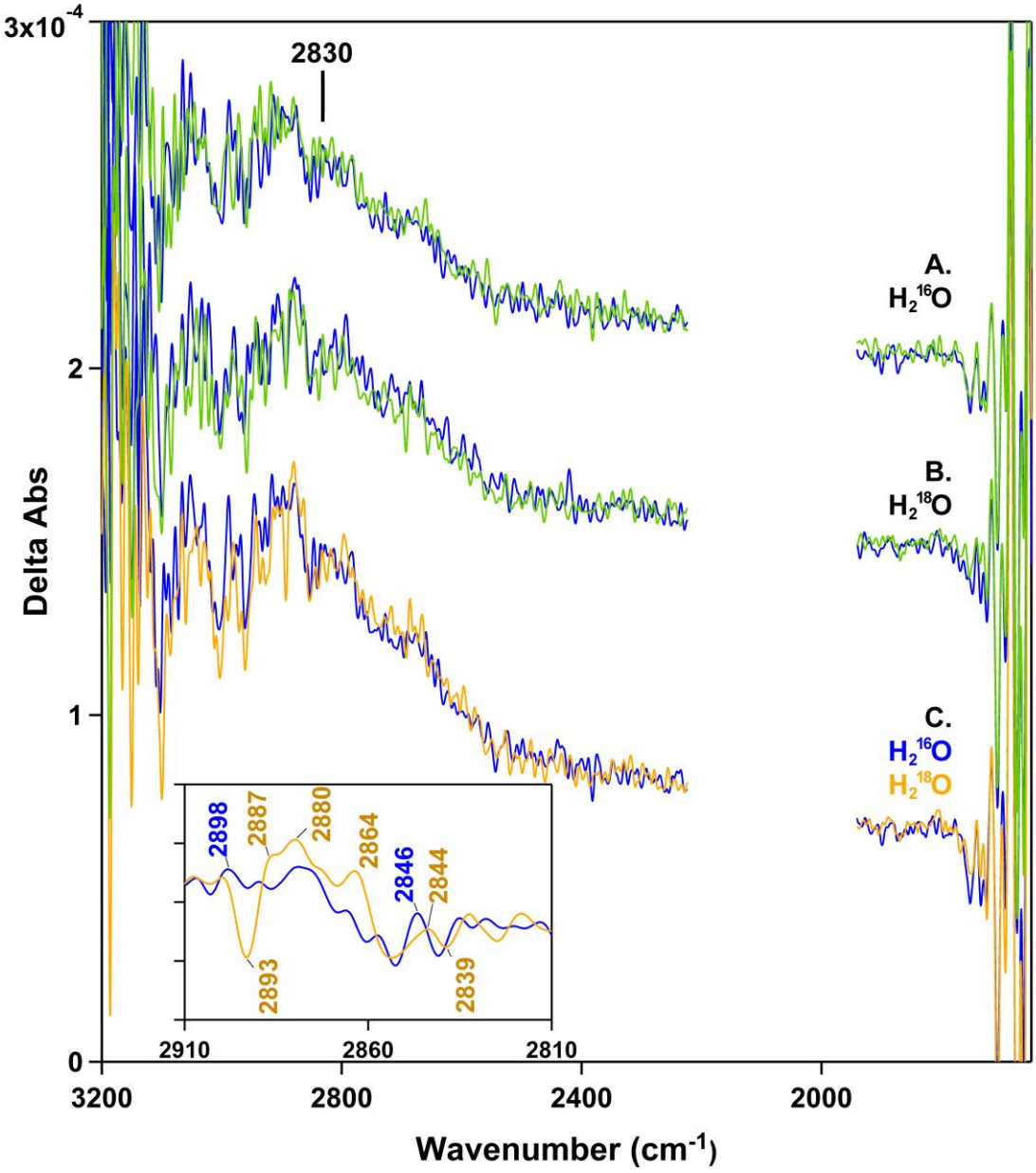

Figure 4.9 Solvent-isotope effects on the W_n^+ infrared band at 283 K and pH 7. RIFT-IR spectra (3200-1650 cm^{-1}) were derived from Cl-PSII in $H_2{}^{16}O$ (A and C, blue) or $H_2{}^{18}O$ (B and C, orange) buffer. In (A, B), the total data set was randomly divided into two pools, each pool was averaged, and then the two sub-averages were superimposed to show reproducibility in this region. In (C), the spectra derived from Cl-PSII in $H_2{}^{16}O$ buffer (blue) and $H_2{}^{18}O$ buffer (orange) are superimposed to show

solvent isotope effects. Data in (A, B) were divided by $\sqrt{2}$ to account for difference in the number of scans. Data were collected at 4 cm^{-1} resolution. A 17-point smoothing has been applied to the data using the Savitzky–Golay algorithm. The data in (C) are reproduced from ref.[11]. The inset shows an expanded view of Figure 4.9C, showing an example of solvent-isotope induced shifts, assignable to the W_n^+ infrared band at 283 K and pH 7.

As previously discussed, the W_n^+ band shifts from 2830 to 2582 cm^{-1} in NO_3-PSII (Figure 4.8, A and B). The same result was obtained using either the ^{14}NO or $^{15}NO_3$ isotopomer (compare Figure 4.8, B and C). Previously, based on QM/MM calculations, this 248 cm^{-1} downshift was attributed to nitrate acting as a stronger conjugate base than chloride, thereby exerting a greater stabilizing influence on W_n^+.[11] Taken together, these observations indicate that the structure of water, as assessed by the signal of W_n^+, is altered by nitrate. Figure 4.10 establishes the reproducibility of peak position for W_n^+ in control PSII samples. In Figure 4.10, A and B, spectra from Cl-PSII in $H_2{}^{16}O$ buffer were sorted randomly into four sets and then averaged to generate sub-averages The four sub-averages are superimposed in pairs in Figure 4.10, A and B. The overlays show that the center frequency and lineshape of the 2830 cm^{-1} band are indistinguishable in the four sub-averages. This is also evident when the peak position is measured as the centroid. The four $H_2{}^{16}O$ sub-averages have centroids of 2831, 2831, 2836, and 2839 cm^{-1}; the overall average has a centroid frequency of 2829 cm^{-1}. This reproducibility is also evident in the overlay of the W_n^+ band, as derived from Cl-PSII in sucrose (black) and trehalose (orange) buffer (Figure 4.10C). This overlay shows that no significant change is observed in band center position and lineshape.

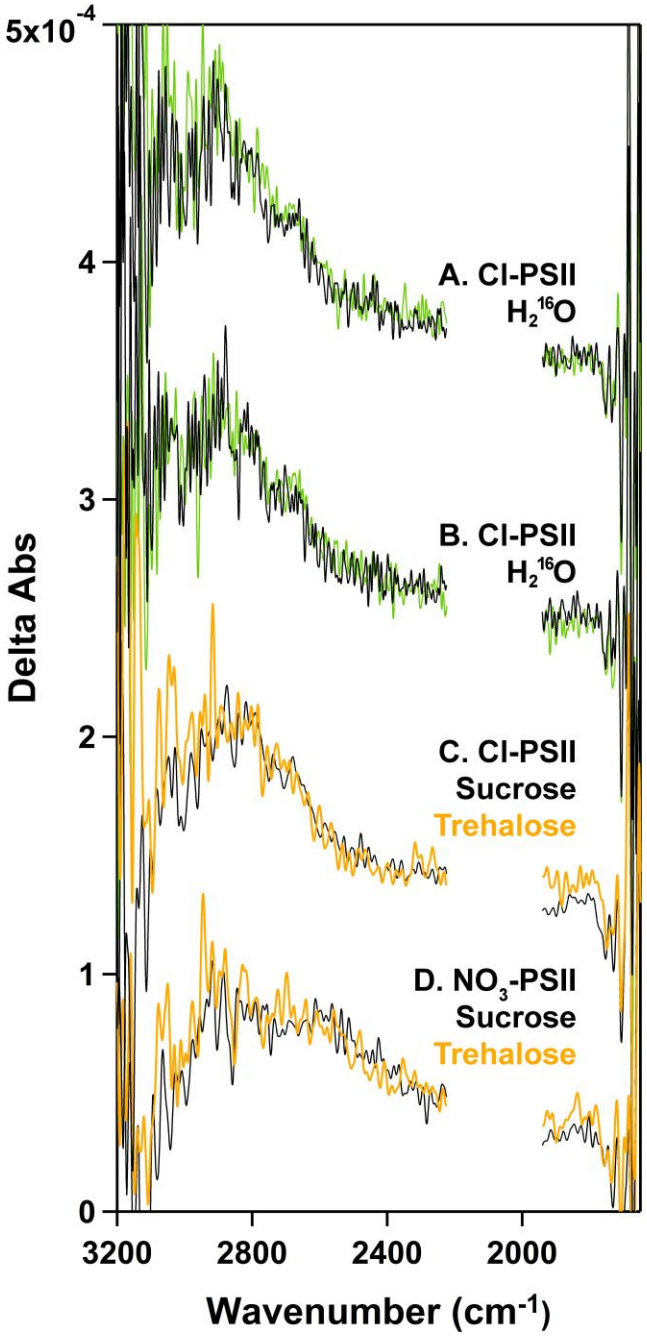

Figure 4.10 Reproducibility of the W_n^+ band peak position in RIFT-IR spectra acquired from Cl-PSII (A-C) and the effect of trehalose treatment on RIFT-IR spectra derived from NO_3-PSII (D). The RIFT-IR spectra (3200-1650 cm^{-1} region) are associated with the S_1 to S_2 transition at pH 7.5 and 283 K. Data were recorded from PSII in (A, B, green and black, and C, D, black) sucrose, (C, D orange) trehalose-containing buffers. In (D), a trehalose-induced shift is observed in NO_3-PSII. In (A, B), the total data set derived from the Cl-PSII samples was randomly divided into four pools. Each pool was averaged, and then superimposed to establish the

reproducibility of the center position of the W_n^+ band in the replicates. Each spectrum is an average of (A, B) 10 and (C, D) 5 data acquisition loops using (A, B) 15 total samples, (C, black) 15, (C, orange) 8, (D, black) 8, and (D, orange) 9 different samples. Spectra in (A, B) were acquired at 4 cm^{-1} resolution; spectra in (C, D) were acquired at 8 cm^{-1} resolution. The infrared bands of ferricyanide/ferrocyanide have been deleted for presentation purposes.

Importantly, however, when NO_3-PSII is suspended in trehalose (Figure 4.8D), the W_n^+ upshifts 68 cm^{-1} to ~2650 $cm^{-1,}$ when compared to its position in sucrose-treated NO_3-PSII (Figure 4.8B). This is evident in the spectral overlay in Figure 4.10D, in which sucrose NO_3-PSII is black or trehalose NO_3-PSII is orange. In the overlay, the 68 cm^{-1} upshift is evident as a spectral intersection at ~2600 cm^{-1}. The upshift of the W_n^+ band in trehalose is consistent with a decrease in the stabilizing influence of the nitrate ion in a re-engineered, trehalose-containing network. Note that in Cl-PSII, which does not contain nitrate, the addition of trehalose had no effect on the position of the W_n^+ band (Figure 4.10D) consistent with its lack of significant impact on the mid-infrared region (Figure 4.7).

4.5 Discussion

Here, we have used RIFT-IR spectroscopy in conjunction with anion exchange experiments to investigate the mechanism of PSII proton transfer. Chloride and bromide substitutions are used as perturbants of the proton transfer pathway. The report of a nitrate-substituted crystal structure supports the idea that nitrate also occupies the chloride binding site.[13] The experiments, which we present here, establish that the proton transfer pathway in PSII is robust and can tolerate substantial changes in internal electrostatic interactions.

We show that bromide substitution causes pronounced changes in the amide I, II, and III regions of the S_1 to S_2 spectrum. One effect of bromide was a downshift of a

derivative-shaped band, with a positive component at 1665 and a negative component at 1643 cm^{-1}. Such a downshift can be caused by vibrational Stark effect.[34] As evident in the literature, the change in ionic radius when chloride is substituted with bromide is expected to lead to such a downshift of solvent vibrational bands.[35] The Stark tuning rate for the C=O band, 0.6-1.8 MV/cm, can be used to calculate a field difference at the C=O group. The bromide-induced spectral shift is 4 cm^{-1}, giving a minimal change of 2.4 MV. Using a correlation (0.4 kcal/mol per 1 cm^{-1}) previously derived, this frequency shift is equivalent to 1.6 kcal/mol or ~1 hydrogen bond.[36-37] Notably, the proton transfer network is functional in Br-PSII, and PSII exhibits nearly normal steady state oxygen evolution rate with this internal change in field. It should be noted that coupling between peptide bonds can be complex. This analysis assumes that the derivative shaped band is the response of a single C=O group to Mn oxidation; more complex models are possible.

In spectra derived from NO_3-PSII, changes are observed throughout the amide I (1630 cm^{-1}), amide II (1531(+)/1522(-) cm^{-1}) and amide III (1390-1330 cm^{-1}) regions, when compared to Cl-PSII or Br-PSII. This is attributed to an increased number of hydrogen bonding interactions between nitrate and its protein environment. (See Supporting Information for comparison to previous reports in the literature). Notably, when PSII is substituted with nitrate, bands at 1630, 1531/1522, and 1396 cm^{-1} are reduced in intensity. One possible reason for the decrease in intensity is the exclusion of a C=O peptide bond from the hydrogen-bonding network when nitrate binds to the chloride site. In this interpretation, the excluded C=O bond is not responsive to changes in charge distribution, caused by manganese oxidation. The effects of trehalose, which partially reverse the nitrate effect, support this interpretation. Previously, trehalose has been shown

to prevent the disruption of hydrogen-bonding networks in PSII by the substrate analog, ammonia.[28] The mechanism by which trehalose exerts its stabilizing influence on proteins has been the subject of several studies.[33] The solvent reorganization time has been reported to be significantly retarded in the presence of trehalose.[38] There is also evidence that trehalose promotes hydration of the protein surface, an idea commonly referred to as the preferential hydration model.[39] The water molecules, which are bound either at the protein surface or in the trehalose-water matrix away from the protein surface, exhibit lower propensity for ice-formation. The effect of trehalose on PSII suggests that retardation of water dynamics and preferential hydration alter the proton transfer network. These experiments suggest that internal water structure plays an important role in proton transfer and storage in PSII.

As stated above, in trehalose buffer, the intensity in nitrate-sensitive bands is recovered (1636, 1532/1526 cm^{-1} and 1390-1330 cm^{-1} region). In addition to these changes, nitrate also causes a substantial 248 cm^{-1} downshift of an infrared signal, which is assigned to a stretching vibration of an internal hydronium ion.[11] However, when NO_3-PSII is suspended in trehalose buffer, this band shifts back toward its original position and appears at ~2650 cm^{-1}. In previous work using anion substiution,[11] a correlation was found between the pK_a value of the corresponding acid and the frequency of this W_n^+ band. For example, bromide has a predicted pK_a of -9, and the W_n^+ frequency was observed at 2917 cm^{-1} in Br-PSII. Chloride has a predicted pK_a of -7 and a frequency of 2830 cm^{-1}, and nitrate has a predicted pK_a of -1.4 and a frequency of 2582 cm^{-1}. It was proposed that the increased basicity of nitrate, when compared to chloride or bromide, stabilizes the hydronium ion through an electrostatic interaction. Based on this argument, the upshift observed in the

nitrate-W_n^+ frequency in trehalose is consistent with a decrease in the basicity of the bound nitrate. This effect is attributed to an increase in hydrogen-bonding interactions between nitrate and the nitrate-W_n^+ hydration shell.[40] Thus, the experiments presented here provide two lines of evidence that nitrate and trehalose alters hydrogen bonding and electrostatics in the OEC. One is derived from analysis of amide intensities; the second is derived from analysis of W_n^+ frequency. Note that in the absence of nitrate, trehalose does not have a significant effect on the W_n^+ or mid-infrared frequencies under these conditions.

Previously, chloride has been proposed to adjust the pK_a of D1-D61 in the proton transfer network (Figure 4.1A and Figure 4.11). Evidence supporting this hypothesis has been obtained from mutagenesis experiments in cyanobacterial PSII,[21-22] computational studies,[19-20] and, recently, a nitrate-substituted structure of cyanobacterial PSII.[13] One proposed mechanism is that chloride prevents salt bridge formation between the side chains of D1-D61 and D2-K317.[18] These previous site-directed mutagenesis studies have revealed alterations in the mid-IR region of the S_1 to S_2 spectrum of the mutants, which are consistent with the amide I and II assignments proposed here. Note that side chain vibrational bands may also contribute to the mid-infrared region if their frequency is perturbed, but lower infrared extinction coefficients and coupling with the peptide backbone complicate direct assignment of their spectral contributions.[27]

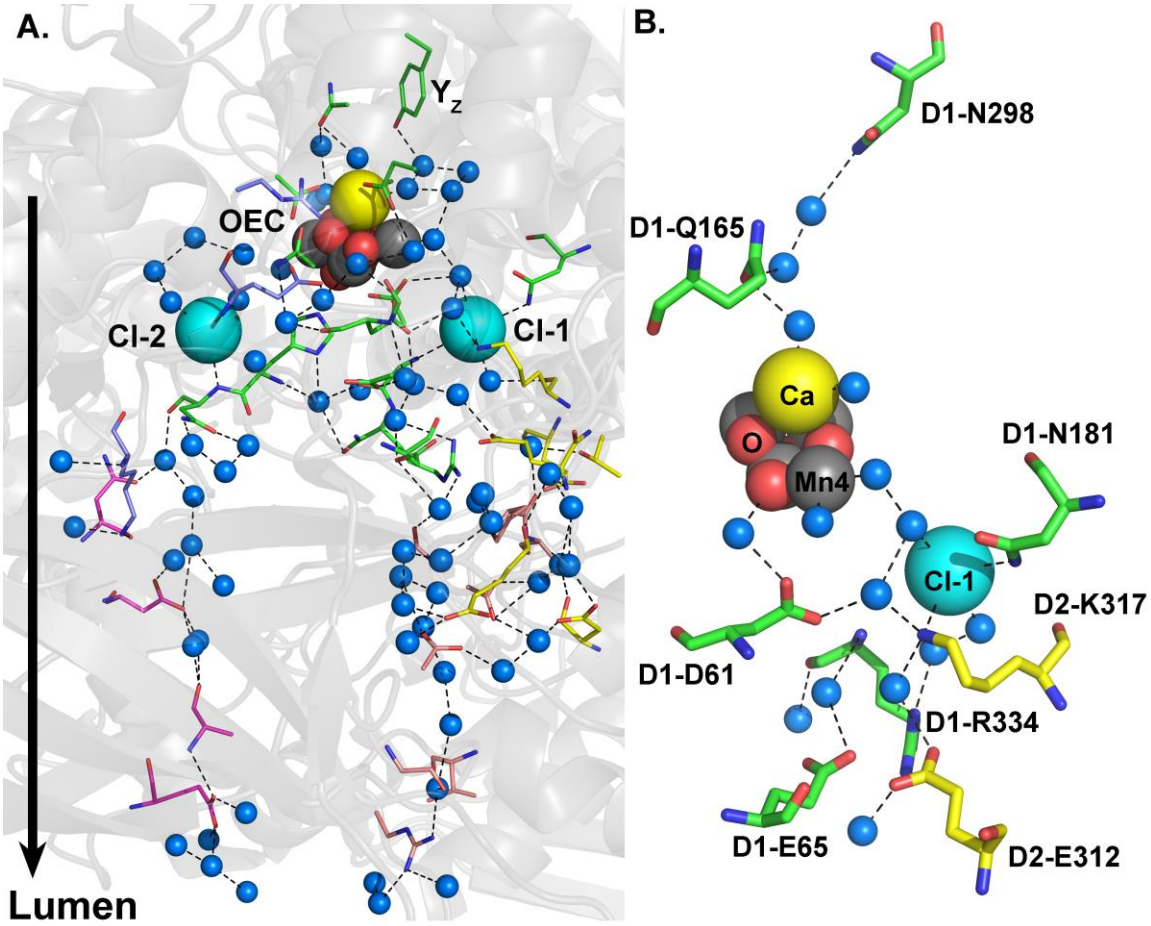

Figure 4.11 Proposed proton exit pathways extending from the OEC to the lumen. The figure was generated from cyanobacterial PSII X-ray structure (PDB ID: 4UB6[2]). The pathways include residues of PSII subunits: D1 (green), D2 (yellow), CP47 (cyan), CP43 (blue), psbO (orange), and psbU (magenta). The pathways are also predicted to include chloride ions (cyan spheres) and water molecules (blue spheres). Hydrogen-bonding interactions are shown as dashed lines. (B) Residues that altered the amide bands in the infrared spectrum, as previously reported in site-directed mutagenesis studies. Color scheme is the same as Figure 4.1. See Table 3 for more information.

A summary of previously residues, targeted for mutagenesis, and the putative proton transfer pathway is presented in Figure 4.11. As shown, D1-D61, D2-K317 and D1-N181 are located in close proximity to Cl-1 (Figure 4.11), and the latter two amino acids are predicted to be ligands to Cl-1. All mutants retained some oxygen evolution activity (Table 3, 10-54% of wildtype).

Table 3 Summary of oxygen evolution rates as observed in PSII, isolated from cyanobacterial PSII mutants

Mutant	Oxygen evolution rate* (% of WT)
D1-D61A[41,42]	16-18
D2-K317A[22]	50-54
D1-N181A[43]	33-36
D1-R334A[44]	39-42
D1-N298A[45]	7-9
D1-Q165E[44]	33-36
D2-E312A[41]	26-28
D1-E65A[41]	14-15

Notably, in the D1-D61A mutant, spectral changes were observed in all three amide regions in the S_2-minus-S_1 spectrum.[42] Specifically, bands in the 1600-1640 cm^{-1} region (amide I) were altered, the 1530(+)/1522(-) cm^{-1} (amide II) feature was eliminated, and changes in the 1350-1400 cm^{-1} (amide III) region were reported. Other mutations, including D2-K317A[22] and D1-N181A[43], were reported to eliminate the 1530(+)/1522(-) cm^{-1} (amide II) feature, but did not induce changes in the other amide regions. In addition, D1-R334A,[44] D1-N298A,[45] D1-Q165E,[44] and D2-E312A[41] altered the 1530(+)/1522(-) cm^{-1} (amide II) and amide I bands but did not eliminate them. The D1-E65A[41] mutation elicited changes only in the amide I region.

Taken together, these previous results show that mutations at amino acid side chains, predicted to participate in the hydrogen-bonded network, all cause similar alterations in the S_1 to S_2 infrared spectrum. The spectral change is assignable to amide I and II bands and to alterations in C=O hydrogen bonding interactions. When combined

with our data, these results predict the existence of a common hydrogen-bonding network, involving peptide carbonyl groups, which connects the side chains of these amino acid residues. Importantly, the spectral effects of the D1-D61A mutation in cyanobacteria are similar to the spectral effect that we report here for nitrate substitution in spinach PSII. This observation suggests that nitrate substitution and mutation at D1-D61 cause similar defects in proton translocation. However, it is important to note that the RIFT-IR spectra of spinach and cyanobacterial PSII are not identical. For example, the negative 1747 cm^{-1} band observed during the S_1 to S_2 transition in cyanobacteria is absent in spinach.[42]

Our data support the conclusion that the hydrogen-bonding network contains trapped water and a hydronium ion, which is produced during the S_1 to S_2 transition. The vibrational spectrum of this hydronium ion, designated W_n^+, contains a broad positive infrared band centered at 2830 cm^{-1}. We have previously employed isotope editing and quantum mechanical calculations to assign this band to a stretching vibration of W_n^+.[11] In the gas phase, similar infrared bands have been reported from protonated water clusters.[46] Notably, bands with similar frequencies have also been assigned to internal, protonated water clusters in the membrane protein, bacteriorhodopsin,[47] and, most recently, a cyanobacterial anion pump.[48] Interestingly, we have shown that $H_2{}^{18}O$ isotope exchange elicits very different responses based on the experimental temperature. At 283 K, small isotope shifts of 10 cm^{-1} are observed in the sharp spectral features of the 2830 cm^{-1} band. The magnitude of the shift is consistent with literature reports.[49] However, at lower temperatures of 190 K[25] and 263 K,[26] the solvent isotope shift is much larger than expected. We attributed the large, apparent isotope shift to cluster size heterogeneity caused by viscosity difference in $H_2{}^{18}O$.[26] Table 1 presents a summary, which has been discussed in

ref.[24-26] It is interesting to note that the D1-D61A mutation leads to the elimination of the 2830 cm^{-1} band,[42] and as discussed above, D1-D61 is predicted to be involved in the proton exit pathway.[18-19]

The observation of nitrate-induced changes in the amide I, II, and III regions is consistent with the disruption of a hydrogen-bonded network when nitrate is substituted at one or more chloride-binding sites. We have previously proposed the existence of such an infrared-detectable, hydrogen bonding network based on substitutions at the calcium site and ammonia-induced inhibition experiments.[28-29] In this present study, we provide insight into the effective design of this proton transfer pathway. The pathway was probed via its infrared signature bands, arising from the peptide backbone and an internal hydronium ion. Remarkably, while bromide and nitrate substitutions lead to spectral changes consistent with substantial alterations in electric field, pK_a, and hydrogen bonding, PSII is functional in each case. Therefore, while bromide and nitrate reorganize the network, the proton transfer pathway is robust and accommodates to these changes. Analogy can be made to the ubiquitous voltage-gated proton channel Hv1, which contains a highly selective proton transfer network.[50] The selectivity of the channel is unaffected by mutation of all but one of the acidic residues proposed to be directly involved in proton transfer. Therefore, it is a robust functional network, similar to the one reported in the current study. A Grotthuss-like hopping mechanism has been proposed for Hv1, involving both internal water molecules along with amino acid side chains. A similar mechanism may operate in PSII. The resiliency of the proton transfer pathway in PSII may be important in preservation of optimum levels of activity under physiological conditions, which are associated with

adaptation from light to dark, pH changes in the thylakoid lumen, and adaptation to oxidative stress.[51]

4.6 References

1. Wydrzynski, T. J.; Satoh, K., *Photosystem Ii: The Light-Driven Water: Plastoquinone Oxidoreductase*. Springer: Dordrecht, 2006; Vol. 22.

2. Suga, M.; Akita, F.; Hirata, K.; Ueno, G.; Murakami, H.; Nakajima, Y.; Shimizu, T.; Yamashita, K.; Yamamoto, M.; Ago, H., et al. Native Structure of Photosystem Ii at 1.95 Å Resolution Viewed by Femtosecond X-Ray Pulses. *Nature* **2015,** *517*, 99-103.

3. Umena, Y.; Kawakami, K.; Shen, J.-R.; Kamiya, N. Crystal Structure of Oxygen-Evolving Photosystem Ii at a Resolution of 1.9 Å. *Nature* **2011,** *473*, 55-60.

4. Wei, X.; Su, X.; Cao, P.; Liu, X.; Chang, W.; Li, M.; Zhang, X.; Liu, Z. Structure of Spinach Photosystem Ii–Lhcii Supercomplex at 3.2 Å Resolution. *Nature* **2016,** *534*, 69-74.

5. Kok, B.; Forbush, B.; McGloin, M. Cooperation of Charges in Photosynthetic O_2 Evolution-I. A Linear Four Step Mechanism. *Photochem. Photobiol.* **1970,** *11*, 457-75.

6. Renger, G.; Renger, T. Photosystem Ii: The Machinery of Photosynthetic Water Splitting. *Photosynth. Res.* **2008,** *98*, 53-80.

7. Gerken, S.; Brettel, K.; Schlodder, E.; Witt, H. Optical Characterization of the Immediate Electron Donor to Chlorophyll a^{+Ii} in O_2-Evolving Photosystem Ii Complexes Tyrosine as Possible Electron Carrier between Chlorophyll A_{ii} and the Water-Oxidizing Manganese Complex. *FEBS Lett.* **1988,** *237*, 69-75.

8. Barry, B. A. Proton Coupled Electron Transfer and Redox Active Tyrosines in Photosystem Ii. *J. Photochem. Photobiol., B* **2011,** *104*, 60-71.

9. Dau, H.; Zaharieva, I.; Haumann, M. Recent Developments in Research on Water Oxidation by Photosystem Ii. *Curr. Opin. Chem. Biol.* **2012,** *16*, 3-10.

10. Haumann, M.; Hundelt, M.; Jahns, P.; Chroni, S.; Bögershausen, O.; Ghanotakis, D.; Junge, W. Proton Release from Water Oxidation by Photosystemii: Similar Stoichiometries Are Stabilized in Thylakoids and Psii Core Particles by Glycerol. *FEBS Lett.* **1997,** *410*, 243-248.

11. Brahmachari, U.; Gonthier, J. F.; Sherrill, C. D.; Barry, B. A. Chloride Maintains a Protonated Internal Water Network in the Photosynthetic Oxygen Evolving Complex. *J. Phys. Chem. B* **2017,** *121*, 10327-10337.

12. Yocum, C. F. The Calcium and Chloride Requirements of the O_2 Evolving Complex. *Coord. Chem. Rev.* **2008,** *252*, 296-305.

13. Umena, Y.; Tamaru, S.; Shen, J.-R. Proton-Transfer Inhibition by Molecular Anion Substitutions in Photosystem Ii. *Acta Crystallographica, Section A: Foundations and Advances* **2017,** *73*, C96.

14. Wincencjusz, H.; van Gorkom, H. J.; Yocum, C. F. The Photosynthetic Oxygen Evolving Complex Requires Chloride for Its Redox State S2→ S3 and S3→ S0 Transitions but Not for S0→ S1 or S1→ S2 Transitions. *Biochemistry* **1997,** *36*, 3663-3670.

15. Wincencjusz, H.; Yocum, C. F.; Van Gorkom, H. J. Activating Anions That Replace Cl-in the O2-Evolving Complex of Photosystem Ii Slow the Kinetics of the Terminal Step in Water Oxidation and Destabilize the S2 and S3 States. *Biochemistry* **1999,** *38*, 3719-3725.

16. Feller, G.; le Bussy, O.; Houssier, C.; Gerday, C. Structural and Functional Aspects of Chloride Binding to Alteromonas Haloplanctis A-Amylase. *J. Biol. Chem.* **1996,** *271*, 23836-23841.

17. Wei, L.; Alhenc-Gelas, F.; Corvol, P.; Clauser, E. The Two Homologous Domains of Human Angiotensin I-Converting Enzyme Are Both Catalytically Active. *J. Biol. Chem.* **1991,** *266*, 9002-9008.

18. Pokhrel, R.; McConnell, I. L.; Brudvig, G. W. Chloride Regulation of Enzyme Turnover: Application to the Role of Chloride in Photosystem Ii. *Biochemistry* **2011,** *50*, 2725-2734.

19. Amin, M.; Pokhrel, R.; Brudvig, G. W.; Badawi, A.; Obayya, S. Effect of Chloride Depletion on the Magnetic Properties and the Redox Leveling of the Oxygen-Evolving Complex in Photosystem Ii. *J. Phys. Chem. B* **2016,** *120*, 4243-4248.

20. Rivalta, I.; Amin, M.; Luber, S.; Vassiliev, S.; Pokhrel, R.; Umena, Y.; Kawakami, K.; Shen, J.-R.; Kamiya, N.; Bruce, D. Structural–Functional Role of Chloride in Photosystem Ii. *Biochemistry* **2011,** *50*, 6312-6315.

21. Suzuki, H.; Yu, J.; Kobayashi, T.; Nakanishi, H.; Nixon, P. J.; Noguchi, T. Functional Roles of D2-Lys317 and the Interacting Chloride Ion in the Water Oxidation Reaction of Photosystem Ii as Revealed by Fourier Transform Infrared Analysis. *Biochemistry* **2013,** *52*, 4748–4757.

22. Pokhrel, R.; Service, R. J.; Debus, R. J.; Brudvig, G. W. Mutation of Lysine 317 in the D2 Subunit of Photosystem Ii Alters Chloride Binding and Proton Transport. *Biochemistry* **2013,** *52*, 4758-4773.

23. Barry, B. A.; Brahmachari, U.; Guo, Z. Tracking Reactive Water and Hydrogen-Bonding Networks in Photosynthetic Oxygen Evolution. *Acc. Chem. Res.* **2017,** *50*, 1937-1945.

24. Polander, B. C.; Barry, B. A. Detection of an Intermediary, Protonated Water Cluster in Photosynthetic Oxygen Evolution. *Proc. Natl. Acad. Sci. U.S.A.* **2013,** *110*, 10634-9.

25. Guo, Z.; Barry, B. A. Cryogenic Trapping and Isotope Editing Identify a Protonated Water Cluster as an Intermediate in the Photosynthetic Oxygen-Evolving Reaction. *J. Phys. Chem. B* **2016,** *120*, 8794-8808.

26. Brahmachari, U.; Barry, B. A. Dynamics of Proton Transfer to Internal Water During the Photosynthetic Oxygen-Evolving Cycle. *J. Phys. Chem. B* **2016,** *120*, 11464-11473.

27. Barth, A.; Zscherp, C. What Vibrations Tell Us About Proteins. *Q. Rev. Biophys.* **2002,** *35*, 369-430.

28. Polander, B. C.; Barry, B. A. A Hydrogen-Bonding Network Plays a Catalytic Role in Photosynthetic Oxygen Evolution. *Proc. Natl. Acad. Sci. U.S.A.* **2012,** *109*, 6112-6117.

29. Polander, B. C.; Barry, B. A. Calcium and the Hydrogen-Bonded Water Network in the Photosynthetic Oxygen-Evolving Complex. *J. Phys. Chem. Lett.* **2013,** *4*, 786-791.

30. Berthold, D. A.; Babcock, G. T.; Yocum, C. F. A Highly Resolved, Oxygen-Evolving Photosystem Ii Preparation from Spinach Thylakoid Membranes: Epr and Electron-Transport Properties. *FEBS Lett.* **1981,** *134*, 231-234.

31. Mishra, R. K.; Ghanotakis, D. F. Selective Extraction of Cp 26 and Cp 29 Proteins without Affecting the Binding of the Extrinsic Proteins (33, 23 and 17 Kda) and the Dcmu Sensitivity of a Photosystem Ii Core Complex. *Photosynth. Res.* **1994,** *42*, 37-42.

32. Cooper, I. B.; Barry, B. A. Perturbations at the Chloride Site During the Photosynthetic Oxygen-Evolving Cycle. *Photosynth. Res.* **2007,** *92*, 345-356.

33. Jain, N. K.; Roy, I. Effect of Trehalose on Protein Structure. *Protein Sci.* **2009,** *18*, 24-36.

34. Boxer, S. G. Stark Realities. *J Phys Chem B* **2009,** *113*, 2972-2983.

35. Marcus, Y. Ionic Radii in Aqueous Solutions. *Chem. Rev.* **1988,** *88*, 1475-1498.

36. Fersht, A. R.; Shi, J.-P.; Knill-Jones, J.; Lowe, D. M.; Wilkinson, A. J.; Blow, D. M.; Brick, P.; Carter, P.; Waye, M. M.; Winter, G. Hydrogen Bonding and Biological Specificity Analysed by Protein Engineering. *Nature* **1985,** *314*, 235.

37. Deng, H.; Callender, R. Raman Spectroscopic Studies of the Structures, Energetics and Bond Distortions of Substrates Bound to Enzymes. *Methods Enzymol.* **1999,** *308*, 176-201.

38. Shukla, N.; Pomarico, E.; Chen, L.; Chergui, M.; Othon, C. M. Retardation of Bulk Water Dynamics by Disaccharide Osmolytes. *J Phys Chem B* **2016,** *120*, 9477-9483.

39. Olsson, C.; Jansson, H.; Swenson, J. The Role of Trehalose for the Stabilization of Proteins. *J Phys Chem B* **2016,** *120*, 4723-4731.

40. Shokri, A.; Abedin, A.; Fattahi, A.; Kass, S. R. Effect of Hydrogen Bonds on P K a Values: Importance of Networking. *J. Am. Chem. Soc.* **2012,** *134*, 10646-10650.

41. Service, R. J.; Hillier, W.; Debus, R. J. Evidence from Ftir Difference Spectroscopy of an Extensive Network of Hydrogen Bonds near the Oxygen-Evolving Mn4ca Cluster of

Photosystem Ii Involving D1-Glu65, D2-Glu312, and D1-Glu329. *Biochemistry* **2010,** *49*, 6655-6669.

42. Debus, R. J. Evidence from Ftir Difference Spectroscopy That D1-Asp61 Influences the Water Reactions of the Oxygen-Evolving Mn_4cao_5 Cluster of Photosystem Ii. *Biochemistry* **2014,** *53*, 2941-2955.

43. Pokhrel, R.; Debus, R. J.; Brudvig, G. W. Probing the Effect of Mutations of Asparagine 181 in the D1 Subunit of Photosystem Ii. *Biochemistry* **2015,** *54*, 1663-1672.

44. Service, R. J.; Hillier, W.; Debus, R. J. Network of Hydrogen Bonds near the Oxygen-Evolving Mn_4cao_5 Cluster of Photosystem Ii Probed with Ftir Difference Spectroscopy. *Biochemistry* **2014,** *53*, 1001-1017.

45. Nagao, R.; Ueoka-Nakanishi, H.; Noguchi, T. D1-Asn-298 in Photosystem Ii Is Involved in a Hydrogen-Bond Network near the Redox-Active Tyrosine Yz for Proton Exit During Water Oxidation. *J. Biol. Chem.* **2017**, jbc. M117. 815183.

46. Headrick, J. M.; Diken, E. G.; Walters, R. S.; Hammer, N. I.; Christie, R. A.; Cui, J.; Myshakin, E. M.; Duncan, M. A.; Johnson, M. A.; Jordan, K. D. Spectral Signatures of Hydrated Proton Vibrations in Water Clusters. *Science* **2005,** *308*, 1765-1769.

47. Garczarek, F.; Gerwert, K. Functional Waters in Intraprotein Proton Transfer Monitored by Ftir Difference Spectroscopy. *Nature* **2006,** *439*, 109-112.

48. Harris, A.; Saita, M.; Resler, T.; Hughes-Visentin, A.; Maia, R.; Pranga-Sellnau, F.; Bondar, A.-N.; Heberle, J.; Brown, L. S. Molecular Details of the Unique Mechanism of Chloride Transport by a Cyanobacterial Rhodopsin. *Phys. Chem. Chem. Phys.* **2018,** *20*, 3184-3199.

49. Kandori, H.; Shichida, Y. Direct Observation of the Bridged Water Stretching Vibrations inside a Protein. *J. Am. Chem. Soc.* **2000,** *122*, 11745-11746.

50. van Keulen, S. C.; Gianti, E.; Carnevale, V.; Klein, M. L.; Rothlisberger, U.; Delemotte, L. Does Proton Conduction in the Voltage-Gated H+ Channel Hhv1 Involve Grotthuss-Like Hopping Via Acidic Residues? *J Phys Chem B* **2017,** *121*, 3340-3351.

51. Pottosin, I.; Shabala, S. Transport across Chloroplast Membranes: Optimizing Photosynthesis for Adverse Environmental Conditions. *Molecular Plant* **2016,** *9*, 356-370.

CHAPTER 5. ACETATE INHIBITS PROTON HOPPING THROUGH INTERMEDIATE WATER BRIDGES IN PHOTOSYNTHETIC OXYGEN EVOLUTION

By

[1,2] Udita Brahmachari, [3,4] Jérôme F. Gonthier[†],

[3,4] C. David Sherrill, and [1,2] Bridgette A. Barry*

[1]Department of Chemistry and Biochemistry,

[2]Petit Institute for Bioengineering and Biosciences,

[3]Center for Computational Molecular Science and Technology, and

[4]School of Computational Science and Engineering,

Georgia Institute of Technology,

Atlanta, Georgia 30332, United States

5.1 Abstract

Proton transfer using water bridges has been observed in bulk water, acid-base reactions and several proton-translocating biological systems. In the water-oxidizing enzyme, photosystem II (PSII), a functional proton transfer network is predicted to be composed of hydrogen-bonded water molecules, amino acid side chains, and peptide carbonyl groups. The network spans 35 Å and shuttles protons away from the oxygen-evolving, Mn_4CaO_5, complex (OEC) to the thylakoid lumen during the five-step water oxidation (S state) cycle. Acetate is a well-known PSII inhibitor, which acts in a chloride-dependent manner. Here, we study the effect of ^{12}C and ^{13}C acetate on one step of the water-oxidizing cycle, the S_1 to S_2 transition, using infrared spectroscopy. PSII was isolated from spinach, and experiments were conducted at pH 7.5, using 532 nm laser flashes to advance the cycle from the dark-adapted state S_1 to the S_2 state. Isotope-editing reveals an infrared spectrum assignable to the protonation of acetate; the S_1 to S_2 transition perturbs the infrared spectrum of the product, bound acetic acid, due to a second-order Stark effect. An accompanying intensity decrease in the 2830 cm^{-1} band, previously assigned to a stretching vibration of a hydrated hydronium ion, W_n^+, is observed. Computational studies using a small OEC model support the spontaneous transfer of the proton from the hydronium ion to the acetate inhibitor, when acetate is substituted at the chloride side. Taken together, these results show that the mechanism of PSII proton transfer involves proton hopping and uses internal water as an essential intermediate.

5.2 Introduction

The mechanism of proton transfer in water has been the subject of numerous theoretical and experimental investigations.[1-2] The von Grotthuss mechanism accounted for the unusually high mobility of protons in water using intermediary water molecules as bridges to allow proton hopping in a sequential manner. Spectral evidence for the hydrated proton has been obtained in the gas phase [3] as well as aqueous solutions.[4] There are several examples in biology of proteins that employ proton transfer to generate transmembrane electrochemical gradients for activity.[5] Bacteriorhodopsin,[6] cytochrome c oxidase,[7] and carbonic anhydrase[8] employ organized hydrogen bonded networks of internal water molecules and amino acid side chains for proton translocation. In these proteins, water acts as an efficient proton donor and acceptor and functions as bridges in stepwise proton transfer.

In photosystem II (PSII), a multisubunit transmembrane protein, efficient proton translocation from the catalytic center is essential for oxygen evolution (Figure 5.1A). [9-11] Step-wise photoinduced oxidations of the oxygen evolving complex (OEC), comprised of a Mn_4CaO_5 cluster, leads to water oxidation (Figure 5.1B). Oxygen is evolved with period four oscillation.[12] Following light absorption, charge separation is initiated in the reaction center of PSII which leads to the formation of a tyrosyl radical, $Y_z^{\bullet}$ **(**Y161 of D1 subunit).[13] The OEC is then oxidized by the powerful oxidant $Y_z^{\bullet}$.[14] Four such oxidations of the OEC leads to water oxidation and thereby resets the OEC back to its most reduced state.[15] The S-state cycle is used to describe the water oxidation cycle (Figure 5.1B), where each state of the OEC is referred to as a S_n state, n indicating the number oxidizing equivalents on the OEC in that state. S_1 is the dark-adapted resting state of the OEC. The first and second

flashes oxidize S_1 to S_2 and S_2 to S_3, respectively.[16-17] The third flash oxidizes and S_3 to S_0 and is accompanied by substrate water oxidation.[12] S_1 is regenerated after the fourth flash.

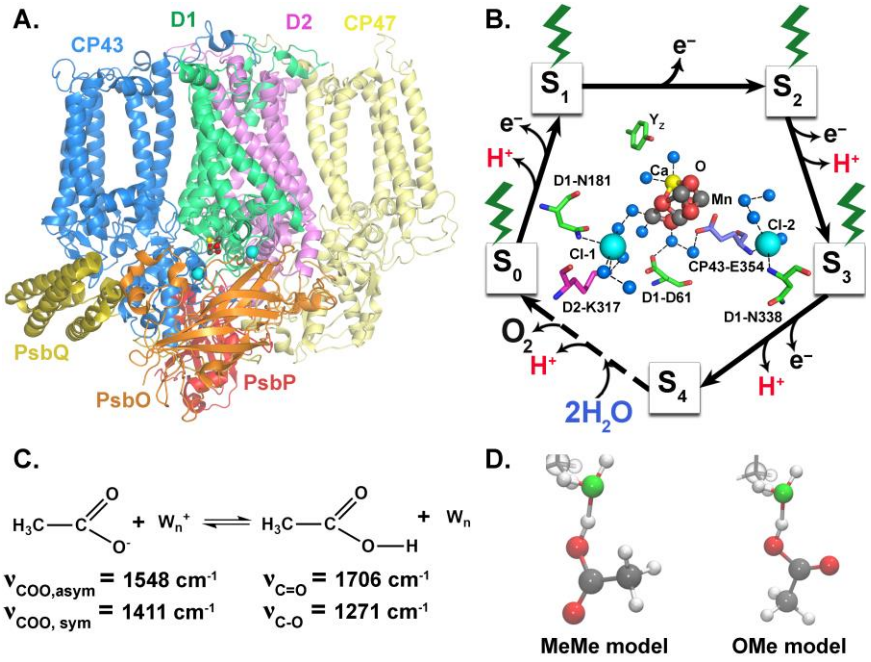

Figure 5.1 Structure of PSII and photosynthetic water oxidation. (A) Spinach PSII structure (PDB ID: 3JCU [11]) showing the integral membrane spanning D1 (green), D2 (magenta), CP43 (marine), and CP47 (yellow) subunits. The three extrinsic subunits PsbP (red), PsbQ (olive), and PsbO (orange) are also shown. (B) S-state cycle of water oxidation and release of molecular oxygen [12]. (B, Inset) Structure of the OEC and ligand environment around the chloride ions (cyan (PDB ID:4UB6 [9]). (C) Schematic representation of acetate removing a proton from the protonated cluster of water molecules, designated W_n^+, during the S_1 to S_2 transition. The literature values for infrared frequencies are noted below the relevant species [18]. (D) The two orientations of the acetate ion substituted at the chloride site predicated by QM after geometry optimization of the small model of the OEC. Full models are shown in the Figure 5.7.

The OEC oxidations lead to concomitant proton release to the lumen. The stoichiometry of proton release in sucrose containing buffers was 1:0:1:2 upon advancing from S_0 to S_1, S_1 to S_2, S_2 to S_3 and from S_3 back to S_0.[19-20] Chloride, an essential cofactor, has been proposed to be mediate proton transfer reactions in PSII.[21] Proton transfer occurs

through an extensive hydrogen-bonded network, spanning over 35 Å, involving amino acid side chains, peptide carbonyl groups and water molecules.[22] Previously, we have demonstrated that chloride is involved in maintaining this network, which remains active in oxygen evolution despite changes in pK_a, ionic strength and hydrogen bonding.[23] The present study obtains incisive information concerning the mechanism of this proton transfer using the chloride-dependent inhibitor, acetate. Vibrational spectroscopy and computational studies of a small model of the OEC indicate that acetate inhibition is associated with interruption of proton hopping through water bridges.

5.3 Materials and methods

PSII was purified by Triton X-100 treatment from market spinach.[24] Octylthioglucoside (OTG) was then used in a second round of detergent treatment.[25] The PSII was suspended in buffer containing 0.4 M sucrose, 50 mM 2-(N-morpholino)ethanesulfonic acid (MES)-NaOH, pH 6.0, and 15 mM NaCl and stored at -70°C. Acetate substitution at the chloride sites on PSII was carried out by resuspending OTG-PSII three times in buffer containing 0.4 M sucrose, 50 mM 2-[4-(2-hydroxyethyl)piperazin-1-yl]ethanesulfonic acid (HEPES)-NaOH, pH 7.5, and 15 mM NaOAc (referred to as OAc-PSII). The chloride-containing control (Cl-PSII) was generated by washing OTG-PSII in the same buffer with 15 mM NaCl instead of the acetate salt. Samples were subsequently aliquoted and frozen at -70°C. The oxygen evolution activity of the PSII samples was assayed using a Clark-type oxygen electrode. Freshly prepared 1 mM potassium ferricyanide ($K_3[Fe(CN)_6]$) and recrystallized 0.5 mM 2,6-dichlorobenzoquinone were used as external electron acceptors. As isolated, OTG-PSII samples exhibited oxygen evolution rates of 1260 ± 150 μmol O_2 (mg Chl-h)$^{-1}$ in pH 6.0 buffer. See Figure 5.2 and Figure 5.3 for more information concerning pH 7.5

and a summary of the effects of the inhibitor, acetate. RIFT-IR spectroscopy and QM/MM calculations were performed by methods previously described.[26] See Chapter 3 for details.

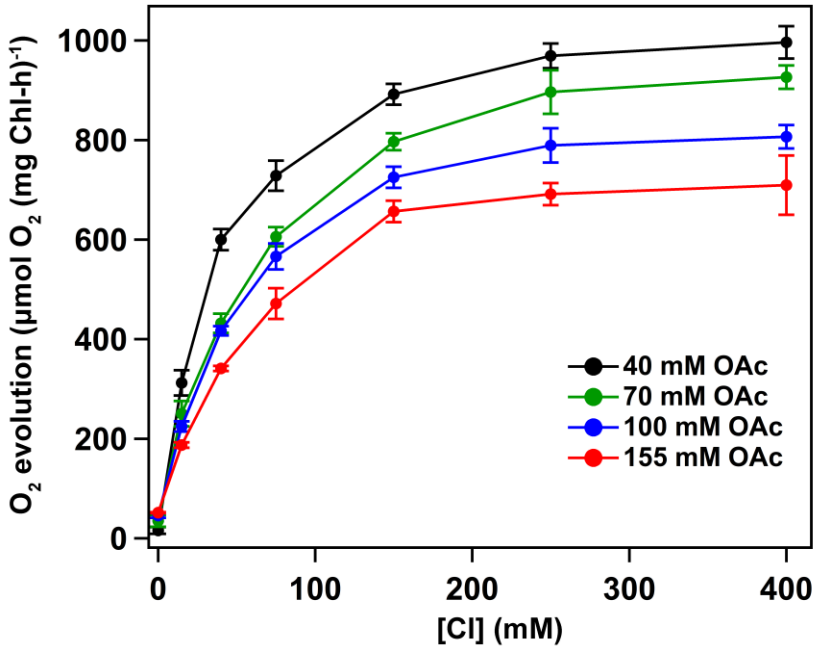

Figure 5.2 Effect of chloride addition on the oxygen evolution activity of acetate-containing PSII samples. Three different acetate concentrations were tested, 40 mM (red), 100 mM (black), and 155 mM (blue). Error bars represent ±standard deviation.

5.4 Results

PSII was isolated from market spinach, using Triton X-100 and octylthioglucoside [24-25]. Samples were suspended at pH 7.5 to deplete the PsbP and PsbQ extrinsic subunits and increase access to the PSII chloride site.[26] Preparations had calcium and chloride dependent rates of oxygen evolution greater than 1260 ± 150 µmol O_2 (mg Chl-h)$^{-1}$. To assess the effect of acetate addition under these conditions, the light-induced steady state rate of oxygen evolution was measured (Figure 5.2). As shown, mM concentrations of acetate inhibits oxygen evolution in a chloride dependent manner. A Lineweaver Burke

plot reveals a mixed inhibition mechanism, suggesting that in this type of PSII preparation, acetate binds at two sites, one of which is only available when chloride is bound (Figure 5.3). X-ray structures of PSII reveal two chloride sites near the OEC, so a mixed inhibition mechanism could be associated with interactions with these two sites if the affinities are different.

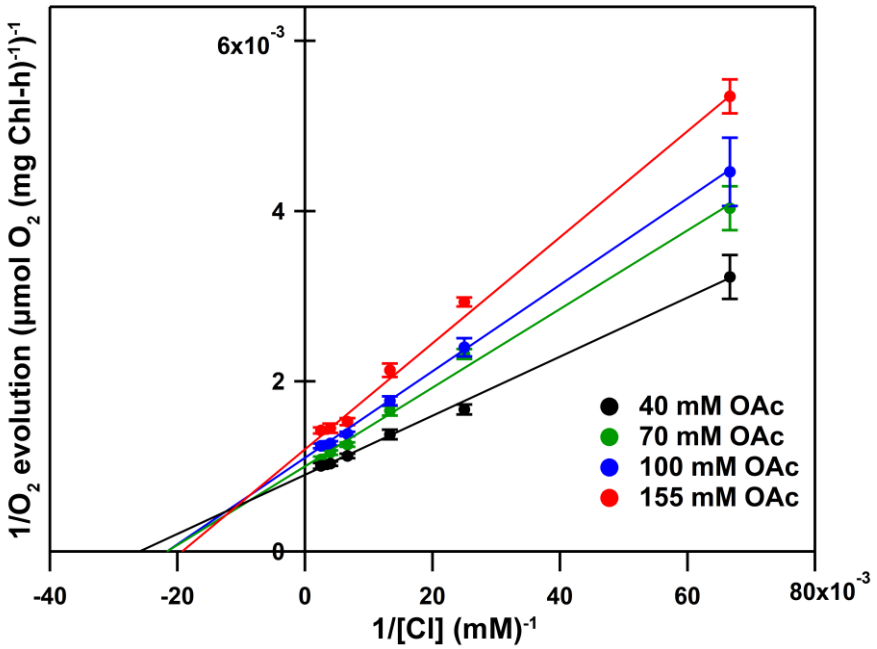

Figure 5.3 Lineweaver-Burk analysis of data shown in Figure 5.2.

To assess the effect of acetate, reaction-induced FT-IR (RIFT-IR) spectroscopy was employed. Samples were preflashed at 532 nm to synchronize in the S_1 state of the S state cycle. An additional flash produces the S_2 state, corresponding to a Mn oxidation reaction.[20] Samples contained potassium ferricyanide to reoxidize the acceptor side. Potassium ferricyanide acted as an external electron acceptor and bands from the CN stretching vibrations of the ferricyanide/ferrocyanide couple are observed at 2115/2038 cm^-

[1]. The intensity of this band is a marker for flash-induced charge separation. The RIFT-IR spectrum associated with the S_1 to S_2 transition is well known,[23, 27] and is dominated by donor side, protein structural changes (Figure 5.4A). In Figure 5.4A and Figure 5.4B, the 3200-1800 cm^{-1} regions of the S_2-minus-S_1 difference spectrum of the chloride-containing control, termed Cl-PSII, are shown (black). The spectra from the chloride control are compared to inhibited samples containing either 40 mM or 155 mM acetate (orange). Note that 10 mM calcium was present in all samples.

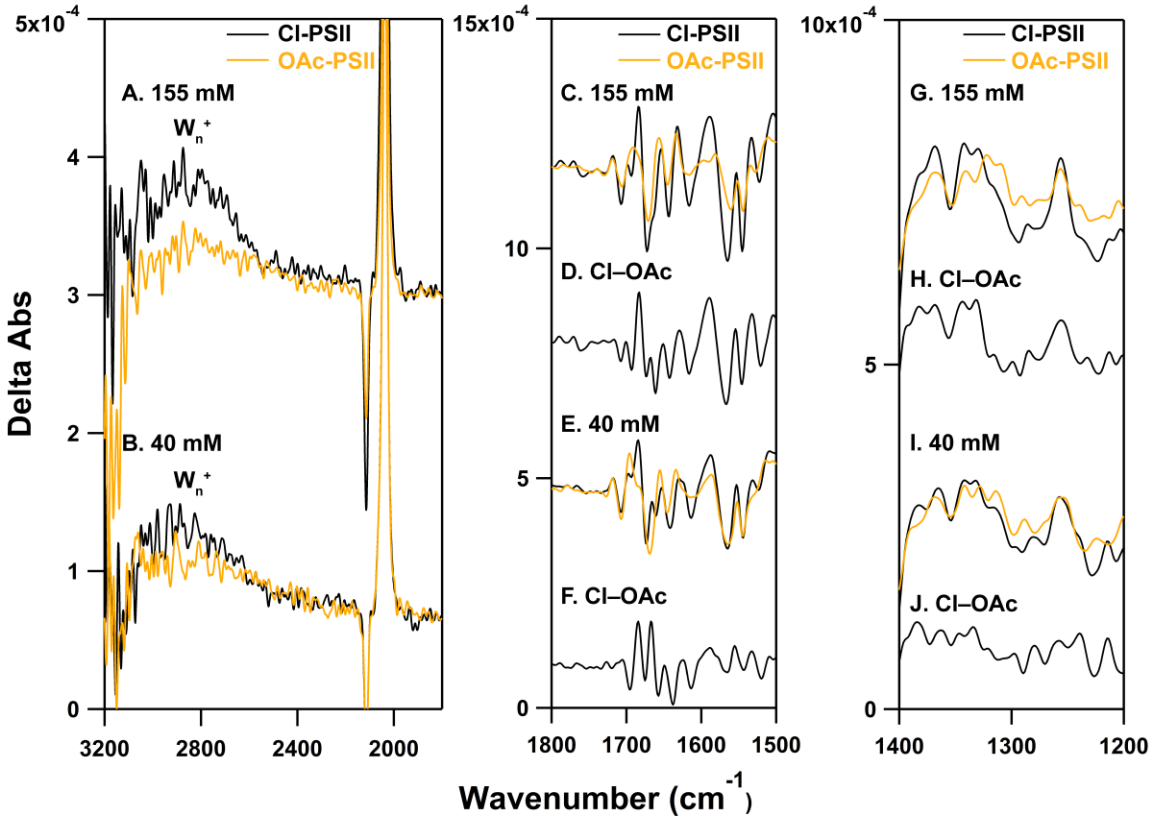

Figure 5.4 Acetate concentration dependence. Effects of acetate substitution in PSII during the S_1 to S_2 transition at pH 7.5, 283 K. The RI-FTIR S_2-minus-S_1 spectrum is presented in the (A, B) 3200-1800 cm^{-1}, (C-F) 1800-1500 cm^{-1}), and (G-J) 1400-1200 cm^{-1} region. In (A, C, G), the anion concentration was maintained at 155 mM while in (B, E, I) it was maintained at 40 mM. Cl-minus-OAc double difference spectra at (D, H) 155 mM, and (F, J) 40 mM anion concentration. Five data acquisition loops were

averaged for each spectrum from (A, C, G, black) 7, (A, C, G, orange) 10, (B, E, I, black) 11, and (B, E, I, orange) 11 individual samples.

In the spectrum of Cl-PSII (Figure 5.4A, black), a broad positive absorption band is observed (labeled as W_n^+); the center can be estimated at 2830 cm^{-1}.[26, 28] See Table 1 for a review of infrared assignments in the 2830 cm^{-1} region. The W_n^+ band is observed at 40 mM and 155 mM chloride (Figure 5.4A and Figure 5.4B, black) with similar intensity. While the addition of 40 mM acetate has little effect on the intensity of the W_n^+ band; the addition of 155 mM acetate eliminates the band (Figure 5.4A and Figure 5.4B, orange).

Figure 5.4C-F and Figure 5.4G-J present the 1800-1500 cm^{-1} and 1400-1200 cm^{-1} regions of the RIFT-IR spectra, as derived from the chloride control and acetate-treated PSII. To accentuate spectral differences, in Figure 5.4C and Figure 5.4G, the chloride control (black) and the 155 mM acetate (orange) treated data are overlaid. Substantial intensity changes and frequency shifts are observed. These differences are further emphasized in the chloride-minus-acetate double difference spectra shown in Figure 5.4D and Figure 5.4H. Interestingly, the intensity differences are much less pronounced when 40 mM acetate is employed (Figure 5.4E and Figure 5.4I). This observation is supported by the chloride-minus-acetate double difference spectra in Figure 5.4F and Figure 5.4J. We conclude that the addition of 155 mM acetate has dramatic spectral effects, both on the W_n^+ band and on the mid-infrared region of the spectrum. The addition of 40 mM acetate has a less dramatic spectral effect. This result is consistent with the oxygen evolution assays reported in Figure 5.2 and Figure 5.3, which show more complete inhibition at 155 mM acetate, compared to the lower acetate concentration.

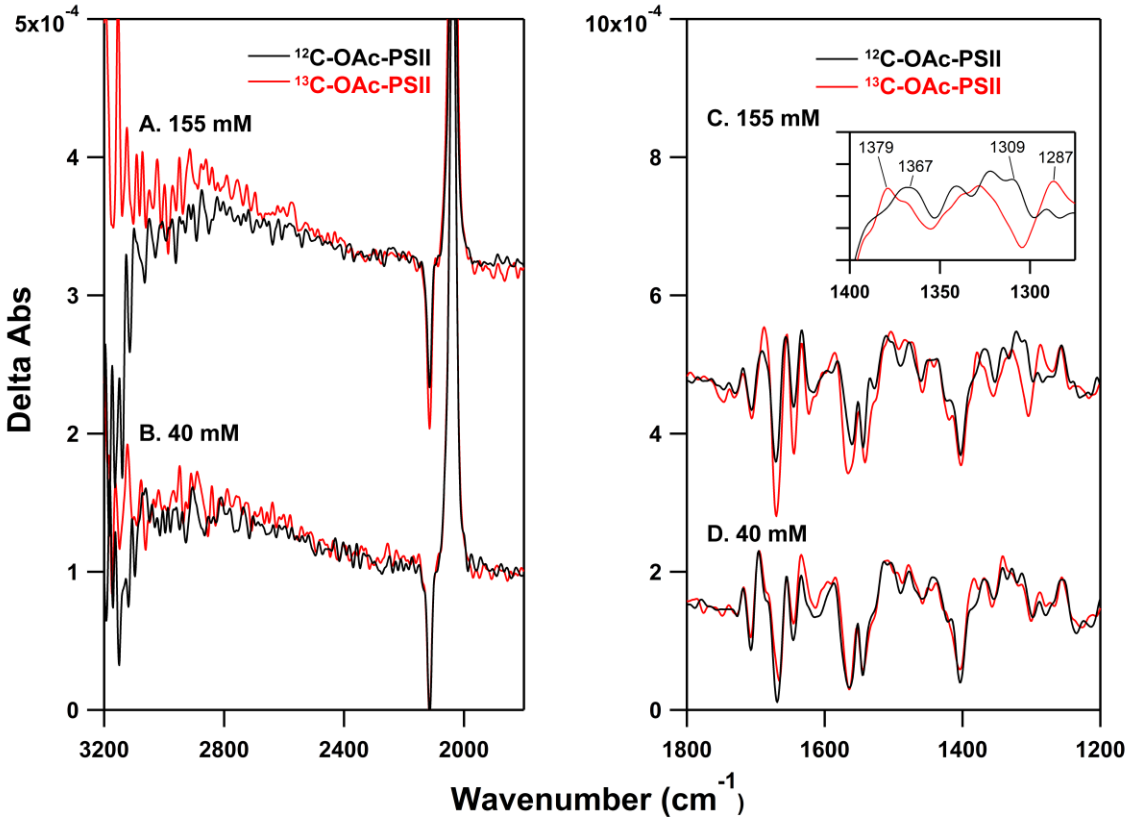

Figure 5.5 Isotope labeling of acetate. RIFT-IR spectra comparing the effects of ^{12}C-acetate (black) and ^{13}C-acetate (red) substitution during the S_1 to S_2 transition at pH 7.5, 283 K. In (A, B), the 3200-1800 cm^{-1} and in (C, D), the 1800-1200 cm^{-1} regions of the S_2-minus-S_1 spectrum are shown. (A, C) contained 155 mM acetate, and (B, D) contained 40 mM acetate. (Inset) Data from (C) in the 1400-1250 cm^{-1} region. The ^{12}C-acetate data are reproduced from Figure 2. Each spectrum contains the averaged data from five acquisition loops using (A, C, black) 10, (A, C, red) 9, (B, D, black) 11, and (B, D, red) 11 different samples.

To definitively identify any spectral contributions of acetate to the RIFT-IR spectra, ^{13}C-acetate was employed. Figure 5.5 compares RIFT-IR spectra acquired with ^{12}C and ^{13}C acetate. The 1800-1200 cm^{-1} regions are presented in Figure 5.5C and Figure 5.5D. With 155 mM acetate treatment, isotope-dependent spectra differences are evident, especially in the 1400-1250 cm^{-1} region (inset). This is a region in which isotope sensitive, symmetric carboxylate stretching bands and CO bands of carboxylic acids are expected.

The spectra in Figure 5.5C also identify changes in the 1700-1600 cm^{-1} region of the spectrum, corresponding to isotope-sensitive C=O stretching vibrations of protonated carboxylic acid. With 40 mM acetate treatment (Figure 5.5D), these changes are not observed. Note that the W_n^+ region is similar in ^{12}C and ^{13}C acetate treated samples (Figure 5.5A and Figure 5.5B).

Figure 5.6A presents a double difference spectrum, constructed from the 155 mM acetate and 40 mM acetate spectra. The double difference spectra are constructed by direct subtraction of the S_2-minus-S_1 spectra. Bands that are in common will cancel, revealing the effects of increase in inhibitor concentration on the data. Notably, this double difference spectrum contains bands both in the 1710-1660 and 1590-1540 cm^{-1} regions. These are regions characteristic of the C=O stretching of carboxylic acids and the asymmetric stretching vibrations of carboxylates. This spectrum suggests that acetate may protonate to form acetic acid during the S_1 to S_2 transition and that the inhibitor may make a direct contribution to the spectrum due to a perturbation caused by the manganese oxidation reaction.

To test this idea, isotope-editing, comparing the effects of ^{12}C and ^{13}C uniformly labeled acetate, was employed. To contribute to an isotope-edited spectrum, a vibrational band must be changed in frequency and intensity by the S_1 to S_2 transition and also involve displacement of the labeled carbon.

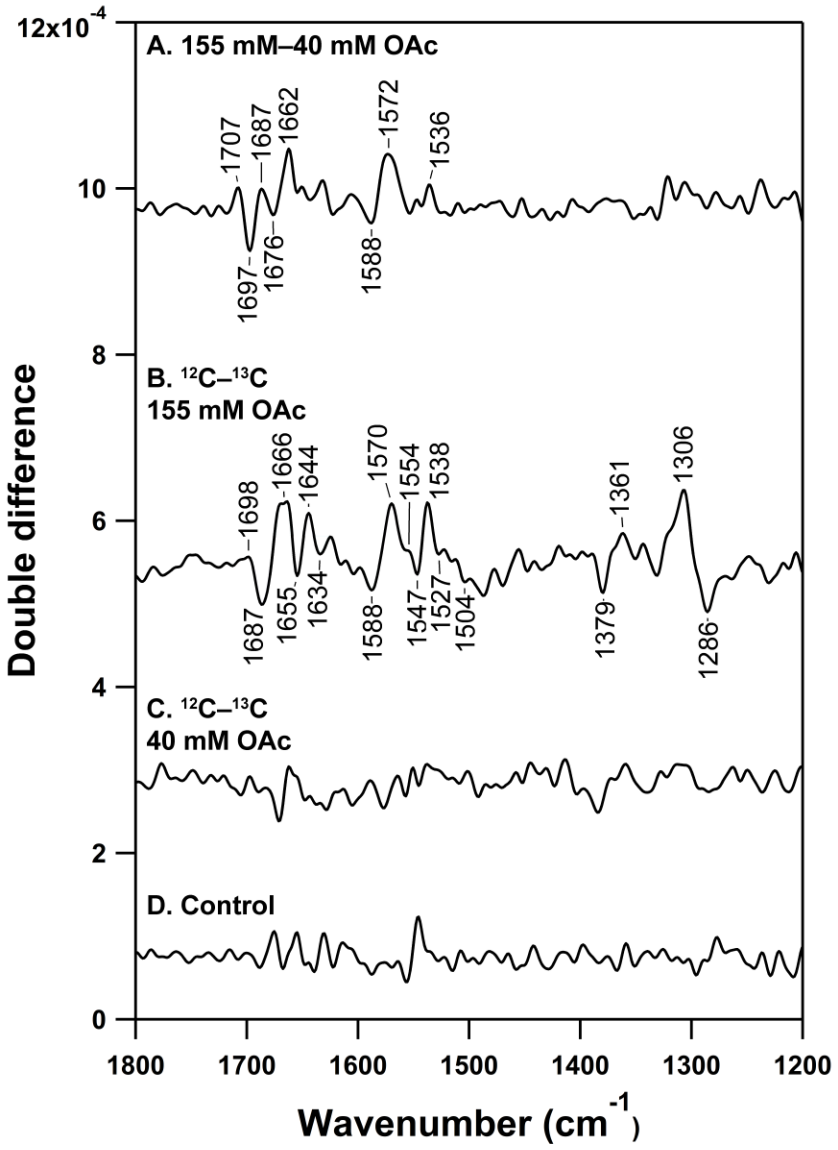

Figure 5.6 Acetate concentration dependence and Isotope-editing using ^{13}C acetate. Double difference spectra, constructed from the S_1 to S_2 transition at pH 7.5, 283 K are shown. In (A), 155 mM acetate-minus-40 mM acetate; in (B), ^{12}C acetate-minus-^{13}C acetate at 155 mM, and in (C), ^{12}C acetate-minus-^{13}C acetate at 40 mM. In (D), the control double difference spectrum. To make the double difference spectra, S_2-minus-S_1 spectra were directly subtracted. The control double difference spectrum was generated by subtracting one half of the corresponding ^{12}C-acetate containing PSII from the other half and the dividing by $\sqrt{2}$.

Figure 5.6B and Figure 5.6C present isotope-edited spectra, ^{12}C-minus-^{13}C, at two different acetate concentrations. With 40 mM acetate, the isotope-edited spectrum is similar to a negative control, which is a double difference spectrum derived just from a ^{12}C acetate data set. This is consistent with the conclusion that isotope labeling of acetate has little spectral effect at 40 mM concentration. However, at 155 mM ^{12}C/^{13}C inhibitor, the isotope-edited spectrum (Figure 5.6B) shows defined bands. The spectrum is constructed: ^{12}C inhibitor (S_2-minus-S_1) - minus ^{13}C inhibitor (S_2-minus-S_1). So, for example, a positive band may arise from a perturbed band of the inhibitor in the S_2 state. Then, the corresponding isotope-shifted band will have an opposite sign and appear as a negative spectral feature. Protonation of acetate to form acetic acid will lead to negative bands in the asymmetric and symmetric CO stretching regions (1548 and 1411 cm^{-1})[18] and produce positive bands in the C=O and CO regions of the carboxylic acid (1706 and 1271 cm^{-1})[18]. The frequencies of these bands are sensitive to environmental interactions and may be shifted when acetate or acetic acid interacts with the OEC.

The isotope-edited spectrum in Figure 5.6B confirms that the S_1 to S_2 transition perturbs the vibrational spectrum of bound acetate and acetic acid in the OEC. Because acetate is added to PSII at pH 7.5, the protonation of acetate occurs in its PSII binding site. So, for example, acetic acid exhibits a second derivative spectrum, with bands at 1698 (+), 1687 (-), and 1666 (+) cm^{-1}. This type of spectral contribution is consistent with a second order Stark effect, which broadens the infrared band of bound acetic acid. In addition, bands are observed at 1655 (-), 1644 (+), and 1634 (-). The spectral lineshape may also be consistent with a Stark effect. Both the acetate and acetic acid bands exhibit isotope sensitive components upon ^{13}C-acetate substitution. Note that the 2830 cm^{-1} region shows

little intensity in the isotope-edited spectrum, either at 155 mM or 40 mM, compared to a negative control. This is consistent with the low intensity expected for the CH vibrational bands of the inhibitor.

To aid in interpretation, QM/MM calculations were conducted on a small model of the OEC used previously.[26] This model was used to elucidate the effects of bromide and nitrate anion exchange at the chloride site.[26] The full geometry-optimized QM models are shown in Figure 5.7. In ref. [26], chloride was found to stabilize an extra proton on a nearby water molecule in this model of the S_2 state. Vibrations of the H_3O^+ core along with solvating waters gave rise to a band that is similar in frequency to the observed W_n^+ band. This band and the hydronium ion were present when bromide and nitrate were substituted for the chloride, but frequency shifts were predicted and observed.[26]

In the present study, acetate is substituted for chloride. Significantly, the proton, stabilized on the hydronium ion in the chloride-containing model, is transferred to acetate to form acetic acid (Figure 5.7). Two different binding orientations of the acetate were tested. In the first conformation, the Me group of the acetate is oriented towards the Me group of the NH_4^+ model ligand (Figure 5.1D, and Figure 5.7A). This orientation will be referred to as the MeMe mode. In the second conformation, the C=O of the acetate is oriented towards the same Me group of NH_4^+ ligand and will be referred to as the O-Me mode (Figure 5.1D, and Figure 5.7B). The MeMe conformation is energetically less favored than the OMe conformation, with a difference of 5 kcal/mol in electronic energies. In both cases, the acetate captures a proton from the water cluster and forms acetic acid.

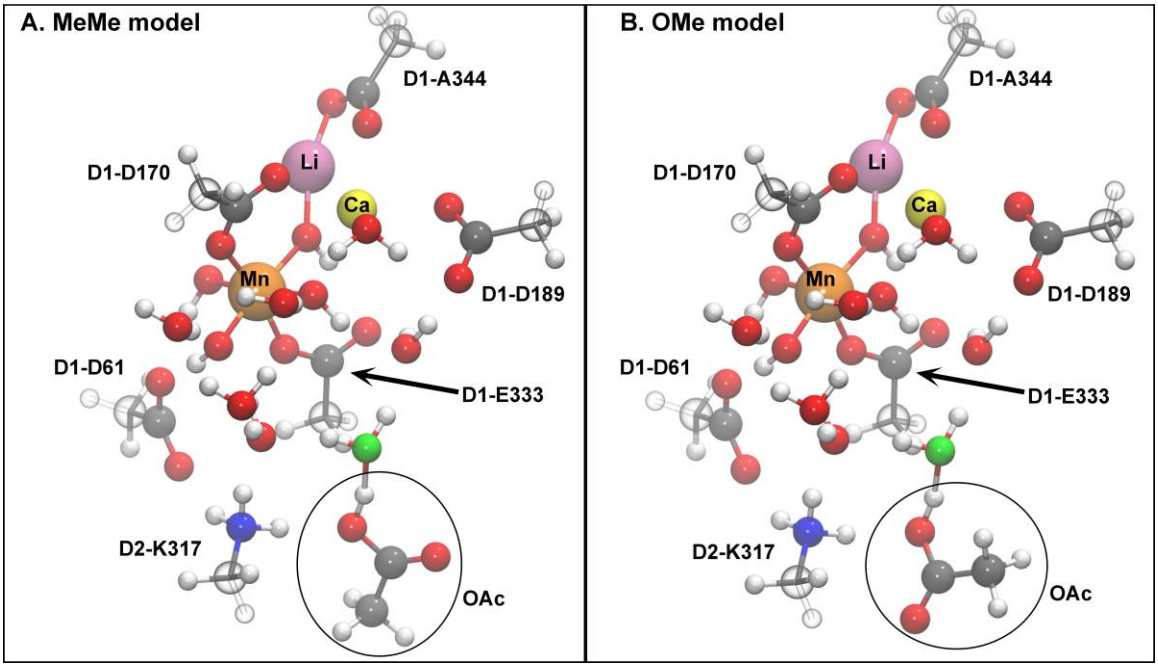

Figure 5.7 Full geometry optimized QM models for acetate substituted PSII. (A) MeMe model with Me group of acetate orientated towards the NH_4^+ group mimicking D-K317. (B) OMe model where C=O group of acetate is oriented towards the adjacent NH_4^+ ligand. The oxygen in green shows the water that accepts the extra proton in chloride containing models. Color of atoms: carbon, gray; nitrogen, blue; oxygen, red; hydrogen, white; manganese, orange; calcium, yellow; and lithium, pink.

The geometry-optimized structures were then used to predict vibrational frequencies. These frequencies are summarized in Figure 5.8. Vibrational bands of the chloride containing model are shown in Figure 5.8A. The predicted acetate spectrum only has contributions from the protonated acid form with bands at 1830/1831 cm^{-1} and 1309/1306 cm^{-1} from the two conformations tested (Figure 5.8B and Figure 5.8D). The predicted isotope shifts for these bands are 42/41 cm^{-1} and 28/31 cm^{-1}, respectively. The difference between the observed and computed frequencies is expected since the minimal model of the OEC does not include the majority of the protein environment.

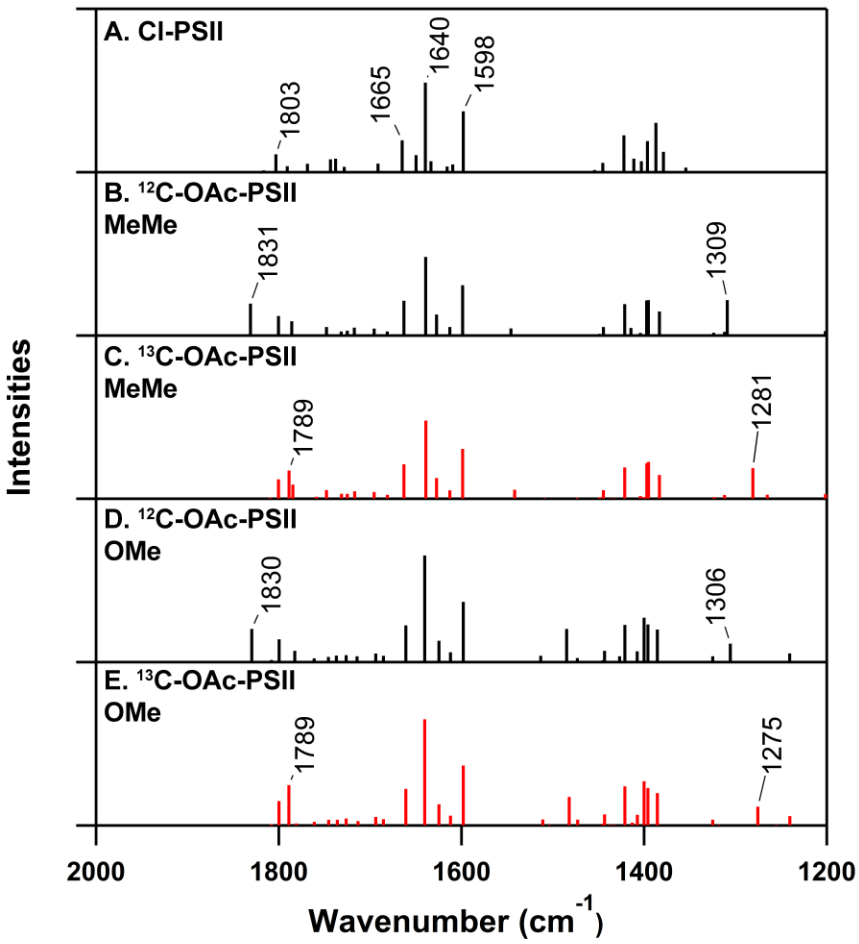

Figure 5.8 Predicted infrared spectrum (2000-1200 cm^{-1}) region from the geometry-optimized model of the OEC containing (A) chloride and (B-E) acetic acid, formed after substitution of acetate at the chloride site. Figure 1D shows the two orientations of acetic acid, referred to as MeMe and OMe. In (B and D), the OEC model contained ^{12}C-acetic acid, (C and E), the OEC model contained ^{13}C-acetic acid.

5.5 Discussion

We have used infrared spectroscopy and QM/MM calculations to provide new information concerning the mechanism of proton transfer in photosynthetic oxygen evolution. Proton transfer occurs over 35 Å from the OEC to the thylakoid lumen. This

proton transfer is critical for photosynthesis, because it leads to acidification of the lumen and a proton gradient that is used to make ATP. This proton transfer must occur under a diverse set of conditions in the plant, including those associated with oxidative stress, increased protein damage, protein turnover, and lumen pre-acidification. The proton transfer network (Figure 4.11A) is robust [23] and functions under a wide set of physiological conditions.

Previous investigations of proton transfer mechanism in PSII have shown that chloride plays an integral role in facilitating this process. The effect of chloride has been proposed to occur by two distinct mechanisms. In the first, chloride prevents a conformational change, organized through a D1-D61 and D2-K317 salt bridge, which closes the channel.[29-32] In the second, chloride stabilizes an intermediary protonated hydronium ion, W_n^+,[23, 26] which is formed by internal water molecules in the network. These two mechanisms are likely to occur simultaneously to optimize the reaction under a variety of conditions. The existence of two mechanisms implies that both protein amino acid side chains and internal water are important participants in the reaction.

Acetate is a well-known inhibitor of PSII, but its mechanism of action has been unclear. A complete block of the S state cycle occurs in the presence of acetate. This block has been documented after formation of the S_2Y_Z radical state, which is formed instead of the S_3 state when acetate is substituted for chloride (ref. [33] and references therein). This has been attributed to exchange and dipolar interaction of $Y_z^\bullet$ with S_2 state of the OEC.[34-36] However, the use of NO to quench the $Y_z^\bullet$ caused the normal S_2 state multiline signal for the Mn cluster to reappear in acetate inhibited PSII. This indicated no direct interaction of acetate with the metal cluster.[37] Simulations of ^{55}Mn ENDOR results showed that the

altered spectrum in acetate inhibited PSII arises from the coupling of $Y_z^{\bullet}$ to the Mn cluster.[33] Oxygen evolution assays have investigated the effect of acetate on activity.[38] One study has been interpreted as showing competitive inhibition between acetate and chloride, although binding of acetate at the non-heme iron site on the PSII acceptor side was also proposed in that work.[38] Note that other anion substitutions at the chloride site can activate or inhibit oxygen evolution.[21] For example, bromide and nitrate support oxygen evolution when substituted for chloride but at lower rates. This is due to a change in rate of the S_3 to S_0 transition.[39] The influences of bromide and nitrate were recently investigated by infrared and QM/MM studies. The effects of bromide and nitrate were attributed to electrostatic effects on the intermediary protonated water cluster based on predicted and observed shifts of W_n^+ band frequency. This study suggests that one effect of acetate could be on the pKa or structure of W_n^+ and that this change in water structure could lead to PSII inhibition.

To test this hypothesis, we performed QM/MM calculations on a small model of the OEC. This model contains one manganese, one calcium, a chloride, and nine water molecules. The essential ligation sphere of these metal ions is maintained. The model provides a high resolution system in which to calculate vibrational frequencies and to explore the effect of metal substitution. When chloride is present, this model predicts stabilization of a hydronium ion on water molecules near the chloride. The frequencies of the hydronium ion are similar to the frequencies observed for W_n^+ in chloride containing PSII.[26] Further the direction of the shift, observed in the W_n^+ band in nitrate and bromide containing PSII, were predicted by the model. In this work, acetate was substituted for chloride. The results predict that the proton is transferred from the hydronium ion to

acetate, forming a hydrogen bonded acetic acid species at the chloride site. Two different conformers of the acetic acid were possible, and the vibrational frequencies were calculated.

The results of the QM/MM study predict that when chloride-depleted PSII is treated with acetate, the inhibitor will protonate to form acetic acid. Therefore, acetate and acetic acid should be detectable in an infrared spectrum of PSII, due to the well-known change in vibrational frequencies when the delocalized CO stretching modes of the carboxylate anion are replaced with the C=O and C−O stretching vibrations of the carboxylic acid. The infrared spectrum of PSII can be obtained with reaction-induced methods; spectra associated with manganese oxidation during the S_1 to S_2 transition are reported here. If this transition perturbs the infrared intensity or frequency of the acetate/acetic acid or leads to protonation, ^{13}C labeling of acetate will identify isotope sensitive bands in the spectrum.

Our infrared results show that both acetate and acetic acid make direct, infrared spectral contributions to the S_2 minus S_1 spectrum. These results conclusively support a mechanism of inhibition in which acetate protonates. The concomitant decrease in the intensity of the W_n^+ band shows that the source of the proton is the hydrated hydronium ion. Taken together, the experiments are consistent with the conclusion that the W_n^+ species plays an essential role in proton transfer and that acetate inhibits oxygen evolution by preventing proton hopping through water.

In the present study, the mechanism of acetate inhibition is revealed mixed Michaelis-Menten inhibition, based on oxygen evolution assays. This would imply multiple binding sites for acetate. One of these binding sites must be chloride dependent

to explain the mixed inhibition pattern. There are at least two possible binding sites for the acetate, one of which is the Cl-1 chloride site (Figure 4.11A). There are several possibilities for the second site.

One is the Cl-2 site, which may have a different affinity for anions (Figure 4.11A). A second is a site somewhere else along the proton transfer pathway (Figure 4.11A). Note that binding of acetate to the acceptor side may occur in some PSII preparations under some conditions, but do not rationalize our results. The infrared spectra acquired in the presence of ferricyanide are regarded to be dominated by donor side structural changes.[40]

The 1698(+)/1687(-)/1666(+) cm^{-1} bands of the bound acetic acid inhibitor are downshifted from the frequency predicted in the calculation and from frequencies typically derived from carboxylic acid residues in proteins. Therefore, the environment around the inhibitor is highly perturbative of the acetate/acetic acid. The C=O frequency has often been correlated with pKa, with a low frequency related to a decrease in pKa.[41-42] The band of the protonated inhibitor has a second derivative shape that is indicative of a Stark effect, which broadens the infrared spectrum.[43] The S_2-minus-S_1 spectrum may arise mainly from electrostatic effects on protein residues in the proton transfer network. Overlap of acetate/acetic acid bands with protein bands is evident when the isotope-edited spectra are compared to the ^{12}C data.

In summary, we use a combination of spectroscopic and theoretical methods to derive information concerning the mechanism of water oxidation. When coupled with infrared spectroscopy, the use of acetate and isotope labeling reveals incisive information about proton transfer mechanism in real time. We report that essential proton hopping

through water bridges occurs in the long-distance proton transfer pathway in PSII. Bacteriorhodopsin and sensory rhodopsin II use a similar mechanism to transport protons [44-45], and the use of water bridges may be a ubiquitous strategy in membrane proteins.

5.6 References

1. Knight, C.; Voth, G. A. The Curious Case of the Hydrated Proton. *Acc. Chem. Res.* **2012,** *45*, 101-9.

2. Marx, D.; Tuckerman, M. E.; Hutter, J.; Parrinello, M. The Nature of the Hydrated Excess Proton in Water. *Nature* **1999,** *397*, 601.

3. Headrick, J. M.; Diken, E. G.; Walters, R. S.; Hammer, N. I.; Christie, R. A.; Cui, J.; Myshakin, E. M.; Duncan, M. A.; Johnson, M. A.; Jordan, K. D. Spectral Signatures of Hydrated Proton Vibrations in Water Clusters. *Science* **2005,** *308*, 1765-1769.

4. Mohammed, O. F.; Pines, D.; Dreyer, J.; Pines, E.; Nibbering, E. T. Sequential Proton Transfer through Water Bridges in Acid-Base Reactions. *Science* **2005,** *310*, 83-86.

5. Xu, J.; Sharpe, M. A.; Qin, L.; Ferguson-Miller, S.; Voth, G. A. Storage of an Excess Proton in the Hydrogen-Bonded Network of the D-Pathway of Cytochrome C Oxidase: Identification of a Protonated Water Cluster. *J. Am. Chem. Soc.* **2007,** *129*, 2910-2913.

6. Garczarek, F.; Gerwert, K. Functional Waters in Intraprotein Proton Transfer Monitored by Ftir Difference Spectroscopy. *Nature* **2006,** *439*, 109-112.

7. Seibold, S. A.; Mills, D. A.; Ferguson-Miller, S.; Cukier, R. I. Water Chain Formation and Possible Proton Pumping Routes in *Rhodobacter Sphaeroides* Cytochrome *C* Oxidase: A Molecular Dynamics Comparison of the Wild Type and R481k Mutant. *Biochemistry* **2005,** *44*, 10475-10485.

8. Silverman, D. N.; McKenna, R. Solvent-Mediated Proton Transfer in Catalysis by Carbonic Anhydrase. *Acc. Chem. Res.* **2007,** *40*, 669-675.

9. Suga, M.; Akita, F.; Hirata, K.; Ueno, G.; Murakami, H.; Nakajima, Y.; Shimizu, T.; Yamashita, K.; Yamamoto, M.; Ago, H., et al. Native Structure of Photosystem Ii at 1.95 Å Resolution Viewed by Femtosecond X-Ray Pulses. *Nature* **2015,** *517*, 99-103.

10. Umena, Y.; Kawakami, K.; Shen, J.-R.; Kamiya, N. Crystal Structure of Oxygen-Evolving Photosystem Ii at a Resolution of 1.9 Å. *Nature* **2011,** *473*, 55-60.

11. Wei, X.; Su, X.; Cao, P.; Liu, X.; Chang, W.; Li, M.; Zhang, X.; Liu, Z. Structure of Spinach Photosystem Ii–Lhcii Supercomplex at 3.2 Å Resolution. *Nature* **2016,** *534*, 69-74.

12. Kok, B.; Forbush, B.; McGloin, M. Cooperation of Charges in Photosynthetic O_2 Evolution-I. A Linear Four Step Mechanism. *Photochem. Photobiol.* **1970,** *11*, 457-75.

13. Barry, B. A. Proton Coupled Electron Transfer and Redox Active Tyrosines in Photosystem Ii. *J. Photochem. Photobiol., B* **2011,** *104*, 60-71.

14. Renger, G.; Renger, T. Photosystem Ii: The Machinery of Photosynthetic Water Splitting. *Photosynth. Res.* **2008,** *98*, 53-80.

15. Gerken, S.; Brettel, K.; Schlodder, E.; Witt, H. Optical Characterization of the Immediate Electron Donor to Chlorophyll a^{+Ii} in O_2-Evolving Photosystem Ii Complexes Tyrosine as Possible Electron Carrier between Chlorophyll A_{ii} and the Water-Oxidizing Manganese Complex. *FEBS Lett.* **1988,** *237*, 69-75.

16. Dau, H.; Zaharieva, I.; Haumann, M. Recent Developments in Research on Water Oxidation by Photosystem Ii. *Curr. Opin. Chem. Biol.* **2012,** *16*, 3-10.

17. Petrie, S.; Pace, R. J.; Stranger, R. Resolving the Differences between the 1.9 Å and 1.95 Å Crystal Structures of Photosystem Ii: A Single Proton Relocation Defines Two Tautomeric Forms of the Water-Oxidizing Complex. *Angew. Chem. Int. Ed.* **2015,** *54*, 7120-7124.

18. Max, J.-J.; Chapados, C. Infrared Spectroscopy of Aqueous Carboxylic Acids: Comparison between Different Acids and Their Salts. *J Phys Chem A* **2004,** *108*, 3324-3337.

19. Bao, H.; Dilbeck, P. L.; Burnap, R. L. Proton Transport Facilitating Water-Oxidation: The Role of Second Sphere Ligands Surrounding the Catalytic Metal Cluster. *Photosynth. Res.* **2013,** *116*, 215-229.

20. Haumann, M.; Hundelt, M.; Jahns, P.; Chroni, S.; Bögershausen, O.; Ghanotakis, D.; Junge, W. Proton Release from Water Oxidation by Photosystemii: Similar Stoichiometries Are Stabilized in Thylakoids and Psii Core Particles by Glycerol. *FEBS Lett.* **1997,** *410*, 243-248.

21. Yocum, C. F. The Calcium and Chloride Requirements of the O_2 Evolving Complex. *Coord. Chem. Rev.* **2008,** *252*, 296-305.

22. Barry, B. A.; Brahmachari, U.; Guo, Z. Tracking Reactive Water and Hydrogen-Bonding Networks in Photosynthetic Oxygen Evolution. *Acc. Chem. Res.* **2017,** *50*, 1937-1945.

23. Brahmachari, U.; Guo, Z.; Konecny, S. E.; Obi, E. N. C.; Barry, B. A. Engineering Proton Transfer in Photosynthetic Oxygen Evolution: Chloride, Nitrate, and Trehalose Reorganize a Hydrogen-Bonding Network. *J Phys Chem B* **2018,** *122*, 6702-6711.

24. Berthold, D. A.; Babcock, G. T.; Yocum, C. F. A Highly Resolved, Oxygen-Evolving Photosystem Ii Preparation from Spinach Thylakoid Membranes: Epr and Electron-Transport Properties. *FEBS Lett.* **1981,** *134*, 231-234.

25. Mishra, R. K.; Ghanotakis, D. F. Selective Extraction of Cp 26 and Cp 29 Proteins without Affecting the Binding of the Extrinsic Proteins (33, 23 and 17 Kda) and the Dcmu Sensitivity of a Photosystem Ii Core Complex. *Photosynth. Res.* **1994,** *42*, 37-42.

26. Brahmachari, U.; Gonthier, J. F.; Sherrill, C. D.; Barry, B. A. Chloride Maintains a Protonated Internal Water Network in the Photosynthetic Oxygen Evolving Complex. *J. Phys. Chem. B* **2017,** *121*, 10327-10337.

27. Polander, B. C.; Barry, B. A. Calcium and the Hydrogen-Bonded Water Network in the Photosynthetic Oxygen-Evolving Complex. *J. Phys. Chem. Lett.* **2013,** *4*, 786-791.

28. Brahmachari, U.; Barry, B. A. Dynamics of Proton Transfer to Internal Water During the Photosynthetic Oxygen-Evolving Cycle. *J. Phys. Chem. B* **2016,** *120*, 11464-11473.

29. Pokhrel, R.; McConnell, I. L.; Brudvig, G. W. Chloride Regulation of Enzyme Turnover: Application to the Role of Chloride in Photosystem Ii. *Biochemistry* **2011,** *50*, 2725-2734.

30. Rivalta, I.; Amin, M.; Luber, S.; Vassiliev, S.; Pokhrel, R.; Umena, Y.; Kawakami, K.; Shen, J.-R.; Kamiya, N.; Bruce, D. Structural–Functional Role of Chloride in Photosystem Ii. *Biochemistry* **2011,** *50*, 6312-6315.

31. Pokhrel, R.; Service, R. J.; Debus, R. J.; Brudvig, G. W. Mutation of Lysine 317 in the D2 Subunit of Photosystem Ii Alters Chloride Binding and Proton Transport. *Biochemistry* **2013,** *52*, 4758-4773.

32. Suzuki, H.; Yu, J.; Kobayashi, T.; Nakanishi, H.; Nixon, P. J.; Noguchi, T. Functional Roles of D2-Lys317 and the Interacting Chloride Ion in the Water Oxidation Reaction of Photosystem Ii as Revealed by Fourier Transform Infrared Analysis. *Biochemistry* **2013,** *52*, 4748–4757.

33. Peloquin, J. M.; Campbell, K. A.; Britt, R. D. 55mn Pulsed Endor Demonstrates That the Photosystem Ii "Split" Epr Signal Arises from a Magnetically-Coupled Mangano−Tyrosyl Complex. *J. Am. Chem. Soc.* **1998,** *120*, 6840-6841.

34. Szalai, V. A.; Brudvig, G. W. Formation and Decay of the S3 Epr Signal Species in Acetate-Inhibited Photosystem Ii. *Biochemistry* **1996,** *35*, 1946-1953.

35. Szalai, V. A.; Kühne, H.; Lakshmi, K. V.; Brudvig, G. W. Characterization of the Interaction between Manganese and Tyrosine Z in Acetate-Inhibited Photosystem Ii. *Biochemistry* **1998,** *37*, 13594-13603.

36. Tang, X.-S.; Randall, D. W.; Force, D. A.; Diner, B. A.; Britt, R. D. Manganese−Tyrosine Interaction in the Photosystem Ii Oxygen-Evolving Complex. *J. Am. Chem. Soc.* **1996,** *118*, 7638-7639.

37. Szalai, V. A.; Brudvig, G. W. Reversible Binding of Nitric Oxide to Tyrosyl Radicals in Photosystem Ii. Nitric Oxide Quenches Formation of the S3 Epr Signal Species in Acetate-Inhibited Photosystem Ii†. *Biochemistry* **1996,** *35*, 15080-15087.

38. Kühne, H.; Szalai, V. A.; Brudvig, G. W. Competitive Binding of Acetate and Chloride in Photosystem Ii. *Biochemistry* **1999,** *38*, 6604-6613.

39. Wincencjusz, H.; Yocum, C. F.; Van Gorkom, H. J. Activating Anions That Replace Cl-in the O2-Evolving Complex of Photosystem Ii Slow the Kinetics of the Terminal Step in Water Oxidation and Destabilize the S2 and S3 States. *Biochemistry* **1999,** *38*, 3719-3725.

40. Polander, B. C.; Barry, B. A. A Hydrogen-Bonding Network Plays a Catalytic Role in Photosynthetic Oxygen Evolution. *Proc. Natl. Acad. Sci. U.S.A.* **2012,** *109*, 6112-6117.

41. Dioumaev, A. Infrared Methods for Monitoring the Protonation State of Carboxylic Amino Acids in the Photocycle of Bacteriorhodopsin. *Biochemistry (Moscow)* **2001,** *66*, 1269-1276.

42. Zscherp, C.; Schlesinger, R.; Tittor, J.; Oesterhelt, D.; Heberle, J. In Situ Determination of Transient Pka Changes of Internal Amino Acids of Bacteriorhodopsin by Using Time-Resolved Attenuated Total Reflection Fourier-Transform Infrared Spectroscopy. *Proc. Natl. Acad. Sci. U.S.A.* **1999,** *96*, 5498-5503.

43. Boxer, S. G. Stark Realities. *J Phys Chem B* **2009,** *113*, 2972-2983.

44. Decoursey, T. E. Voltage-Gated Proton Channels and Other Proton Transfer Pathways. *Physiological reviews* **2003,** *83*, 475-579.

45. Mohrmann, H.; Kube, I.; Lórenz-Fonfría, V. A.; Engelhard, M.; Heberle, J. Transient Conformational Changes of Sensory Rhodopsin Ii Investigated by Vibrational Stark Effect Probes. *J Phys Chem B* **2016,** *120*, 4383-4387.

CHAPTER 6. CONCLUSIONS

In summary, this thesis investigates the functional proton transfer network in photosystem II (Figure 4.11A). RIFT-IR spectroscopy has been utilized to obtain information from several components of the network. Taken together the work provides methods for obtaining high resolution detailed information about dynamic hydrogen-bonded proton transfer networks in proteins spanning distances of more than 35 Å.

First, the infrared signal assignable to the stretching vibrations of protonated internal water cluster was identified. It was found to oscillate in a S-state dependent manner. Based on several experiments, including solvent isotope exchange [1]and others [2-3], we proposed that internal water acts as proton donor and acceptor transiently to form a necessary proton transfer intermediate at two stages in the photosynthetic oxygen evolution process.

The second study involved investigating the role of chloride ions in mediating proton transfer events in PSII. Chloride is an extremely rare cofactor in biology and PSII is one of three enzymes known to exhibit chloride dependence of enzymatic activity [4]. By analogy with the other chloride-dependent enzymes, experimental and theoretical studies (ref. [5] and references therein) it has been proposed that chloride facilitates proton transfer by preventing salt bridge formation between and aspartic acid side critical for proton transfer and a nearby lysine residue [6]. Using RIFT-IR spectroscopy and QM calculations, we observed an additional role for the chloride ions in PSII. It was found to exert a stabilizing influence on a neighboring protonated water cluster formed in the S_2 state. The infrared signal from the protonated water cluster had demonstrated very high and unusual

isotope shift upon $^{18}OH_2$ substitution (~100 cm^{-1}) at 263 K. However, at 283 K the isotope shifts observed ~10 cm^{-1} matched closely with expected literature values. We attributed these observations to a cluster size heterogeneity at lower temperature which is no longer present at higher temperature.

The third study used the spectroscopic signals from peptide carbonyl groups as reporters for monitoring the dynamic proton transfer network. Electric field alteration using bromide and hydrogen bonding perturbation using nitrate led to changes in the spectrum but retention of oxygen evolution activity. Substitution of the cryoprotectant trehalose for sucrose reversed some of the hydrogen bonding changes that affected amide infrared bands. Several mutations in cyanobacterial PSII had elicited similar changes in vibrational frequencies. Taken together, we proposed that PSII proton transfer network which involves peptide carbonyl groups, amino acid side chains, internal water moles and hydronium ion, is robust and can successfully adapt to changes in electric field, pK_a, and hydrogen bonding.

In the fourth study, we have investigated whether the formation of the protonated water cluster intermediate is necessary for proton transfer in PSII. The inhibitory anion acetate was used to disrupt proton transfer to water during the first S-state transition. The effect on the activity was dramatic reduction of the oxygen evolution rates. The infrared signal from the internal protonated water cluster was eliminated. Using isotope-editing with ^{13}C-aceatate, infrared bands from acetic acid were observed. The results matched with those observed from the QM model where acetate accepted a proton from the neighboring hydronium ion to form acetic acid when substituted at the chloride site. Based on these results we proposed that proton hopping through water bridges is necessary for photosynthetic oxygen evolution.

To probe the PSII proton transfer network further, future work can involve engineering new infrared probes into the proton transfer pathway to identify key residues. Previously, 7-azatryptohan was incorporated into PSII via the disordered extrinsic subunit PsbO [7]. Other probes such as fluoro-tryptophans and fluoro-tyrosines can be included to monitor the pathway. The pattern of proton release can also be monitored as a function of S-state progression to evaluate effects of pH, anionic substitutions and unnatural amino acid incorporation. To this end various dyes,[8-9] and infrared signals from 2-(N-morpholino)ethanesulfonic acid, commonly employed as a buffering agent, can be utilized.[10] To reconcile the spectroscopic evidence with the structure, several theoretical approaches can be employed. The QM model reported in this thesis can be increased in complexity to include peptide carbonyl groups, all metal ions of the OEC and ligands to the OEC. Molecular dynamics can be used to model the proton exit pathway and has been recently utilized to investigate hydrogen bonding networks in PSII.[11] Nuclear quantum vibrational perturbation (QVP) method[12] can be used to generate models to the vibrational frequencies of an acetate probe and can thereby provide more information regarding the PSII proton exit pathway.

6.1 References

1. Brahmachari, U.; Barry, B. A. Dynamics of Proton Transfer to Internal Water During the Photosynthetic Oxygen-Evolving Cycle. *J. Phys. Chem. B* **2016,** *120,* 11464-11473.

2. Polander, B. C.; Barry, B. A. Detection of an Intermediary, Protonated Water Cluster in Photosynthetic Oxygen Evolution. *Proc. Natl. Acad. Sci. U.S.A.* **2013,** *110,* 10634-9.

3. Guo, Z.; Barry, B. A. Cryogenic Trapping and Isotope Editing Identify a Protonated Water Cluster as an Intermediate in the Photosynthetic Oxygen-Evolving Reaction. *J. Phys. Chem. B* **2016,** *120*, 8794-8808.

4. Wincencjusz, H.; Yocum, C. F.; van Gorkom, H. J. S-State Dependence of Chloride Binding Affinities and Exchange Dynamics in the Intact and Polypeptide-Depleted O2 Evolving Complex of Photosystem Ii. *Biochemistry* **1998,** *37*, 8595-8604.

5. Brahmachari, U.; Gonthier, J. F.; Sherrill, C. D.; Barry, B. A. Chloride Maintains a Protonated Internal Water Network in the Photosynthetic Oxygen Evolving Complex. *J. Phys. Chem. B* **2017,** *121*, 10327-10337.

6. Rivalta, I.; Amin, M.; Luber, S.; Vassiliev, S.; Pokhrel, R.; Umena, Y.; Kawakami, K.; Shen, J.-R.; Kamiya, N.; Bruce, D. Structural–Functional Role of Chloride in Photosystem Ii. *Biochemistry* **2011,** *50*, 6312-6315.

7. Offenbacher, A. R.; Pagba, C. V.; Polander, B. C.; Brahmachari, U.; Barry, B. A. First Site-Specific Incorporation of a Noncanonical Amino Acid into the Photosynthetic Oxygen-Evolving Complex. *ACS chemical biology* **2014,** *9*, 891-6.

8. Saphon, S.; Crofts, A. R. Protolytic Reactions in Photosystem-Ii - New Model for Release of Protons Accompanying Photooxidation of Water. *Z. Naturforsch C.* **1977,** *32*, 617-626.

9. Auslander, W.; Junge, W. Neutral Red, a Rapid Indicator for Ph-Changes in Inner Phase of Thylakoids. *Febs Lett.* **1975,** *59*, 310-315.

10. Suzuki, H.; Sugiura, M.; Noguchi, T. Monitoring Proton Release During Photosynthetic Water Oxidation in Photosystem Ii by Means of Isotope-Edited Infrared Spectroscopy. *J. Am. Chem. Soc.* **2009,** *131*, 7849-7857.

11. Guerra, F.; Siemers, M.; Mielack, C.; Bondar, A.-N. Dynamics of Long-Distance Hydrogen-Bond Networks in Photosystem Ii. *J Phys Chem B* **2018,** *122*, 4625-4641.

12. Garcia-Viloca, M.; Nam, K.; Alhambra, C.; Gao, J. Solvent and Protein Effects on the Vibrational Frequency Shift and Energy Relaxation of the Azide Ligand in Carbonic Anhydrase. *J Phys Chem B* **2004,** *108*, 13501-13512.